ABSTRACT

Title of Dissertation: ON THE CONTROL OF ROBOTIC PARASITIC ANTENNA ARRAYS

Jeffrey N. Twigg
Doctor of Philosophy, 2022

Dissertation Directed by: Professor Nikhil Chopra
Department of Mechanical Engineering

Wireless networking is challenging in safety, security, and rescue contexts where network infrastructure may be damaged or compromised. Radio communication between ground robots at the lower end of the Very High Frequency (low-VHF) band is generally more reliable in complex indoor and urban environments when compared to communication systems such as Wi-Fi and cellular, which operate at Ultra High Frequencies (UHF) and higher frequencies. Exciting antenna design research in the last 5 to 10 years has approached what is theoretically possible to create compact, moderately high bandwidth antennas at low-VHF. At the beginning of this dissertation research, we discovered that we could distribute these low-VHF antennas across closely positioned ground robots to create a robotic parasitic antenna array. When these robots are optimally positioned, they create a directional signal through the mutual coupling of their antennas. Consequently, these low-VHF arrays have the potential to extend the communication range of a reliable signal in urban and indoor environments with a proportionally small amount of robotic motion. In this dissertation, we research the control of robotic platforms constituting these

arrays from two perspectives. First, we research how robots control their positions to optimize or maintain the gain of a single robotic parasitic array to improve the quality of a communication link. Then, we investigate where these robots should collect to form an array in a network of robotic parasitic arrays to increase a metric of overall network connectivity.

To improve individual network communication links, we consider a two-element parasitic array formed by a static antenna and a ground robot, and propose a technique by which this array can increase its gain in a direction of interest. First, we propose and test a calibration approach for actuating the spacing between the two antennas and the passive antenna length to increase gain. Next, we propose and test an approach that uses robotic motion to rotate the antenna array. In these experiments, we show that the robotic parasitic antenna array can provide a gain of $2\,\mathrm{dB}$ which is close to twice the effective transmission power in line-of-sight and non-line-of-sight conditions.

From a network perspective, we research where robots should form arrays to maintain a metric of overall connectivity. However, existing control formulations for maintaining connectivity are not general enough to support this new capability. We first propose a generalized model that we integrate into a Fiedler value maximization approach for maintaining communication. Afterward, we develop approaches for allocating a finite number of robots for forming these robotic parasitic arrays while ensuring that our metric for overall network connectivity between robotic parasitic array forming robots remains lower bounded.

ON THE CONTROL OF ROBOTIC PARASITIC ANTENNA ARRAYS

by

Jeffrey N. Twigg

Dissertation submitted to the Faculty of the Graduate School of the
University of Maryland, College Park in partial fulfillment
of the requirements for the degree of
Doctor of Philosophy
2022

Advisory Committee:
- Dr. Nikhil Chopra, Chair/Advisor
- Dr. Shapour Azarm
- Dr. Yancy Diaz-Mercado
- Dr. Dinesh Manocha, Dean's Representative
- Dr. Brian M. Sadler
- Dr. Miao Yu

Dedication

I would like to dedicate this dissertation to my pragmatic and loving wife, who pushed me towards getting this degree with an eye towards the future. In addition, I would like to dedicate this to my parents, who pushed me to pursue every opportunity to learn more about how things work, as well as my siblings and aunt, who are consistently enthusiastic and supportive.

Acknowledgments

First, I would like to acknowledge my advisor, Dr. Nikhil Chopra, for his guidance throughout my coursework and research. In addition, Dr. Brian Sadler has provided a wide range of meaningful perspectives before and during my Ph.D. work. His guidance pushed me to work towards pursuing a Ph.D. and catalyzed this research into robotic parasitic arrays. Dr. Chopra and Dr. Sadler's feedback on research ideas and papers we have written has been incredibly helpful and enlightening. I would also like to acknowledge Dr. Fikadu Dagefu. His insight into antenna design, wave propagation modeling, and experiments has been critical to the success of this research. His foundational simulation work and corresponding models have informed my thoughts about appropriate control approaches, while his positive attitude and meticulous approach to problem-solving are attributes I appreciate and seek to emulate. Additional recognition should be given to the members of the Intelligence for Robotics Branch at the Army Research Laboratory; their enthusiasm and deep knowledge of robotics have motivated, educated, and challenged me.

Table of Contents

Dedication ii

Acknowledgements iii

Table of Contents iv

List of Tables vi

List of Figures vii

List of Abbreviations x

Chapter 1: Introduction: The Robotic Communications Problem and the State of the Art 1
- 1.1 Low-Frequency Channels and Novel Antennas . . . 4
- 1.2 Robotic Parasitic Arrays . . . 6
- 1.3 Dissertation Outline . . . 9

Chapter 2: Background in Robotic Communication for Robotic Parasitic Arrays 12
- 2.1 Multi-Element Antenna Arrays . . . 15
  - 2.1.1 Parasitic Arrays . . . 17
- 2.2 Network Connectivity Maintenance . . . 23

Chapter 3: Calibrating a Parasitic Array for Increased Gain 32
- 3.1 Approach to Calibrating the Array . . . 33
  - 3.1.1 Parasitic Array Formation . . . 34
  - 3.1.2 Full-wave FDTD Simulations . . . 35
  - 3.1.3 Increasing Received Power . . . 37
  - 3.1.4 Setup . . . 39
- 3.2 Experiments . . . 41
- 3.3 Results and Discussion . . . 42

Chapter 4: Robotic Parasitic Array Control for Increased RSS in Non-Line-of-Sight 47
- 4.1 Approach . . . 49
  - 4.1.1 Robotic Parasitic Array Boresight Rotation . . . 49
  - 4.1.2 Actuating the Array to Maximize RSS . . . 53
- 4.2 Experiments . . . 54
- 4.3 Results and Discussion . . . 60

Chapter 5: Optimizing Overall Network Connectivity of Parasitic Arrays 65
5.1 Approach to Connectivity Maintenance . . . 66
5.1.1 System Model and Problem Formulation . . . 67
5.1.2 Graph of Agent Connectivity . . . 70
5.1.3 Fiedler Optimization . . . 72
5.2 Derivation of Controller . . . 75
5.2.1 Maintaining Connectivity While Pursuing Other Objectives . . . 77
5.3 Simulations . . . 78
5.3.1 Verifying Communications Maintenance . . . 78
5.4 Results and Discussion . . . 80
5.4.1 Effects of Array Forming on Operational Range . . . 81
5.4.2 Multiple Trials . . . 82

Chapter 6: Reallocation of Array Forming Robots with Constraints 85
6.1 Related Work . . . 88
6.2 Approach . . . 89
6.2.1 Connectivity Maintenance Control for All Arrays . . . 90
6.2.2 Additional Motion Control Input for Motion-Controlled Arrays . . . 92
6.2.3 Allocating Constraints on the Number of Passive Antenna Agents for All Arrays . . . 95
6.2.4 Passive Antenna Agent Deallocation for Relay Arrays . . . 97
6.2.5 Motion Compensation Control for Relay Arrays . . . 97
6.3 Simulations . . . 99
6.4 Results and Discussion . . . 102

Chapter 7: Contributions and Conclusions 105
7.1 Contributions . . . 105
7.2 Array Gain Control . . . 107
7.2.1 Future Control Research in Array Creation . . . 108
7.3 Network Connectivity Maintenance . . . 109
7.3.1 Future Connectivity Research with Robotic Arrays . . . 109
7.4 New Research Threads . . . 110

Bibliography 112

List of Tables

5.1 System States and Variables [1] ©2020 IEEE 67
5.2 Gain of a Yagi-Uda Parasitic Antenna Array [1] ©2020 IEEE 70

6.1 Robotic Array i States and Control Inputs 90
6.2 The directions that arrays are guided when they assume the motion-controlled role ($u_{i,3:4}^{mc} = 0$). 100

List of Figures

1.1 Several ground robots occupy a complex environment. The image zooms in on one of them to show its low-VHF antenna. The concentric circles around one of the robots show that it is radiating equally in all directions using this low-VHF antenna. 6
1.2 Several ground robots maneuver to form a robotic parasitic array to create a higher gain and more directional signal. 7
1.3 Ground robots establish an ad-hoc network enabled by low-VHF communication. Robots with active low-VHF antennas are shown with larger light-blue circles. . 9
1.4 Ground robots establish an ad-hoc network enabled by low-VHF communication. 10

2.1 Electromagnetic radiation of a single, low-VHF electrically small antenna mounted on a ground robot. [2] ©2019 IEEE 20
2.2 Parasitic antenna array created by a second robot with a passive antenna that mutually couples with the antenna of the robot in Fig 2.1. The direction of the boresight and the spacing d between antennas are also shown. [2] ©2019 IEEE . 20
2.3 Low-VHF robotic parasitic antenna array feasibility experiment. [3] 22
2.4 Our robotic Yagi-Uda arrays are composed of a driven/excited antenna (solid circle) and passive antennas (numbered in the order in which they are added to increase gain). The arrow points in the direction of maximum gain of the array pattern (dashed line). An array with more passive antenna agents has a higher gain when these antennas are optimally spaced. [1] ©2020 IEEE 23
2.5 Four robotic agents are represented by nodes with weighted edges indicating the strength of their respective links. 26

3.1 This is a diagram of the robot that changes d, the distance from the robot to the reflector, in order to maximize the reception power measured by the radio on the robot. The static transmitter is not depicted. [2] ©2019 IEEE 35
3.2 Full-wave FDTD simulation results show the gain of a two-element parasitic array as a function of antenna spacing. Four different values of the length of the parasitic element are considered. The excited element for this simulation is 0.46λ long. The result shows that the antenna spacing that provides the peak gain varies depending on the length of the parasitic element. [2] ©2019 IEEE 36
3.3 The adjustable reflector is electrically coupled with the ESA, which is mounted on a robot. The transmitter is roughly $25\,\mathrm{m}$ from the robot. The robotic parasitic array is on almost level ground near the top of a hill. [2] ©2019 IEEE 40

3.4 Change in received power as a function of robot position with and without the reflector. [2] ©2019 IEEE . . . 41
3.5 Change in gain as a function of robot position for a reflector length of $1.94\,\mathrm{m}$ [2] ©2019 IEEE . . . 43
3.6 Change in gain as a function of reflector length with the robot in a calibrated position. [2] ©2019 IEEE . . . 44
3.7 Change in gain as a function of robot position in a dynamic environment [2] ©2019 IEEE . . . 46

4.1 The positions and orientations of UGV and reflector and the mobile node . . . 49
4.2 The robotic parasitic array is formed by the UGV and reflector. A camera on the UGV allows it to localize the reflector. . . . 55
4.3 This is a system of coordinate frames for localizing the reflector, UGV, and the mobile node. . . . 56
4.4 Array gain at different boresight angles and reflector-UGV spacings . . . 57
4.5 RSS v. boresight angle with optimal reflector and UGV spacing. . . . 57
4.6 Satellite view of a complex environment where we test the robotic parasitic array. 59
4.7 Distortion of array pattern when ground impinges on the signal. . . . 60
4.8 Array gain with fixed boresight in LOS and NLOS conditions . . . 61
4.9 Array gain achieved by rotating the boresight using mobile node telemetry at LOS and NLOS positions . . . 62
4.10 The left y-plot shows the change in boresight angle during gradient ascent. The right y-plot shows the steady growth in RSS. . . . 63

5.1 Connectivity indicated by the color-scale between agent i, located at (0,0), and agent j in different (x, y) positions, both with fixed values of θ and ρ. [1] ©2020 IEEE . . . 72
5.2 Connectivity indicated by colorscale and z-axis plotted between agent i, located at (0,0), and agent j in different (x, y) positions, both with fixed values of θ and ρ. 73
5.3 Trajectories of active antenna agents. Square markers denote the final positions of the single, non-array-forming agents which employ a disk model. Circle markers denote the final positions of the array forming active antenna agents. [1] ©2020 IEEE . . . 79
5.4 Fiedler value over time for both trials of agents shown in Fig. 5.3. [1] ©2020 IEEE 80
5.5 Parasitic effect (ρ) of the 4 arrays over time. The plot colors match the agents' colors from the trajectories in Fig.5.3 ending with the circle marker. [1] ©2020 IEEE . . . 81
5.6 Maximum distance between 2 active antenna agents which form parasitic arrays. Each plot corresponds to the number of passive agents available to form arrays. [1] ©2020 IEEE . . . 82
5.7 Trajectories and final positions of each of the four active antenna agents is initialized at random locations . . . 83
5.8 Fiedler value of each of the four active antenna agents initialized at random locations. . . . 84

6.1 A motion-controlled array needs to acquire a passive antenna agent from a relay array to move in a desired direction while maintaining connectivity. However, the proposed reallocation shown by the green arrow can instantaneously reduce the overall connectivity of the arrays. 86
6.2 Trial with a simple approach to reallocating agents 87
6.3 The energy function of λ_2 where $\epsilon = 0$ 91
6.4 Comparison of the parasitic effect with and without the deallocation controller described in Sec. 6.2.4 101
6.5 Fiedler value over time for 3 different methods of (re)allocating passive antenna agents 103
6.6 Trajectories created by different approaches: Points with the smallest array distances are at the beginning of time interval t as the additional motion control increases the spacing between motion-controlled arrays. The values at the end of each interval are marked with a star. 103

List of Abbreviations

ESA	electrically small antenna
FDTD	finite-difference time-domain
HF	high frequency (3 MHz- 30MHz)
LOS	line-of-sight
NLOS	non-line-of-sight
RSS	received signal strength
UHF	ultra high frequency (300 MHz - 3 GHz)
VHF	very high frequency (30 MHz - 300 MHz)

Chapter 1: Introduction: The Robotic Communications Problem and the State of the Art

Wireless networking is challenging in safety, security, and rescue contexts where network infrastructure may be damaged or compromised. As a result, maintaining communication between mobile autonomous agents operating in these situations is difficult. The contexts of these missions are often dense, physically complex environments where conventional communication systems that operate at ultra high frequency (UHF [$300\,\mathrm{MHz}$ to $3\,\mathrm{GHz}$]) and higher frequencies (e.g., implementations of the IEEE 802.11 standards at $2.4\,\mathrm{GHz}$ and $5\,\mathrm{GHz}$, cellular) used by roboticists are unreliable [4]. In these complex environments, received signal strength (RSS), an indicator of successful wireless communication, fluctuates due to multipath fading and rapidly diminishes with the increased range at these higher frequencies. Another aspect of multipath is that signals' RSS rapidly changes with small changes in position. This phenomenon is more prevalent in complex environments where densely spaced objects (e.g., walls, buildings, vehicles, and people) reflect UHF signals. Simultaneously, these frequencies are rapidly attenuated by walls and other objects; for example, a robot navigating around the corner of a building could instantly lose a communication link.

Despite the increasing maturity of these UHF and higher frequency technologies, it is reasonable to investigate how novel communications capabilities can augment multi-robot systems

and vice-versa. In fact, the advancements in industry and academia indicate a convergence and growing overlap of wireless communication and mobile autonomy solutions. Research on designing compact, robot-mountable antennas for longer-range, reliable communication in these environments [5] is one such example. These antennas radiate at the lower end of the very high frequency (VHF [$3\,\mathrm{MHz}$ to $300\,\mathrm{MHz}$]) band and have been demonstrated to penetrate dense structures with reduced variation in signal strength. In addition, preliminary research shows that it is possible to create arrays and establish long-range, directional communication links when several of these antennas are deployed in an array.

In this dissertation, we research how to control robotic agents wielding these low-VHF antennas to create and articulate the arrays from two perspectives. One perspective is focused on maximizing received RSS for a communication link enabled by a robotic parasitic array. Next, from a wider perspective, we examine the positioning and creation of multiple parasitic arrays that form and maintain communication links to increase a metric of overall network connectivity. Before discussing this in detail, we position this preliminary research in the state of the art of wireless communication and robotic research.

Current wireless communication solutions often use some or all of the following: elevated cellular towers, wireless access points, dedicated and densely configured sensor network infrastructure, and/or extensive databases of site-specific radio signal measurements for predicting connectivity. Given that 80% of the world's population is expected to reside in urban environments by 2050 [6], such rapid global urbanization and the ever-increasing need for reliable communications necessitate new communications paradigms for such challenging environments. Consequently, there is a frenzy of commercial effort to deliver wireless technologies that are capable of supporting the explosion of devices (e.g., smart buildings and the internet of things), as well as network requirements

(e.g., virtual reality and self-driving vehicles). Much of this work is focused on radio hardware and software development. The notion of combining a variety of approaches to tackle complex network challenges is evident in commercial 5G cellular networks to address the ever increasing densification and demand for data in such networks [7]. Enabling technologies that may be leveraged include software-defined networking [8], Heterogeneous Networks (HetNets), distributed antenna systems, millimeter-wave (i.e., 30 GHz to 300 GHz) communications [9], massive multi-input/multi-output (MIMO) [10, 11], and three-dimensional beamforming [12]. While these technologies may be relevant to varying degrees to ad-hoc first-responder networks, the different applications and opportunities associated with these networks imply that a larger diversity of solutions are required. For example, unlike commercial networks, these ad-hoc networks cannot depend on established infrastructure. Also, in contrast to typical commercial applications with static infrastructure, these networks must provide connectivity in extremely harsh conditions, even if only at significantly degraded data rates (e.g., providing only voice communications or telemetry). In addition, networks created by first-responders often rely on low-power, compact radio and antenna systems configured in an ad-hoc manner in infrastructure-poor environments where many commercial approaches are insufficient. In these contexts, small movements can cause large variations in signal quality, compromising communication in a complex and dangerous situation. To mitigate this danger, first-responders could deploy and coordinate with robotic agents.

Autonomous robotics technology has recently seen significant advances as well. These systems require lower bandwidth and less frequent communication to complete complex tasks. This autonomy is enabled by advanced perception, statistical machine learning, and navigation techniques as well as robust solutions to the simultaneous localization and mapping (SLAM)

problem. When successfully integrated, these technologies enable robots to autonomously create models of their environment, evaluate the utility of possible actions, and then act to achieve increasingly complex mission objectives. Advances in machine learning and optimal control have led to highly agile ground vehicles [13] and agile aerial systems [14]. From drones to autonomous cars, the capabilities of intelligent systems are rapidly approaching the point where partially and fully autonomous systems will be ubiquitous. It is clear that autonomous systems, with rich sensing and onboard computation, will be a significant part of future first-responder systems with capabilities such as enhanced situational awareness. However, this capability comes at the cost of increased communication requirements and network load. The current practice treats communication hardware as a separately developed system that has its own states and control inputs, rather than co-designed and integrated with autonomous vehicle control. However, we assert that these systems provide the intelligence and adaptability that are essential for long-range reliable communication necessary in safety, security, and rescue contexts. Communication could be especially important for commanding and controlling robotic agents that can compensate for limited bandwidth using autonomy.

1.1 Low-Frequency Channels and Novel Antennas

Lower frequency communication bands from $10\,\mathrm{MHz}$ to $100\,\mathrm{MHz}$ (HF and low-VHF) often receive limited attention because of their inherently reduced bandwidth in comparison with microwave bands ($300\,\mathrm{MHz}$ to $300\,\mathrm{GHz}$). However, recent studies of the propagation characteristics of low-frequency channels through physics-based simulation and extensive measurements in various line-of-sight (LOS), non-line-of-sight (NLOS), indoor, and outdoor scenarios show

favorable channel characteristics for these bands. These favorable characteristics include improved penetration and channel time coherence, a longer-range with low transmit power, and reduced multipath fading and phase distortion [15–17]. This suggests that low-power, short-range persistent one-hop communications have the potential to dramatically impact autonomous tactical networking challenges. Despite these advantages, applications in the low-VHF band are limited by the prohibitively large size of conventional antennas or high power requirements due to the poor efficiency of existing small antennas. However, researchers at the DEVCOM Army Research Laboratory have pioneered the development of novel miniature passive and active antennas that can approach Chu's fundamental limit at low VHF [18–21]. This advancement means that these antennas can achieve higher bandwidth than is possible on most commercially developed low-VHF antennas. These electrically small antennas (ESAs) transmitting at 300 mW have a range of hundreds of meters and can penetrate obstacles without a decrease in reliability from multipath fading [22]. An example of one of these antennas is shown on a ground robot in Fig. 1.1 These ESAs have higher bandwidth so as to be appropriate for low-power, moderate-rate communications, and networking [22–25]. Researchers have demonstrated they can provide enough bandwidth for streaming video, as well as sharing images and telemetry. These properties make these compact low-VHF antennas ideal for coordinating autonomous systems in complex environments. In outdoor experiments, this radio and antenna achieved a range of $200\,\mathrm{m}$ in the presence of multiple cinder-block buildings with very low power transmission (300 mW) [26]. For comparison, a transmitter operating at $1\,\mathrm{W}$, $2.4\,\mathrm{GHz}$ has an intermittent range of roughly 75 m in this environment. However, as wavelength increases, so does the required size of high gain, directional antennas. The overall gain of these low-VHF ESAs is relatively small due to the highly limited physical aperture of the antenna, and smaller antennas inherently tend to have

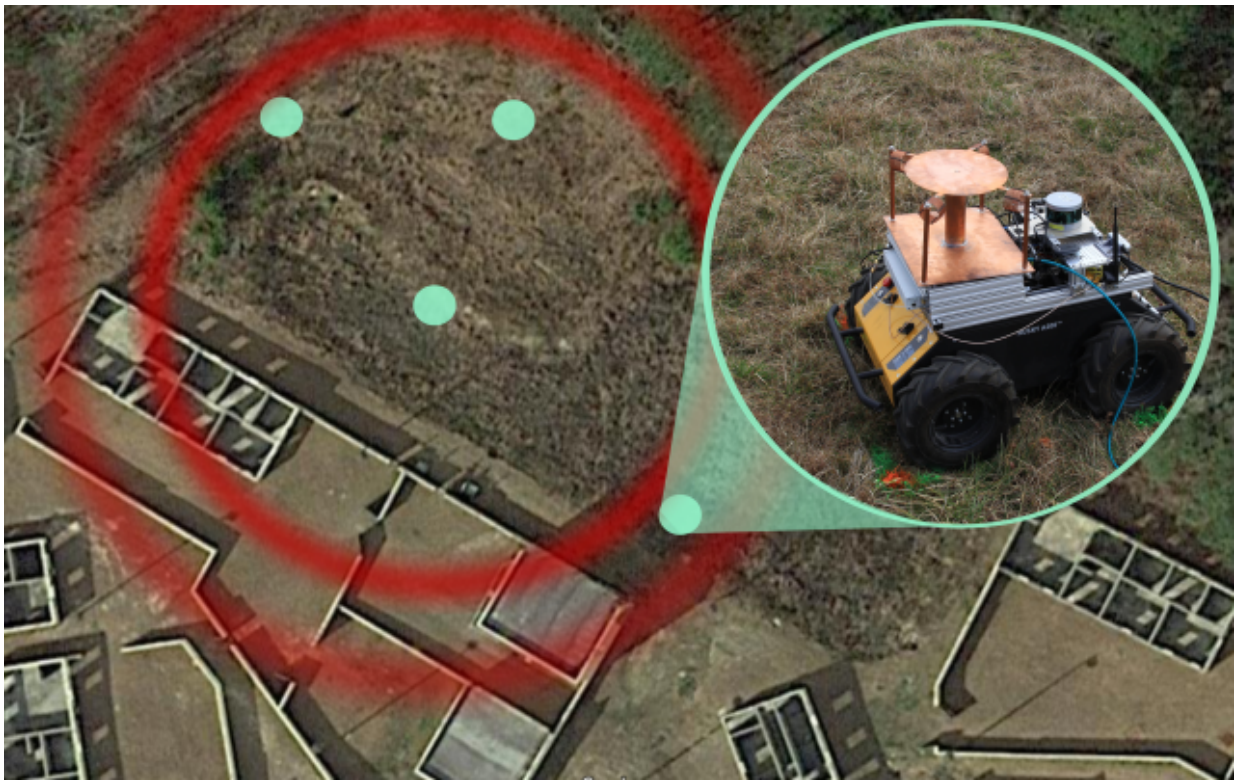

Figure 1.1: Several ground robots occupy a complex environment. The image zooms in on one of them to show its low-VHF antenna. The concentric circles around one of the robots show that it is radiating equally in all directions using this low-VHF antenna.

omnidirectional patterns [27]. A directional antenna enhances the range and reduces radiation in unwanted directions. Unfortunately, deploying a robot with a large directional antenna and/or a powerful radio is not feasible, especially with compact, limited-power robotic platforms. An off-the-shelf directional antenna at these lower frequencies is 1.5 m long and would impose mobility constraints. Consequently, extending the communication range using a conventional low-VHF directional antenna is not feasible for small ground robots.

1.2 Robotic Parasitic Arrays

In the last few years, we demonstrated a new way for robotic systems to act in order to extend the communication range in order to establish a link. Specifically, we showed that it

is feasible for ground robots to form a particular type of antenna array composed of multiple robots wielding these compact low-VHF antennas. This antenna array is a parasitic array, more specifically a Yagi-Uda array [3]. The Yagi-Uda antenna array is a well researched type of parasitic array [28] [29]. These arrays are composed of one active antenna, which is by definition connected to a radio, and one or more passive antennas that are not connected to a radio. It is often designed using empirical models before being deployed in real-world environments. When implemented on ground robotic agents, there are new research areas to explore in control array formation and positioning. Fig. 1.2 is a conceptual graphic showing robots equipped with ESAs moving to form a parasitic array for longer-range communication. Here, four robots form an array. By adding additional antennas, it is possible to achieve an even higher gain in the array, but the increase in gain diminishes with each additional antenna element. While we focus on the

Figure 1.2: Several ground robots maneuver to form a robotic parasitic array to create a higher gain and more directional signal.

increased range through increased directionality, a parasitic array could also be used to radiate more covertly, thus reducing the risk of being detected. In addition, directional radiation could be used to limit interference from nearby agents that are using the same low-VHF bands. When optimally designed, these arrays can increase transmitted or received power by 30 to 54 times, which equates to an array gain of 14.8–17.3 dB [30] in front of the antenna array.

Extending the range of this reliable, low-VHF signal would have a variety of uses for robotic systems. Autonomous robots could deploy more sophisticated approaches for planning to create communication links. Since robots can perceive and act in their environments, they often do not require a large amount of bandwidth to execute a task. Even for systems that use large bandwidths, this low bandwidth channel could support a recovery action that re-enables communication at higher frequencies. We posit that such a technology would in turn enable a reliable, evolving network of autonomous agents that could act and adapt in complex environments where safety, security, and rescue missions occur. To approach the formulation of such a system, consider a network of robots in a complex environment communicating on a low-VHF band, as shown in Fig. 1.3. In this conceptual graphic, there are four robots actively transmitting and receiving using a low-VHF antenna. These robots are transmitting omnidirectionally since nearby robots are not positioned to form parasitic arrays. These other array-forming robotic agents have passive low-VHF antennas and communicate at a UHF band, which means they can only communicate with other nearby robotic agents. In this initial configuration, a metric of overall network connectivity between these four agents is low. If these robotic agents form arrays and move closer together, they can increase the overall metric of network connectivity as shown in Fig. 1.4. By increasing overall network connectivity, the individual communication links between the parasitic arrays are maintained and likely improved.

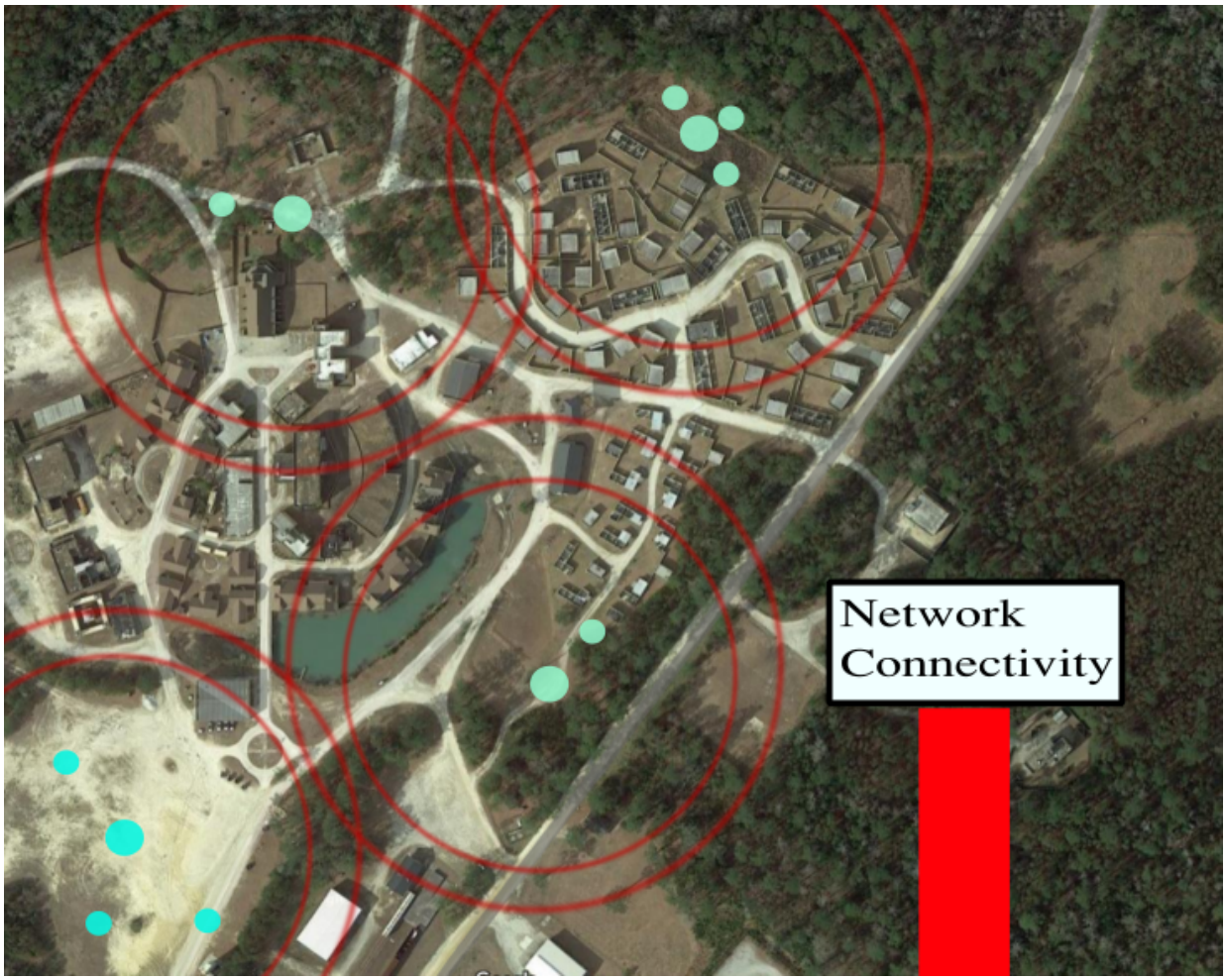

Figure 1.3: Ground robots establish an ad-hoc network enabled by low-VHF communication. Robots with active low-VHF antennas are shown with larger light-blue circles.

1.3 Dissertation Outline

In Chapter 2, we review research and technological development in the areas of robotics and wireless communication. We also discuss multi-agent antenna and robotic research. Then, we focus on issues of controlling the motion of robotic agents forming the array and the motion of robotic parasitic arrays. While some of this background covers research conducted by the author, the work covered in subsequent chapters constitutes work conducted primarily by the author in pursuit of a doctorate.

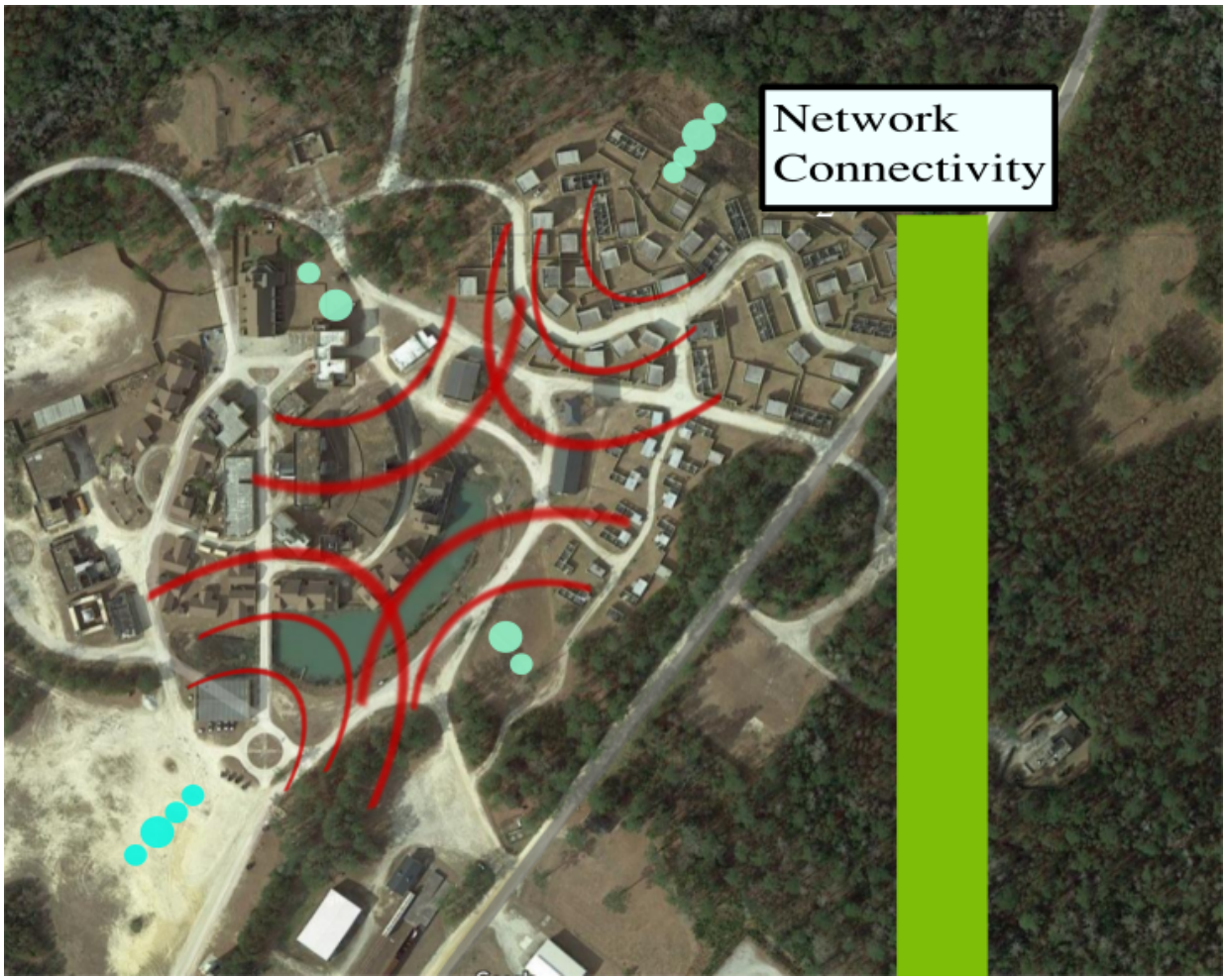

Figure 1.4: Ground robots establish an ad-hoc network enabled by low-VHF communication.

First, we consider the calibration of a robotic parasitic array through the collaborative manipulation of robotic platforms to increase gain/directionality control and effective communication range in Chapter 3. This research reflects the work we published in [2]. Building on this approach, we hypothesize a method for maintaining the gain of a parasitic array with two antenna elements. Using this, we propose and test an approach for maintaining the gain created by this array in LOS and NLOS conditions in Chapter 4 which corresponds to our submitted journal paper [31]. Next, we create a simplified model of how robots form arrays to create a controller that determines where robots should move and form robotic arrays in Chapter 5 which is based on our journal

paper [1]. In Chapter 6, we show that this system maintains a metric of overall connectivity that is lower bounded and remains lower bounded after we constrain the number of robots that can be used to form these robotic arrays; this corresponds to work we will soon submit for publication. Finally, we discuss our conclusions and future work in Chapter 7.

Chapter 2: Background in Robotic Communication for Robotic Parasitic Arrays

There is a wealth of research at the intersection of robotics and wireless communication. This chapter discusses this broad area of research briefly and then presents relevant research in the fields of distributed antenna array formation and design, with additional emphasis on parasitic antenna arrays. Afterward, it provides the foundation for understanding this dissertation's approach to optimizing overall network connectivity between these arrays.

Robots can sense wireless signals and move to improve the reliability of receiving data packets over a wireless radio channel. While networking, signal and information processing, and antenna design are fields of research that impact the reliability of communication for robots, the ability to perceive the physical environment and act is what distinguishes robotic communications research. Simultaneously, communication is very important for deploying robotic systems [4]. In safety, security, and rescue contexts, there are environments where communication infrastructure is not sufficient to meet the needs of single or multi-robot systems. To address this issue, there is a spectrum of autonomous approaches for operating within the confines of limited wireless infrastructure for robots to improve communication and/or take the role of wireless infrastructure (e.g., mobilizing robots to maintain communication [32]). On one side of the spectrum, researchers have developed methods where robots plan for periodic communication [33] or developed approaches for multi-agent exploration with communication constraints [34]. Often, communications constraints

[35] are considered with other constraints as well [36]. One example is a joint communication and fuel constraint problem [37]. Another example is minimizing the turning of robotic agents while maintaining communication [38].

In complex environments, defining the area over which communication is possible is a complex task in itself. Much of this research on communication maintenance for robots is at industry-standard Wi-Fi frequencies (e.g., $2.4\,\mathrm{GHz}$, $5\,\mathrm{GHz}$). This frequency is favorable because of the high bandwidth and easily configurable off-the-shelf hardware. As stated earlier, in complex and dense environments (e.g., indoors, urban areas), the received signal strength (RSS) at this frequency varies rapidly with position and time. This rapid variation is due to the constructive and destructive interference of waves from a single transmitter that reflect and diffract off of objects in the environment; this effect is called multipath fading. At UHF and higher frequencies, many surfaces common in indoor and urban environments reflect and attenuate these signals. Research for modeling and adapting to this phenomenon include efficient channel estimation by considering online models [39], efficient sampling strategies for mapping the boundary between good and bad communication [40], developing minimalist models [41] for radio signal propagation, and multi-robot construction of communication maps [42]. In environments where communication is difficult to model, researchers have developed and experimentally tested approaches for using mobility to improve a single communication link [43, 44] or localizing a transmitter [45]. Researchers have also explored controlling other degrees of freedom for maintaining communication by adapting transmission power [46], actuating directional antennas [47] [48], and changing frequency [49]. A multi-frequency approach can be further developed to create a hybrid network for more reliable communication and localization [50]. Another promising approach to making a link more resilient is to intelligently alter the encoding used

by a radio on a mobile robot [51]. While there are a wide variety of approaches for modeling and maintaining communication, there are two somewhat divergent philosophies of research for maintaining connectivity among a network of multi-robot systems as they increase in scale. Here, connectivity refers to overall communication within a group of robotic agents. One philosophy is experimental [52–55]. However, these approaches cannot make strong guarantees about maintaining communication because of the challenges of a complex environment. The other connectivity maintenance philosophy is theoretical and models increasingly complex robotic agents [56–60]. These approaches rely on rigorous proof, but depend on assumptions about the radio channel model. These approaches are addressed later in the chapter. First, it is appropriate to discuss how robotic parasitic arrays improve communication links to inform the discussion of connectivity maintenance from a network perspective.

Our approach to improving communication links described in this dissertation is rare within the field of robotics. We use robotic mobility to change the electromagnetic properties of the receiving/transmitting antenna. In some ways, this is more similar to multi-robot approaches for physical object manipulation [61]. Just as multiple robots can transport physical objects [62] [63], and work with humans to manipulate objects [64], the tight coordination of agents enables a new capability that is beyond the sum of the agents' individual capabilities. Collective behavior enables multi-robot systems to achieve goals that are impossible for a single robot [65]. In this dissertation, we investigate a collective behavior that enables the ability to create parasitic antenna arrays composed of unmanned ground robots [3] that can be controlled to maintain communication over long ranges (100-300 m) [1].

2.1 Multi-Element Antenna Arrays

Within the antenna design community, multi-antenna arrays and array processing techniques have been a widely researched area for many decades. Often, the relative position and radiation of these antennas are carefully adjusted and measured in controlled laboratory environments. This research enables antenna arrays to create *beams* and *nulls* simultaneously. Beams exist in sectors around an antenna array that are more sensitive to signals received from specified directions and/or are high power transmission in desired directions. Nulls are less sensitive to reception and are less powerful sectors of transmission. This shift in received/transmitted power in a direction around an antenna array is referred to as gain. Beamsteering and directional networking have applications in communications, localization, and radar [66]. Synthetic aperture arrays formed by a single antenna moving in a precisely known path have also been exploited both for radar and localization applications [67, 68]. More recently, distributed beamforming with mobile and stationary nodes has been considered by various researchers. In distributed beamforming, all antennas are active and therefore connected to a radio but are physically disconnected. This approach yields n^2 gain, where n is the number of antenna elements constituting the beamforming array. A numerical investigation of beamforming for a location-aware distributed antenna system with location and communication constraints was presented in [69], where a mobile node was simultaneously tasked with both extracting the data as well as localizing itself. In [70], a simulation-based study of a distributed transmit beamformer was presented, where a subset of the nodes moved in addition to updating the excitation phases of the individual antennas, with the goal of iteratively improving the beam quality by exploiting signal-strength trends. Robots have also collaborated to configure their locations with the goal of maximizing the signal-to-noise-ratio

(SNR) based on feedback from a common receiver [71]. In [72], the mobility of the nodes was considered as a new dimension to improve the signal-to-interference-plus-noise-ratio (SINR), accounting for varying levels of interfering signals using sequential quadratic programming. In [73], the cooperative transmission of common information via beamforming with mobile agents under a reception quality requirement was investigated based on simulations where the channel was either known or the mobile agents could probabilistically predict the wireless channel from each robot to the common receiver. Finally, the directionality of a beamforming array means that researchers can minimize gain in desired directions, thus creating a null [74]. In addition, there is growing interest in using machine learning for antenna, design [75]. Given the popularity of machine learning, research in this area of study will only increase.

At the DEVCOM Army Research Laboratory, there is also a significant research on distributed beamforming as well. When multiple antenna agents are radiating, mobility adds an additional degree of freedom, which enables greater control of which directions the antenna array radiates [76, 77]. Researchers have explored how to achieve the desired array pattern by changing the phase, amplitude, and position at which different active antenna element agents radiate [78, 79]. These researchers have used the ability to change the phase at which antenna element agents radiate in order to steer nulls into adversaries [80–82]. These approaches require tightly synchronized operation among all the agents, as well as a highly accurate estimation of the joint positioning and pose of each agent, requirements that significantly complicate distributed array use. An additional consideration that arises with low-frequency operation is the mutual coupling that occurs between antenna elements that are closely spaced relative to the signal wavelength (denoted by λ). These coupling effects, if not accounted for, can significantly degrade array performance [83–86]. The result of mutual coupling and poor synchronization is a beam that

is wider and has lower gain. In the course of this research at the DEVCOM Army Research Laboratory, we attempted to limit the effects of mutual coupling between antennas forming the array, as this phenomenon could reduce the gain [87]. Further research led us to discover that mutual coupling could create a directional gain on these ground robotic platforms [3]. This is fundamentally how parasitic arrays operate. In fact, this robotic parasitic array could be described as a Yagi-Uda array where the antenna elements are distributed across robotic agents. This discovery presented an opportunity for us to conduct experiments on the effects of motion control on gain and connectivity for robotic agents forming these arrays without addressing the complexity of synchronizing the nodes. A parasitic array, however, will not create the narrow, extremely high-power beams that a beamforming array would.

2.1.1 Parasitic Arrays

Parasitic arrays have been exploited for various applications (e.g., localization, directional communications) to enable directional radiation using multi-element antenna systems. Some parasitic arrays, such as the ones researched in this dissertation, only require a single driven element, meaning that only one antenna in the array is connected to a radio in transmission. When acting in reception, this antenna is called the *excited* antenna element. In both cases, this antenna is called the active antenna element. Other antennas that are unconnected from a radio, are positioned in a way to provide preferential reflection and phasing and thereby yield directionality. These antennas are called passive antenna elements. In our research, we focus on the Yagi-Uda parasitic array. This type of array has only one active antenna. However, parasitic arrays can have combinations of multiple exciters/drivers and passive elements can be employed [88] [89]. There

is already substantial research on novel ways to configure or electrically actuate parasitic antenna arrays [90]. Researchers have investigated actuating a parasitic array by short or open-circuiting a circular array of passive antennas [91]. This effectively removes and adds antenna elements to the parasitic array.

Research on low-VHF antennas has shown that robots, if correctly positioned, create a passively coupled antenna array that communicates farther than any of the agents could individually [3]. This directional robotic antenna array, as shown in Fig. 2.2, is fundamentally different from a single antenna that creates an omnidirectional beam pattern, as shown in Fig. 2.1. For insight into passive coupling between these antennas, consider a two-element parasitic array in free space consisting of a length $\lambda/2$ antenna and a parasitic element that is also $\lambda/2$ long. Here and in the sequel, λ is the center frequency of the antenna. Without loss of generality, let us also assume the elements are vertically oriented along the z direction, which is orthogonal to the ground. Then, the gain pattern of the two element antenna system (in the ϕ plane) relative to the single half-wave dipole (ignoring the loss resistance in the dipoles) can be written as:

$$G_d(\phi) = \left[\frac{R_{11}}{R_{11} - \left|\frac{Z_{12}^2}{Z_{22}}\right| \cos(2\tau_m - \tau_2)}\right]^{0.5} \left(1 + \left|\frac{Z_{11}}{Z_{22}}\right| \angle\xi\right), \tag{2.1}$$

where,

$$\xi = \pi + \tau_m - \tau_2 + \frac{2\pi d}{\lambda} \cos(\phi), \tag{2.2}$$

$$\tau_m = \arctan\left[\frac{X_{12}}{R_{12}}\right] \quad \text{and} \quad \tau_2 = \arctan\left[\frac{X_{22}}{R_{22}}\right], \tag{2.3}$$

The $Z \in \mathbb{R}^{4\times4}$ is the impedance matrix of the two antennas. The diagonal elements are the self-impedance of the i^{th} element, while the off-diagonal elements are the mutual impedance of the two elements. Similarly, $R_{ii} \in \mathbb{R}$, $X_{ii} \in \mathbb{R}$, and $X_{ij} \in \mathbb{R}$ are the self-resistance of the i^{th} element, self-reactance of the i^{th} element, and the mutual-reactance of the two elements, respectively, as stated in [3]. A more in-depth derivation can be found in [86]. Note that when considering more than two antennas, deriving the equation becomes intractable. If the impedance, resistance, and reactance are fixed in Eqn. 2.2, then Eqn. 2.1 is a function d, the distance between the two antennas and ϕ, the orientation of the two antennas. However, the design of these antennas must be optimized with respect to these antenna properties to achieve a desired gain.

As a demonstration of gain, we show full-wave finite-difference time-domain (FDTD) simulation results for two cases. First, the radiation pattern of a quarter-wave monopole antenna on a robot is shown in Fig. 2.1. Here, the robot's antenna radiates in a nearly omnidirectional pattern except along the axis of the antenna itself. As shown in Fig. 2.2, after positioning a UGV with a passive antenna close to the left of the first antenna, the radiated power shifts. This shift in power reaches its maximum in a direction called the *boresight* of the array, which is by definition the front of the antenna array. The increase in RSS along the boresight is caused by mutual coupling between the two antennas and the ground medium the robots occupy. In this dissertation, we refer to this increase in RSS from forming the array as *array gain*. However, this is a slight abuse of the term since we use it to describe the gain measured in a complex environment and not one approximating free space (e.g., an anechoic chamber). This gain enables greater range in one direction and increased covertness in others. It should be noted that the parasitic array achieves the same gain in reception and transmission.

A Yagi-Uda parasitic array is particularly appealing for implementation by a group of

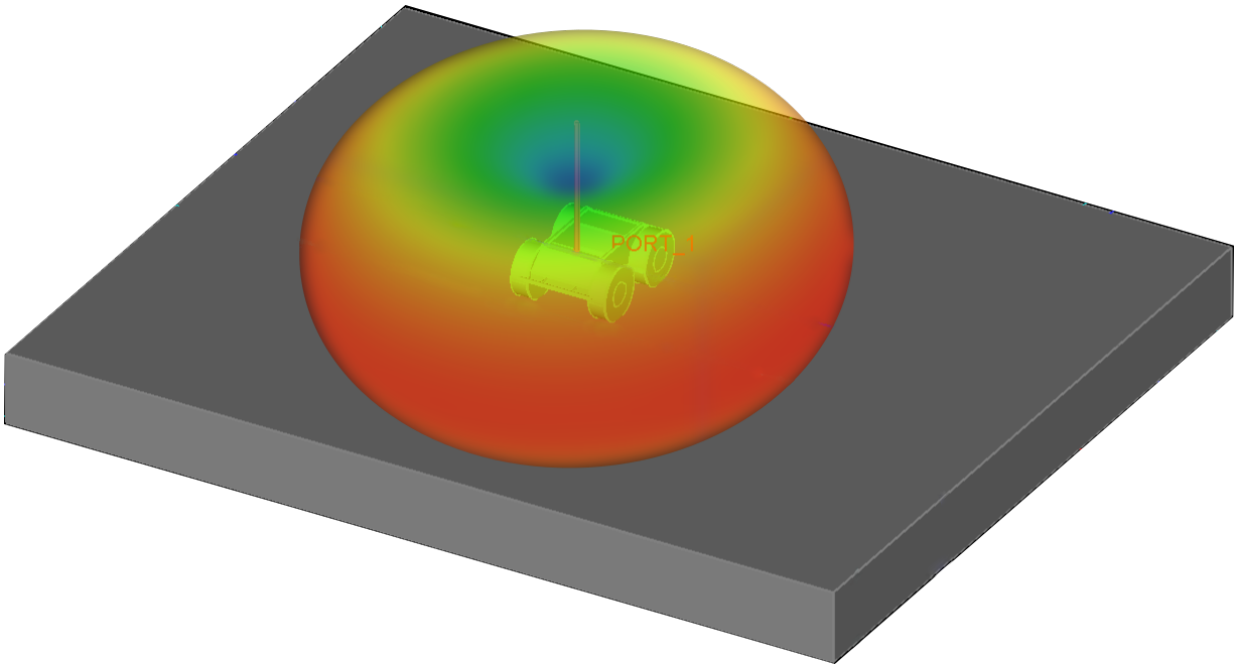

Figure 2.1: Electromagnetic radiation of a single, low-VHF electrically small antenna mounted on a ground robot. [2] ©2019 IEEE

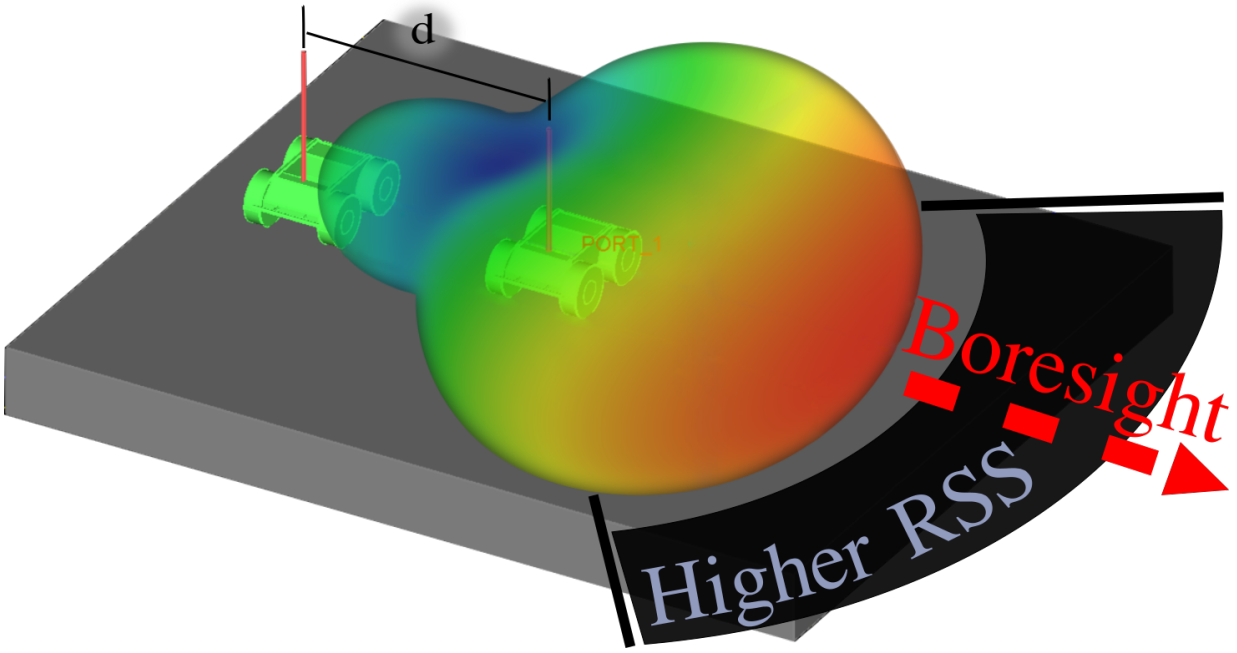

Figure 2.2: Parasitic antenna array created by a second robot with a passive antenna that mutually couples with the antenna of the robot in Fig 2.1. The direction of the boresight and the spacing d between antennas are also shown. [2] ©2019 IEEE

robotic unmanned ground vehicles (UGVs) since these robots can autonomously sense (through camera and lidar) each other and calibrate their positions within the array without a radio on each robot.

The Yagi-Uda array is composed of two types of antenna elements that may be mounted on small ground robots. There is the active antenna element (i.e., an excited/driven antenna element) and other elements that are passive (i.e., not connected to a radio). These passive antennas absorb energy at their resonant frequency and retransmit it. Antenna arrays that use these types of passive elements are called parasitic arrays as these passive elements are not 100% efficient in retransmission. In a Yagi-Uda array, these passive elements are called *reflectors* or *directors*. When the array is acting in transmission, the reflector absorbs radiation from the excited element and retransmits the signal in the direction from which it was received. When the driven element and reflector are spaced properly, the phases of the transmitted and reflected signal align such that there is constructive interference, resulting in a gain in signal strength measured by the radio. When the array is receiving, the reflector adds the same gain by retransmitting the incoming signal towards the driven element. Director elements work in the same way as the reflector, except that their electromagnetic properties cause absorbed energy to be retransmitted in the same direction as the original signal. In Fig. 2.3, a parasitic array with a reflector, an excited/driven antenna, and a director are deployed in a preliminary test. This array is recording a signal that is transmitted by the antenna, which is 3 wavelengths away. In this test, the array achieved a gain of $3.2\,\mathrm{dB}$ while the free space simulation of this configuration predicted a gain of $6.5\,\mathrm{dB}$. By adding additional directors, it is possible to achieve an even higher gain in the array, but the increase in gain diminishes with each additional antenna element. When creating parasitic arrays experimentally or in simulation as described in this dissertation, we add antennas to the array in

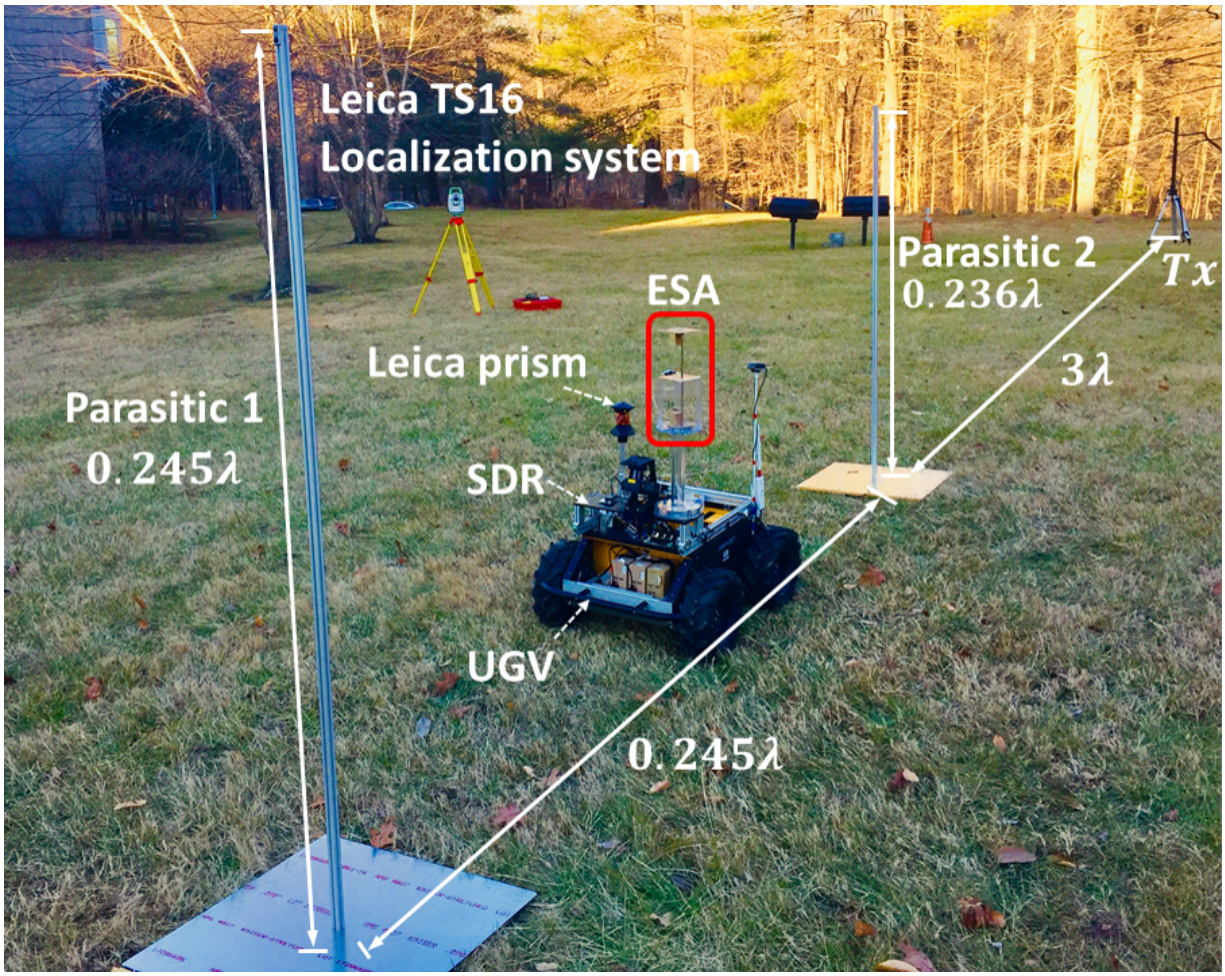

Figure 2.3: Low-VHF robotic parasitic antenna array feasibility experiment. [3]
©2019 ICMCIS

the following order, as shown in Fig. 2.4. In this figure, the reflector is added first. Next, directors are added. If there are no passive antennas, the driven/excited antenna radiates omnidirectionally as in Fig. 2.1.

Classic parasitic array designs are typically carried out for elevated deployment and assume the antenna is in free space. These antennas are a single structure with antenna elements mounted at a fixed spacing. As wavelength increases, so does the required size of high gain, directional antennas. However, deploying a robot with a large directional antenna and/or a powerful radio is not feasible, especially with compact, limited-power robotic platforms. An off-the-shelf low-

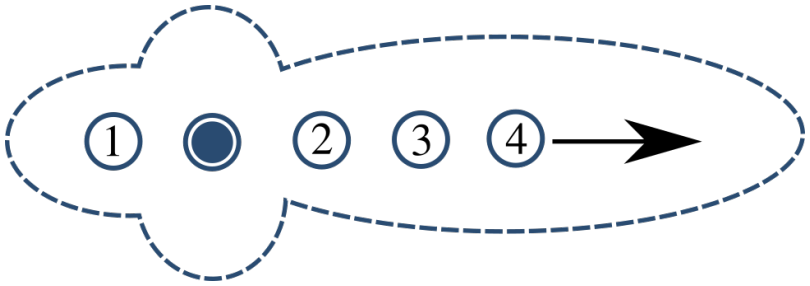

Figure 2.4: Our robotic Yagi-Uda arrays are composed of a driven/excited antenna (solid circle) and passive antennas (numbered in the order in which they are added to increase gain). The arrow points in the direction of maximum gain of the array pattern (dashed line). An array with more passive antenna agents has a higher gain when these antennas are optimally spaced. [1] ©2020 IEEE

VHF directional antenna is 1.5m long and would impose mobility constraints on a ground robot. Here, we consider control for ground-based applications mounted on small robots, as the proximity to the ground can degrade the array gain of existing designs. In Chapter 3 we focus on just the addition of a reflector, since a reflector adds the most gain of all of the passive elements. The theoretical maximum gain for adding a reflector is around 5dB gain. In Chapter 4 we propose and test an approach for rotating the boresight to show that the gain created by the array can be controlled and maintained in line-of-sight (LOS) and non-line-of-sight (NLOS) situations.

2.2 Network Connectivity Maintenance

As stated in Chapter 1, this research is focused on the control of mobile robots forming parasitic arrays. Specifically, we focus first on optimizing the gain of the robotic parasitic arrays and then on where to form these arrays to optimize the overall network connectivity. A controller that increases the level of connectivity between all agents must be able to do so from any system state, if it is able to do so, communication will always be maintained. This is the central tenet of formation/swarm control and consensus research. Achieving this goal is a topic of robotics

research [34, 35, 92] as well as research on mobile ad-hoc networks (MANETs) and wireless sensor networks (WSNs). Despite differing degrees of computational capability and autonomous mobility in these communities, many of the communications problems and solutions are relevant. Communication can be maintained in a decentralized or centralized way depending on these differing platform capabilities and environments [92]. We have already covered how robots maneuver to maintain communication, but there are other approaches to maintaining connectivity that are relevant. Mobility planning approaches for maintaining LOS among agents help to avoid issues with NLOS and multipath fading [93, 94], but these approaches are very conservative in order to be reliable. The rapid change in RSS with Wi-Fi diminishes the value of modeling an antenna's directionality, which is why communications maintenance literature often assumes a disk model for communication between agents [59, 60, 95].

One could consider either sector visibility [96, 97] or range as an initial sensing model for communication between robotic arrays. Visibility is inherently directional. The visibility of one agent by another does not imply joint visibility. However, radio reception/transmission for parasitic arrays is undirected. Sector visibility is one of several sensing geometries for defining when agents can create an edge with each other for the purpose of communication [56]. The other model that is pertinent to our research is the range-based disk model for radio signals. The disk model, however, carries a number of assumptions. Researchers often assume that vehicles are in LOS and that the sector is a full circle around the agent. Wi-Fi, an industry-standard, is favored by many researchers because of its low cost, high bandwidth, and small antenna size. However, Wi-Fi frequencies (2.2 GHz to 5 GHz) are hard to model in NLOS situations, which means that disk model approaches will not be reliable in most indoor and outdoor environments.

Researchers have developed approaches for maintaining LOS among agents to avoid issues

with NLOS [93,94], but these approaches must be very conservative to ensure reliability. Alternatively, researchers use heuristics for maintaining communication with varying degrees of success. Another aspect of multi-agent coordination/allocation is to achieve some mixed objectives of communication and achieving other tasks [42]. There is plenty of research on planning with communications constraints given a noisy radio propagation model [98–100]. In many environments where obstacles create NLOS situations, directionality at Wi-Fi frequencies is not valuable to model because the increased gain in signal strength would be comparable to the change in signal strength due to multipath. As a result, few if any robotics researchers have considered a more realistic antenna model than the disk model. While a sector is directional and is employed in many visibility models, it does not capture the continuous spatial variation in signal strength that occurs with changing the orientation of an antenna array. In addition, in a graph of agents, a link formed by an agent in a sector visibility model is directed, whereas links between parasitic arrays are undirected. Range-based models (e.g., the disk model), on the other hand, are not directional but are often used for modeling radio propagation between robots.

Researchers have used range-based models to develop formation stabilization and consensus in groups of mobile autonomous agents [58, 101]. One approach has been to implement coverage control through Voronoi decomposition [102]. Multi-robot systems can also optimize their connectivity with respect to graph-theoretic metrics such as the Fiedler value using a mix of graph-theoretic constraints and objectives [57, 59]. Variations on this research allow the network to be more distributed [95], and more robust [60]. There are other metrics for assessing the quality of a network of agents, such as the Cheegar value [103] or age of information as implemented in [104] along with motion constraints. Another approach to controlling multi-agent systems is using potential fields [105].

However, approaches for optimizing the Fiedler value are the most appealing and applicable when considering maintaining connectivity between robotic parasitic arrays because it is easy to compute for small and large networks. This is the work we build upon in Chapters 5 and 6. To prepare the reader for this discussion, we offer an example weighted graph, shown in Fig. 2.5 from which we calculate the Fiedler value. From this weighted graph, we can calculate and

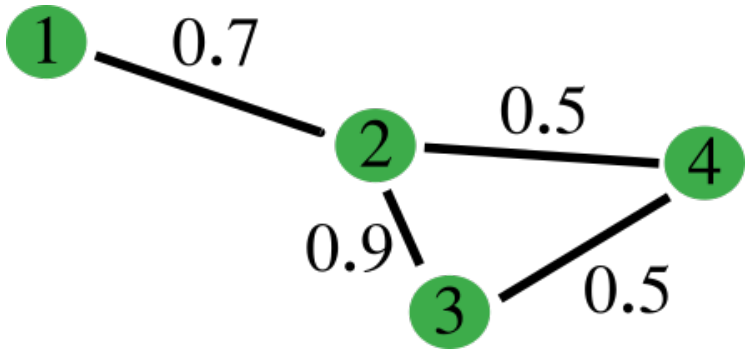

Figure 2.5: Four robotic agents are represented by nodes with weighted edges indicating the strength of their respective links.

adjacency matrix $A \in \mathbb{R}^{n \times n}$. In this context, n is the number of robotic agents A is indexed by $i \in [1, n]$ and $j \in [1, n]$. Note that $A_{i,j} \geq 0$. The adjacency matrix for Fig. 2.5 is as follows.

$$A = \begin{bmatrix} 0.0 & 0.7 & 0.0 & 0.0 \\ 0.7 & 0.0 & 0.9 & 0.5 \\ 0.0 & 0.9 & 0.0 & 0.5 \\ 0.0 & 0.5 & 0.5 & 0.0 \end{bmatrix} \tag{2.4}$$

Notice that this adjacency matrix is symmetric since Fig. 2.5 displays an undirected graph. This means that agents have symmetric communication links and therefore receive data at the same rate when communicating through an edge. The degree of each node as $D_{ii} = \sum_{j=1}^{n} A_{i,j}$ where $D \in \mathbb{R}^{n \times n}$. In this example, the degree is calculated as follows.

$$D = \begin{bmatrix} 0.7 & 0.0 & 0.0 & 0.0 \\ 0.0 & 2.1 & 0.0 & 0.0 \\ 0.0 & 0.0 & 1.4 & 0.0 \\ 0.0 & 0.0 & 0.0 & 1.0 \end{bmatrix} \tag{2.5}$$

The Laplacian $L \in \mathbb{R}^{n \times n}$ is defined as $L = D - A$. The resulting Laplacian is as follows.

$$L = \begin{bmatrix} 0.7 & -0.7 & 0.0 & 0.0 \\ -0.7 & 2.1 & -0.9 & -0.5 \\ 0.0 & -0.9 & 1.4 & -0.5 \\ 0.0 & -0.5 & -0.5 & 1.0 \end{bmatrix} \tag{2.6}$$

It is positive semidefinite as it is symmetric and all of its eigenvalues are non-negative, as seen in the following decomposition.

$$L = Q\Lambda Q^T =$$

$$\begin{bmatrix} -0.50 & 0.81 & 0.17 & 0.27 \\ -0.50 & 0.02 & -0.23 & -0.83 \\ -0.50 & -0.33 & -0.65 & 0.47 \\ -0.50 & -0.49 & 0.70 & 0.10 \end{bmatrix} \begin{bmatrix} 0.0 & 0.0 & 0.0 & 0.0 \\ 0.0 & 0.69 & 0.0 & 0.0 \\ 0.0 & 0.0 & 1.62 & 0.0 \\ 0.0 & 0.0 & 0.0 & 2.89 \end{bmatrix} \begin{bmatrix} -0.50 & -0.50 & -0.50 & -0.50 \\ 0.81 & 0.02 & -0.33 & -0.49 \\ 0.17 & -0.23 & -0.65 & 0.70 \\ 0.27 & -0.83 & 0.47 & 0.10 \end{bmatrix} \tag{2.7}$$

Each column of Q is an eigenvector and the diagonal of Λ are the eigenvalues. For a positive semi-definite Laplacian, $\lambda_1 = 0$. The Fiedler value λ_2 is the second smallest eigenvalue of the Laplacian; in this example, $\lambda_2 = 0.69$. If there were only one link connecting a node to the

rest of the nodes, and this link was to approach zero, the Fiedler value would approach zero as well. Consequently, many approaches for maintaining the connectivity between a graph of nodes are formulated around maintaining the Fiedler value above a given threshold. By bounding the Fiedler value from below, the graph remains unpartitioned. However, the Fiedler value cannot fully define the communication between nodes in a graph. For example, it does not indicate if individual links are above a given level.

Researchers have matured the approaches for Fiedler value optimization in various ways. In [56, 58, 59, 95, 106], the authors propose and use additional properties or expressions of the Fiedler value that is the fundamental to the work in this dissertation. Following the proofs of [107, 108], which we restate here, the Courant-Fisher Theorem provides one such expression of the Fiedler value. An abbreviated version is provided below.

Theorem 1: The matrix L has eigenvalues $\lambda_1 \leq \lambda_2 \leq ... \leq \lambda_n$ and corresponding eigenvectors $v_1, v_2, ..., v_n$. Then

$$\begin{aligned} \lambda_1(L) &= \min_{\|p\|=1} \quad p^T L p = \min_{\|p\|\neq 0} \quad \frac{p^T L p}{p^T p} \\ \lambda_2(L) &= \min_{\|p\|=1, p\perp \mathbf{1}} \quad p^T L p = \min_{\|p\|\neq 0, p\perp \mathbf{1}} \quad \frac{p^T L p}{p^T p} \end{aligned} \tag{2.8}$$

Where $p \in \mathbb{R}^n$ and $\mathbf{1}_i = 1$ such that it is a column vector of size n with the value 1. The term $p \perp \mathbf{1}$ indicates that $\mathbf{1} \cdot p = 0$, meaning that $\mathbf{1}$ and p are orthogonal. In general, for $1 \leq k \leq n$, let S_k denote the space of $v_1, ..., v_k$ (with $S_0 = \{0\}$), and let $S_k^{\perp}$ denote the orthogonal complement of S_k. Then

$$\lambda_k(L) = \min_{\|p\|=1, p\in S_{k-1}^{\perp}} \quad p^T L p = \min_{\|p\|\neq 0, p\in S_{k-1}^{\perp}} \quad \frac{p^T L p}{p^T p}. \tag{2.9}$$

Proof. As in [108], let $L = Q^T \Lambda Q$ be the eigendecomposition of L. Note that $p^T Lp = p^T Q^T \Lambda Q p$ = $(pQ)^T \Lambda (Qp)$. In addition, since Q is orthogonal, and $\|v_i\| = 1, \|Qp\| = \|p\|$. Therefore, it is sufficient to consider the case where $L = \Lambda$ is a diagonal matrix with the eigenvalues $\lambda_1 \leq \lambda_2 \leq ... \leq \lambda_n$ along the diagonal. Then we can write.

$$p^T Lp = \begin{bmatrix} p_1 & p_2 & \dots & p_n \end{bmatrix} \begin{bmatrix} \lambda_1 & & & \\ & \lambda_1 & & \\ & & \ddots & \\ & & & \lambda_n \end{bmatrix} \begin{bmatrix} p_1 \\ p_2 \\ \vdots \\ p_n \end{bmatrix} = \sum_{i=1}^{n} \lambda_i p_i^2 \tag{2.10}$$

Note that when L is diagonal, the eigenvectors of L are $v_k = e_k$, which is the standard basis vector in $\mathbb{R}^n$, therefore $(e_k)_i = 1$ if $i = k$ and $(e_k)_i = 0$ otherwise. Then $p \perp e_i$, for $i = 1, \dots, k-1$, so $x_i = x_i \cdot e_i = 0$. Therefore, for $p \in S_{k-1}^{\perp}$ with $\|p\| = 1$, we have

$$p^T Lp = \sum_{i=1}^{n} \lambda_i x_i^2 = \sum_{i=k}^{n} \lambda_i x_i^2 \geq \lambda_k \sum_{i=k}^{n} x_i^2 = \lambda_k \|p\|^2 = \lambda_k \tag{2.11}$$

However, substituting $p = e_k \in S_{k-1}^{\perp}$ yields $p^T Lp = (e_k)^T L e_k = \lambda_k$. This shows that

$$\lambda_k(L) = \min_{\|p\|=1, p \in S_{k-1}^{\perp}} \quad p^T Lp = \min_{\|p\| \neq 0, p \in S_{k-1}^{\perp}} \quad \frac{p^T Lp}{p^T p} \tag{2.12}$$

If we substitute in $k = 2$, we see that $p \in S_{k-1}^{\perp}$. This is equivalent to stating that $p \perp \mathbf{1}$, since the eigenvector of a symmetric real-valued Laplacian is $v_1 = a\mathbf{1}$, where $a \in \mathbb{R}$. Therefore,

$$\lambda_2(L) = \min_{\|p\|=1, p \perp \mathbf{1}} \quad p^T Lp = \min_{\|p\| \neq 0, p \perp \mathbf{1}} \quad \frac{p^T Lp}{p^T p}. \tag{2.13}$$

□

In addition, the product of $p^T Lp$ over the edges (E) in the graph (G) then it can be re-evaluated as

$$p^T Lp = \sum_{i,j \in E}^{n} A_{i,j}(p_j - p_i)^2 \tag{2.14}$$

This result is an algebraic simplification of the product [109]. After substituting this value in Eqn. 2.13, the Fiedler value can be defined as.

$$\lambda_2(L) = \min_{\|p\|=1, p \perp \mathbf{1}} \quad p^T Lp = \min_{\|p\|=1, p \perp \mathbf{1}} \quad \sum_{i,j \in E}^{n} A_{i,j}(p_j - p_i)^2 \tag{2.15}$$

This expression is the foundation of several approaches. Researchers have used this expression to take the derivative of the Fiedler value with respect to agent positions. Using this derivative, robotic vehicles can be controlled to move in directions that increase Fiedler value. As a result, the edge weights of the graph increase as well and overall network connectivity is maintained or increased. These approaches are called *subgradient* methods since this derivative does not align with the direction of increasing the Fiedler value at the highest rate. Researchers build on this subgradient method. In [95], an approach for estimating the eigenvectors of the Laplacian enabled the motion control of individual agents to be decentralized. In [106, 110], researchers proved the ability to maintain the Fiedler value in the presence of other control inputs, which allows for formation control and individual robots to achieve other goals

In this chapter, we have described the state of the art in robotics and communication, as well as mobile/distributed antenna arrays. We have also provided the mathematical foundations for formulating controllers that increase the strength of individual communication links and for

increasing overall network connectivity between mobile agents. In Chapters 5 and 6, we consider utilizing the multi-agent parasitic arrays as a means of enhancing directional gain to increase the Fiedler value.

Chapter 3: Calibrating a Parasitic Array for Increased Gain

In this chapter, we investigate how a single unmanned ground vehicle (UGV) with a low-VHF antenna forms a parasitic antenna array to create a directional signal on different terrain types. Specifically, we consider the coordination of two antennas to form a parasitic antenna array, which is composed of an excited antenna and a shorted antenna (i.e., a passive antenna); each of these antennas may be mounted on a mobile ground robot. This chapter's research is documented in [2] . In this experimental research, the excited antenna is connected to the radio onboard the UGV. The input of the second antenna is simply short-circuited, making it a passive antenna. The second antenna couples electromagnetically with the excited antenna and the ground medium. If it is placed at a strategic location and has the appropriate length, it can enhance the directional radiation of the overall system. The size of the individual antennas, their relative locations, and the ground characteristics, as well as any nearby scatterers, have to be taken into account to determine the optimal configuration to increase directional radiation.

Robots have used a rotating reflector for localization [111] and localizing wildlife carrying tracking devices by employing multiple robots to form an array [112]. To our knowledge, there is no prior work on autonomous positioning of parasitic array elements that are physically disconnected (e.g., not on a common platform or structure). The optimal design (i.e., the best positions and lengths) of the antenna elements of Yagi-Uda arrays are well understood for radiating

in free space (i.e., a vacuum). However, ground robots need to create an array in the presence of a lossy ground medium where the optimal design varies with the electromagnetic properties of the ground medium . Electromagnetic properties of the ground are difficult to determine by appearance. These properties change with the ground type (e.g., grass/dirt, asphalt, concrete) and other factors such as water saturation level. In addition, there may be sub-surface materials or objects in a given environment that affect the near-ground antennas. These ground properties are difficult to estimate since the ground is often inhomogeneous and its characteristics could change with time. Consequently, whenever a robotic system creates an array, it may have to determine the maximum gain configuration online using a calibration approach. Our contributions to automating this calibration are the following:

- Bounds for antenna element spacing and parasitic element length from simulation and parasitic array design techniques
- Approach for calibrating robot-reflector spacing and reflector length which is verified experimentally
- Comparison of optimal configurations in the presence of different ground media

In our research, we only consider the calibration with the addition of the reflector. However, adding director elements is a reasonable next step.

3.1 Approach to Calibrating the Array

Utilizing intelligent ground agents to form parasitic arrays that can operate in realistic environments is a relatively unexplored research area. Here, we focus on creating configurations that maximize the directionality of a robotic parasitic array in the presence of realistic ground. First, we describe an algorithm for creating the robotic parasitic array. This array will achieve sub-optimal gain, so it will be necessary for the robotic agents to test different configurations and determine an optimal one. We use full-wave simulation to inform our knowledge of the gain

function we wish to increase and the bounds of possible configurations.

3.1.1 Parasitic Array Formation

We envision a ground robot that uses a low-VHF radio system to communicate with a static agent at a known position in a complex environment. If a variable-length reflector is present in this environment, either on another robot or stationary platform, the robot with the low-VHF antenna can use this antenna as the excited/driven element to form a parasitic antenna array that has a higher gain in the direction of the static agent. The robotic system (i.e., the ground robot and the variable-length reflector) would use the following algorithm.

Algorithm 1 Robot Joining Parasitic Array

```
if Robot not mutually coupled with reflector then
    Robot move near reflector
end if
if Robot not in-line with reflector and Tx then
    Robot move to position on line reflector/Tx line segment
    Robot rotate to face reflector
end if
if Robot facing and alignedwith reflector then
    Robot calibrate position with respect to reflector.
end if
```

Given the reliability of existing simultaneous localization and mapping (SLAM) approaches, maneuvering a robot into roughly the correct position to create the parasitic array is well understood. Experiments described in our previous work [3] show that it is possible to create the parasitic array by placing antennas in a sub-optimal configuration outdoors; we assume small alignment errors with the transmitter will not cause a significant loss in gain. Of course, there are different algorithms that are necessary if the reflector is mounted on the robot and the excited/driven element is stationary, or both elements are mobile. The consistent goal is to maneuver antenna elements to be close enough for mutual coupling to occur; they must be aligned, and then the antenna spacing must be calibrated. Therefore, we focus our approach on the step where we calibrate the position of one excited element with respect to a stationary reflector and the length

of the reflector. This setup is shown in Fig. 3.1.

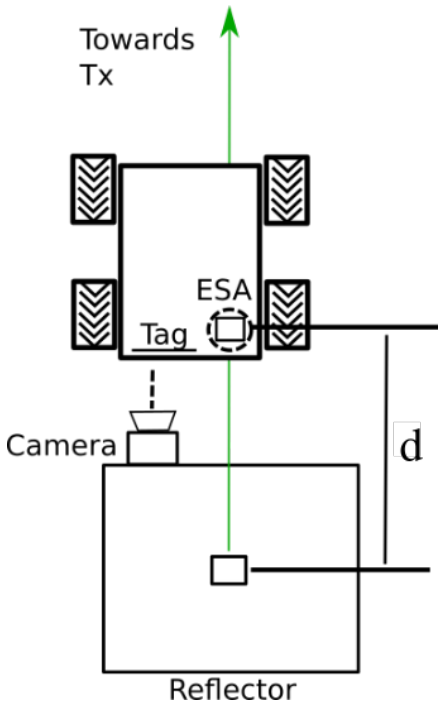

Figure 3.1: This is a diagram of the robot that changes d, the distance from the robot to the reflector, in order to maximize the reception power measured by the radio on the robot. The static transmitter is not depicted. [2] ©2019 IEEE

From this point forward, we refer to the calibration of the excited antenna element position, the calibration of antenna spacing, and the calibration of robot position interchangeably. Once the robot is close enough to the reflector to enable mutual coupling between the reflector and the excited element, these two antenna elements form the parasitic array. When the robot and reflector are close, they are electrically coupled, and the robot receives a signal from a stationary transmitter through the parasitic array. The robotic system is configured to move to a robot position and/or reflector length configuration, then stop and record data to estimate the signal power.

3.1.2 Full-wave FDTD Simulations

We utilize FDTD based numerical codes to solve Maxwell's equations in the time domain that provide accurate solutions in terms of the mutual coupling between the antenna elements

as well as the radiation pattern and radiation efficiency of the antenna system. These full-wave simulations provide insight into the gain variation as a function of the parameters of interest (i.e., parasitic reflector length and antenna element spacing. The placement of parasitic elements with respect to the driven/excited element that maximizes gain in power is well understood for the well-known Yagi-Uda array in free space [113]. The exact array configuration varies depending on the specific type of antenna element used. Here, we show an example simulation for two antennas to study the gain as a function of element spacing and reflector length for two dipoles.

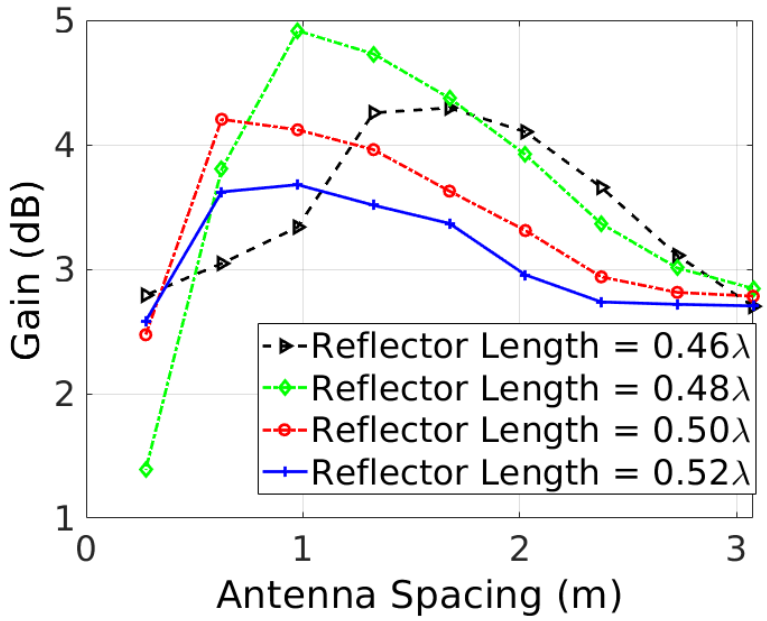

Figure 3.2: Full-wave FDTD simulation results show the gain of a two-element parasitic array as a function of antenna spacing. Four different values of the length of the parasitic element are considered. The excited element for this simulation is 0.46λ long. The result shows that the antenna spacing that provides the peak gain varies depending on the length of the parasitic element. [2] ©2019 IEEE

In Fig. 3.2 a free space model shows that the gain as a function of robot position has a single maximum within a bounded region. We also see that there is roughly $4\,\mathrm{dB}$ of variation in gain by changing the antenna spacing. While free space models tell us that the optimal spacing of the two-element arrays is $\lambda/4$, $1.875\,\mathrm{m}$ for $40\,\mathrm{MHz}$, this length changes slightly depending on the specific antenna type and parasitic length. The influence of the ground medium means that the optimal spacing should be in $\mathbb{X} = [0.8, 2.4]$. The lower threshold exists since spacing

the antennas too closely will affect the resonant frequency of the excited antenna; this is called de-tuning the antenna. If the antenna spacing is greater than the upper threshold, mutual coupling is reduced. When the antenna spacing is outside of these bounds, the two antennas do not form a parasitic array.

Full-wave analysis shows there is a maximum of $1.3\,\mathrm{dB}$ of gain associated with changing the reflector length. Antenna design research indicates that a reflector monopole must be at least $\lambda/4$, $1.875\,\mathrm{m}$ for $40\,\mathrm{MHz}$. Since our reflector has a maximum actuation distance of $0.16\,\mathrm{m}$, we know that we must actuate it such that the reflector length inside set $\mathbb{L} = [1.875, 2.035]$. The maximum gain for a reflector and an excited element pair of dipoles is roughly $5\,\mathrm{dB}$. Depending on the length of the ESA and the parasitic element used, the maximum achievable gain could be slightly less.

3.1.3 Increasing Received Power

Our goal is to enable the robot to autonomously find an array configuration to maximize the gain of the robotic parasitic array. This means maximizing the received power measured by the radio on the robot. In addition, we want to achieve greater insight into the shape of the received power function under various configurations. In order to be resilient to noise sources in different environments, we use linear regression. Full-wave simulation results indicate that we can simplify our problem by assuming that any term that couples the robot position and reflector length is negligible in the presence of other noise sources. Therefore, received power as a function of either robot position or reflector length takes the following form:

$$y(d) = w_0 + w_1\zeta + w_2\zeta^2 + \epsilon \tag{3.1}$$

In this equation, $y \in \mathbb{R}^N$ is the received power and a function of $d \in \mathbb{S}^N$ where N is the number of statistically independent samples. The variable ζ is a placeholder for either d the robot position or l the reflector length. The set $\mathbb{S}$ is a placeholder for the robot positions set $\mathbb{X}$ or the

reflector length set $\mathbb{L}$. The weight matrix $w \in \mathbb{R}^{3\times1}$ is the group of coefficients we want to approximate. Noise in the environment, $\epsilon \in \mathbb{R}^N$, is approximated by $\epsilon_i \sim \mathcal{N}(\mu = 0, \sigma^2)$. We hypothesize this noise arises from small errors in sensing robot position, sensing reflector length, and background radiation. It also results from small variations in the ground medium over the range of robot positions. In addition, small changes in position relative to the transmitter may also cause variation in received power. This change in received power as a result of position in the environment is something we will test as well.

We use the following feature transform

$$z_i = [1, \zeta_i, \zeta_i^2] \tag{3.2}$$

which allows us to consider our non-linear hypothesis such that $z \in \mathbb{R}^{N\times3}$. Then we can formulate the following regression problem [114].

$$y_i = wz_i + \epsilon_i \tag{3.3}$$

Solving for the w which minimizes in-sample error by approximating the true value of y using the pseudo inverse, we get the following equation:

$$w = (z^T z)^{-1} z^T y \tag{3.4}$$

The weights allow us to find the extreme point of the parabola we are approximating.

$$\zeta^* = -\frac{w_1}{2w_2} \tag{3.5}$$

In this case, ζ^* is the value that maximizes the approximation of the received power. In summary, we use linear regression to approximate the received power as a function of robot position and then command the robot to move to the position that maximizes the received power. Afterward, we use the same process to approximate the received power as a function of reflector length and

then move the antenna to the maximized length. Using linear regression to find a maximum is not bounded so our approach could specify a point outside of $\mathbb{X}$ or $\mathbb{L}$. If the optimal robot position is outside of $\mathbb{X}$ we know that the linear regression failed and it is likely the sampled data is too noisy, as exceeding these bounds on robot position diminishes the effectiveness of the array. If the optimal reflector length is less than the lower bound, we set the value to the lower bound for an antenna to act as a reflector, which may be the optimal length for a reflector in all environments. If the antenna threshold is too high, we set the antenna to its upper bound since this is the physical limit of the system. Given our understanding of antenna spacing and reflector length in the parasitic array, an out-of-bounds antenna spacing is more problematic than an out-of-bounds reflector length.

When we record independent samples of either robot position or reflector length for linear regression, these samples are chosen from a uniform distribution in the set $\mathbb{X}$ or $\mathbb{L}$ for the robot position and reflector length, respectively. In order to decrease sampling time, we assume that sample independence is not affected by sampling order, so we sort the samples by increasing magnitude to reduce sampling time. We chose to optimize the robot position first because it has the largest effect on array gain as predicted by simulation. After the robot is in the optimal position, we optimize the reflector length. This is our procedure for calibrating the parasitic array to achieve higher gain.

3.1.4 Setup

In order to test the properties of this two-element parasitic array, we placed a $10\,\mathrm{dB}$, $39.95\,\mathrm{MHz}$ signal generator connected to a one-sixth wavelength antenna radiating at roughly $25\,\mathrm{m}$ from the parasitic array. The reflector and the excited element are aligned as shown in Fig. 3.1. The robot has an ESA that is one-fiftieth of the wavelength. An Ettus N210 software-defined radio is mounted on the robot for recording signal power information within the array. For each signal power sampling, the radio records $M = 100,000$ magnitude and phase (I/Q) samples over $0.05\,\mathrm{s}$. The strength of the signal is calculated as

$$y_i = 10\log_{10}(\frac{1}{M}\sum_{j=1}^{M}(I_j^2 + Q_j^2)); \tag{3.6}$$

where y_i is the received power for every i sample in y. The signal magnitude $I \in \mathbb{R}^M$ and the phase $Q \in \mathbb{R}^M$ samples are values that are measured by the software-defined radio.

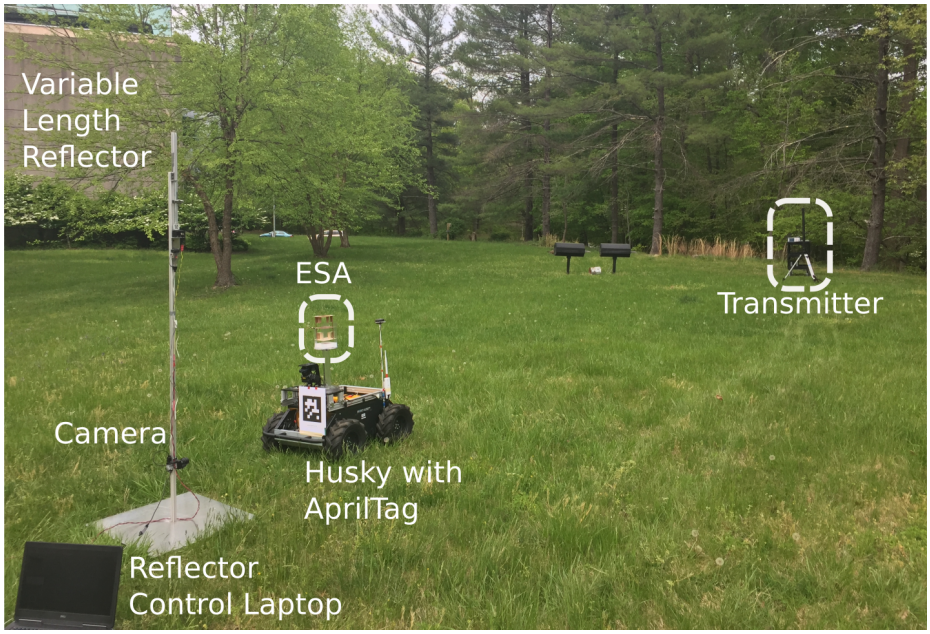

Figure 3.3: The adjustable reflector is electrically coupled with the ESA, which is mounted on a robot. The transmitter is roughly $25\,\mathrm{m}$ from the robot. The robotic parasitic array is on almost level ground near the top of a hill. [2] ©2019 IEEE

The robot we use in these experiments is a modified Clearpath Husky, seen in Fig. 3.3. It is a skid-steer, wheeled research platform. We use a camera and AprilTags [115, 116] to localize the robot relative to the position of the reflector. In this set-up, the reflector is at the origin. This is a convenient convention for allowing comparison between signals recorded with and without the reflector.

The variable-length reflector is a monopole made out of a 0.46 x 0.46 m^2 aluminum sheet used as a ground plane and a $1.7\,\mathrm{m}$ bar. At the top of the antenna is a Dynamixel servo, which is tasked by a laptop running ROS. The laptop is connected wirelessly to the Clearpath Husky using a $2.4\,\mathrm{GHz}$ PicoStation. The Dynamixel servo turns a threaded rod which raises and lowers another $0.3\,\mathrm{m}$ aluminum bar. These two bars are connected through a linear bearing, which

maintains an electrical connection between the two bars. By actuating the servo, the reflector's length and electromagnetic properties also change. We assume that the wires and servo do not change the electromagnetic properties of the reflector.

3.2 Experiments

We want to understand the significance of antenna position and parasitic element length in the calibration of the robotic parasitic array. We also want to determine the optimal configurations of this array in the presence of different ground media.

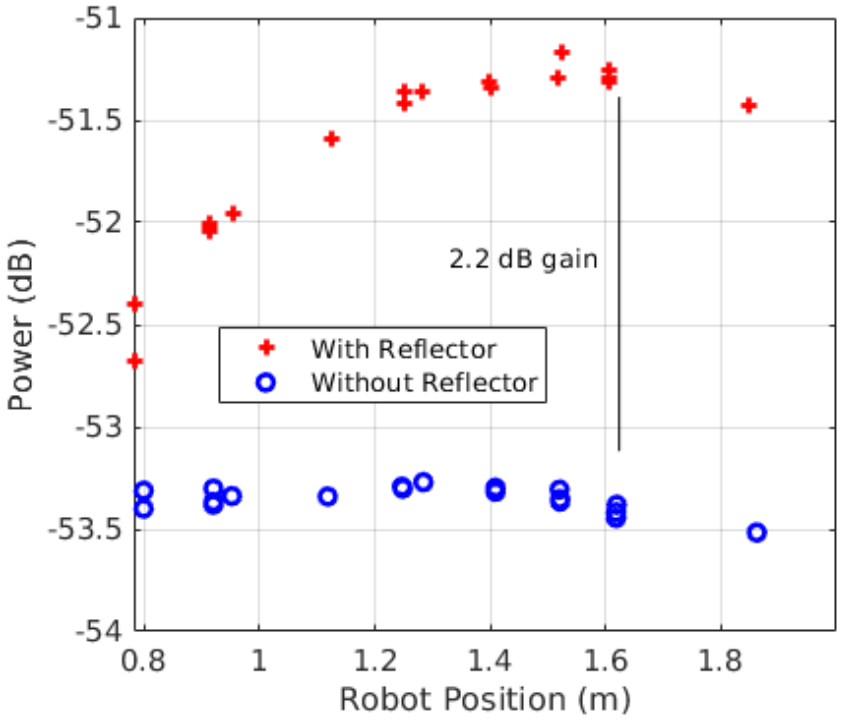

Figure 3.4: Change in received power as a function of robot position with and without the reflector. [2] ©2019 IEEE

In Fig. 3.4 we plot the received power as a function of distance with and without the reflector. Even when the robot does not move, there are changes in recorded power. After sampling, the robot determines the optimal position to be $1.58\,\mathrm{m}$ from the reflector. By changing position, the robot is able to achieve a gain of $2.2\,\mathrm{dB}$. Note, a change in signal power of $3\,\mathrm{dB}$ is 2

times the received power; in creating the array, the robotic system has achieved almost twice the received power.

Once the robot and reflector spacing are increased, we choose a set of reflector lengths to sample from a uniform distribution. Changing the reflector length over this range does not change the gain significantly, about $0.5\,\mathrm{dB}$ to $1\,\mathrm{dB}$. In this experiment, the data was too noisy to identify a trend. The small change in gain makes the optimal reflector length difficult to locate when it is compared to the noise in the environment.

We tested the robotic parasitic array experimentally and in the presence of different additional ground media in a relatively static environment. Simulation results suggest that media with different electromagnetic properties will have different radiation characteristics. We tested the robotic parasitic array on three different types of terrain:

- Grass and dirt which are dry
- Grass and dirt which are dampened by $90\,\mathrm{L}$ of water
- Dry asphalt

We plot gain instead of power as a function of robot position and reflector length to show the change in power possible by forming the parasitic array. To be clear, array gain $g \in \mathbb{R}^N$ where $g = y_{parasitic} - \bar{y}_{alone}$; this is the difference between the y power received in the array ($y_{parasitic}$) minus the mean of power samples collected on the robot with the reflector removed ($\bar{y}_{alone}$).

In the dry and wet grass tests, the robotic parasitic array and transmitter are in the same positions on a relatively flat surface near a hill. The asphalt test places the transmitter and robotic parasitic array on a hill. The results from these tests are shown for calibrating the position of the robot in Fig. 3.5 and calibrating the length of the antenna in Fig. 3.6.

3.3 Results and Discussion

We can estimate the benefit of the increased range which is possible by robots creating a two-element parasitic array. By modifying the Friis Transmission Equation (Eqn. 3.7) for

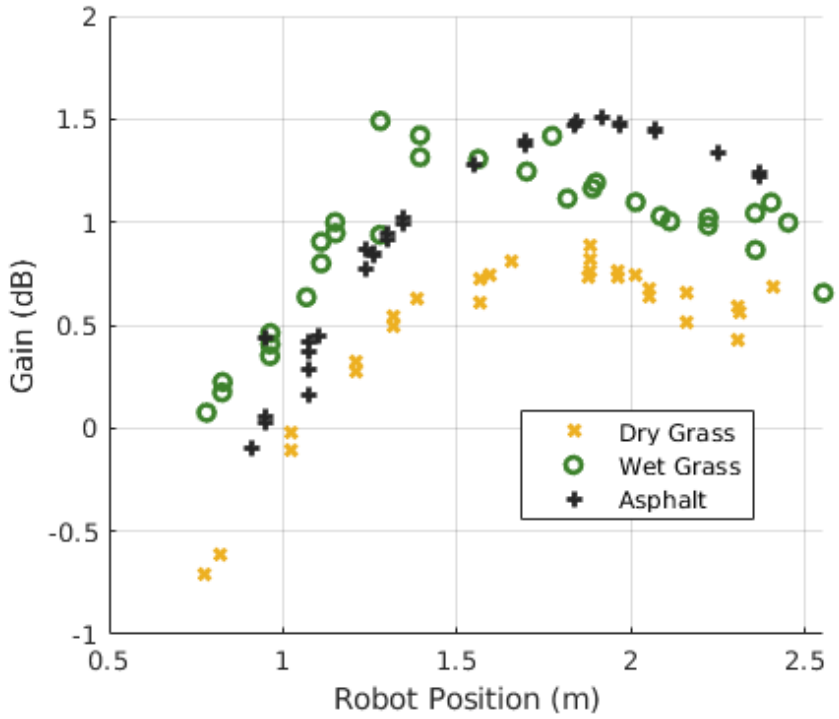

Figure 3.5: Change in gain as a function of robot position for a reflector length of $1.94\,\mathrm{m}$ [2] ©2019 IEEE

received power P_r, we can approximate the change in range R to gain.

$$P_r = \frac{P_T G_T G_R c^2}{(4\pi R f)^2} \tag{3.7}$$

Gains G_T and G_R are unitless multipliers of the transmitting antenna and the receiving antenna, respectively. The transmission power P_T, and the frequency f are constant. The speed of light is c. We can equate the reception power with and without the parasitic element to solve for the array range. The following relationship between the new array range R_{array}, array gain G_{array}, and the range without parasitic elements present R_{alone} is shown in Eqn. 3.8.

$$R_{array} = \sqrt{G_{array} R_{alone}^2} \tag{3.8}$$

In Fig. 3.4 a gain of $2.2\,\mathrm{dB}$ is achieved by forming the array. This is 1.7 times the power of

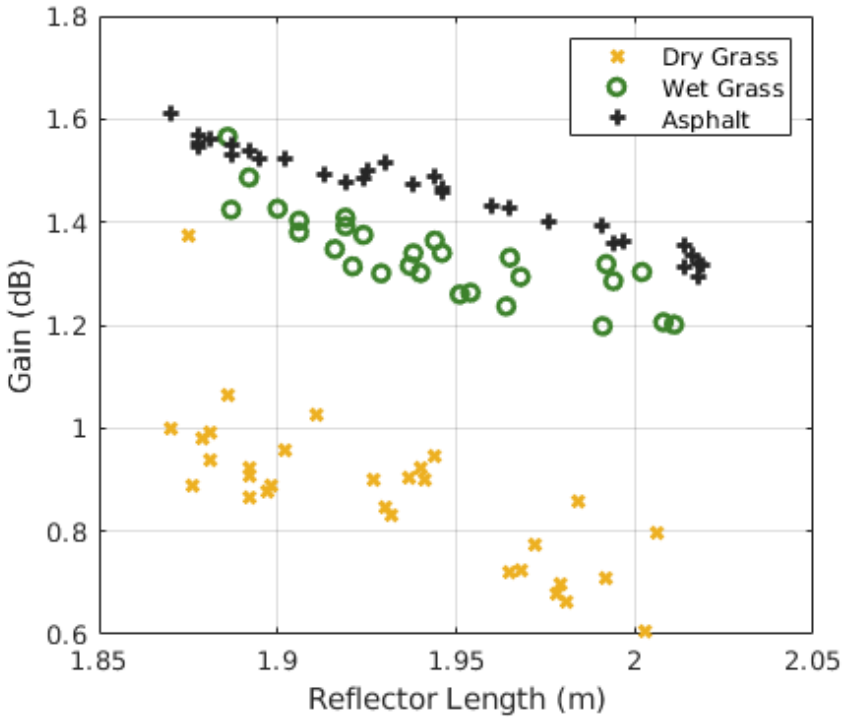

Figure 3.6: Change in gain as a function of reflector length with the robot in a calibrated position. [2] ©2019 IEEE

the original signal. Previous results show this radio/antenna has a range of $200\,\mathrm{m}$ when without the reflector [5]. Adding the reflector creates the array, which increases the estimated range to $258\,\mathrm{m}$ in the desired direction. Clearly, when robots are capable of forming a parasitic array and are within some distance of each other, it is more advantageous to create this parasitic array with these two agents than to use one of them as a relay node to extend the communications range.

Our tests also show there is a discernible difference between the optimal spacing of antenna elements for the wet and dry ground media. The calculated optimal positions for the robot to be positioned were $1.86\,\mathrm{m}$, $1.78\,\mathrm{m}$, and $1.94\,\mathrm{m}$ for dry grass, wet grass, and asphalt, respectfully. One interesting aspect of these results for the robot position is that the dry grass and asphalt can be fitted to a parabola with less error than the test on the wet grass. We hypothesize that this difference with the wet grass is because of the lack of uniformity of moisture content in the area around the parasitic array. While we attempted to apply water evenly to the ground, the lack of uniformity of the ground medium is apparent in the results. This suggests that ground that

changes material within a wavelength of the parasitic array will distort the gain as a function of position. This could be an area of further research. Another observation from these tests is that there is variation in the highest gain achieved by forming the parasitic array. It is not clear if this difference in the highest gain resulted from terrain composition or topology.

The antenna tests suggest that the maximum gain is achieved when the antenna is near $1.875\,\mathrm{m}$ which is the minimum length we specify based on our simulations. In addition, adjusting the reflector only had a small effect on the gain (roughly 0.5 dB). This shows that our dipole assumption in the simulation merits further investigation. We also predict that the addition of more antenna elements (i.e., directors) will make reflector length a more significant factor. The electromagnetic properties of the antenna regulate the phase at which the received energy is retransmitted. Having these antennas set to the proper length in relation to the ground medium will maximize the constructive interference between signals from the antenna elements.

Sampling time is one area where this linear regression approach is not ideal for arriving at the maximum gain configuration. Gradient descent is one option for reducing optimization time as long as the environment remains static during calibration. Data from a more complex environment with trucks near the array and people walking in between the transmitter and the robotic parasitic array is too noisy to establish an optimal configuration. As shown in Fig. 3.7, noise levels were too high for an optimal configuration to be found. Gradient descent would not work in this approach. However, given enough samples, an optimal configuration could be found with linear regression. Another approach to optimizing gain in a noisy, dynamic environment is to move the robotic antenna elements into a known sub-optimal configuration. Our results show that $1.5\,\mathrm{m}$ to $2.2\,\mathrm{m}$ is a near-optimal position spacing for the ground robots at 40 MHz. The penalty for a sub-optimal spacing is $0.25\,\mathrm{dB}$.

In this chapter, we demonstrated the ability to calibrate the reflector's length and spacing with respect to the excited/driven antenna in the presence of different ground media to increase gain. We also demonstrated that different ground media have different optimal configurations for the antenna array. The robotic parasitic array we characterize in this chapter could be created at

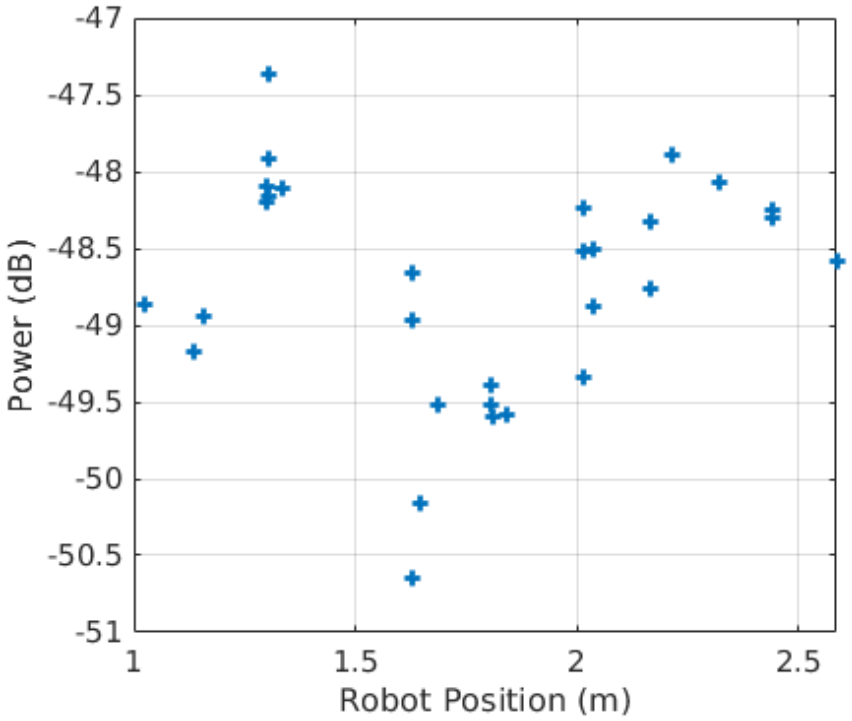

Figure 3.7: Change in gain as a function of robot position in a dynamic environment [2] ©2019 IEEE

frequencies other than 40 MHz, but the antenna size will vary inversely with frequency. However, as the frequency increases, the spacing between the antennas will shrink as the optimal antenna spacing is roughly $\lambda/4$. At some higher frequency, antenna elements would need to be spaced more closely than would be physically possible, as two objects cannot occupy the same space. At higher frequencies, it would be more appropriate to use an off-the-shelf directional antenna. However, as the frequency increases, the prevalence of multipath interference increases, while the range and through-building-penetration benefits decrease as well.

Chapter 4: Robotic Parasitic Array Control for Increased RSS in Non-Line-of-Sight

In order to benefit from the increased received signal strength (RSS) created by the robotic array, it must rotate its boresight (i.e., its direction of maximum gain) to point towards the agent with which it is communicating. Otherwise, the directionality created by forming the array can reduce instead of increase RSS. Addressing how a robotic array rotates is the topic of this chapter and our recent journal submission [31]. In a robotic parasitic array, the boresight can only be rotated by moving the robots that compose the antenna array relative to each other. We hypothesize the UGVs must maintain a formation (i.e., the relative positions and orientations of the antennas) within some tolerance to maintain this gain. Our contributions toward testing this hypothesis and improving wireless communication through actuating a robotic parasitic array are as follows. We propose a method for rotating a formation of two antennas through the controlled motion of a UGV carrying one of the antennas. During this rotation of the array, we show that the array gain is reliably maintained. Next, we describe two scenarios where the robotic parasitic array must rotate to maintain or increase RSS when receiving a signal from a transmitting, mobile node. In the first scenario, this mobile node moves through a complex environment and communicates with the parasitic array. In response to this motion, the robotic parasitic array must rotate to track the mobile node and maintain enhanced RSS. In the second scenario, the array and mobile node are far apart, but the array can detect the RSS of the mobile node. In response, the robotic parasitic array must rotate to increase RSS. For these two scenarios, we propose and experimentally test approaches for controlling the robotic array to increase RSS. The results show that the robotic parasitic array maintains a higher RSS than a signal transmitted through a single

antenna. This is significant, as these compact, low-VHF antennas already have an improved range over UHF systems in line-of-sight (LOS) and non-line-of-sight (NLOS) conditions.

There are some important considerations to discuss before formulating an approach. When antennas forming this type of array are distributed across robots, they must be spaced within $\sim$0.25 λ of each other (i.e., $2\,\mathrm{m}$ at $40\,\mathrm{MHz}$). Once positioned, passive antennas reradiate energy to effectively reflect and focus signal energy that is transmitted and received through the excited/driven antenna. Preliminary experiments indicate that each additional robot with a passive antenna will sharpen the beam and increase the array gain in a similar fashion to a free-space Yagi-Uda array [3]. Complex multi-robot coordination approaches would be required however to align larger arrays and optimize the spacing between robots. Conversely, the simplest of robotic parasitic arrays is one composed of a static reflector and UGV carrying the excited/driven antenna. In this configuration, all of the RSS sampling and motion for optimizing gain and rotation is controlled by one UGV in the antenna array. In this chapter, we research how to control robotic motion to actuate the boresight of the aforementioned array to take advantage of the array gain.

Antenna boresight actuation is researched for contexts outside robotics, such as tracking satellites [117] and maintaining communication between wind turbines [118]. Robotics researchers have used servos [119, 120] and robotic motion [111] to actuate directional UHF antennas for localization and RSS maximization. Maintaining mutual coupling between the antennas and ground medium while the formation of antennas rotates is a unique challenge for actuating robotic parasitic arrays. The results of Chapter 3 showed that these low-VHF antennas can vary $\pm 0.15\,\mathrm{m}$ around the optimal spacing while maintaining maximum gain on a uniform ground medium. However, this optimal spacing can vary $0.75\,\mathrm{m}$ on different ground media. Since the terrain of most environments is not homogeneous, maintaining the array gain while the formation of antennas rotates is not trivial.

4.1 Approach

We investigate the issues of robotic parasitic array actuation in complex environments with a robotic parasitic array comprised of a static reflector and a UGV carrying the excited/driven antenna. While the reflector is fixed, the direction of the peak gain (i.e., the boresight) of the array can be controlled by moving the UGV around the reflector at a fixed radius. A mobile node traverses a complex environment while transmitting the signal that is measured by the UGV to calculate RSS. Our objective is to maximize the RSS of the signal received from a mobile node by changing the position of the UGV with respect to the reflector; this increase in RSS extends the effective communication range with this mobile node.

4.1.1 Robotic Parasitic Array Boresight Rotation

A critical hypothesis in this work is that the array gain can be sustained if the formation of the UGV, excited/driven antenna, and reflector maintain their relative positions and orientations. In order to test this hypothesis, we repurpose a boundary following control approach developed in [121] to rotate the parasitic antenna array. In this implementation, the UGV is a non-holonomic, differential-drive platform that rotates the antenna array by orbiting the reflector. Since the reflector is symmetric about its vertical axis, it is stationary. The reflector is modeled as an obstacle with an imaginary boundary. While, this approach for moving the UGV avoids collisions with the reflector, orbiting the reflector maintains the relative orientation and spacing of the UGV with respect to the reflector.

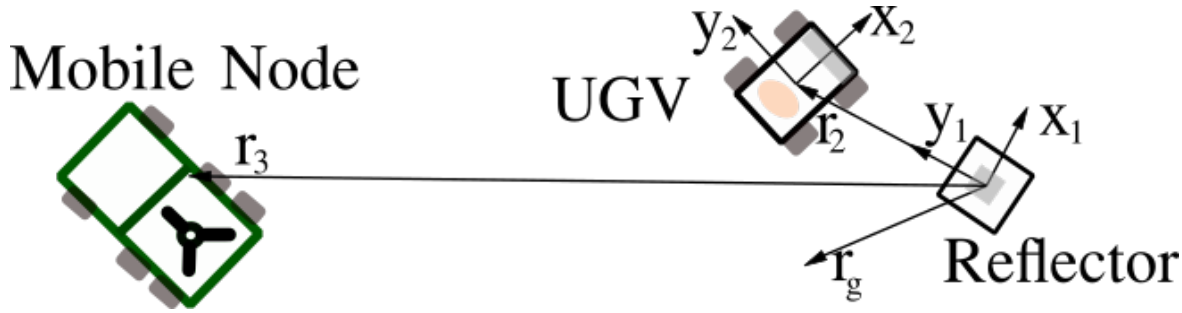

Figure 4.1: The positions and orientations of UGV and reflector and the mobile node

The center of the reflector defines the origin of the relative coordinate system. From the origin, vector $r_2 \in \mathbb{R}$ connects to the center of the UGV. The boresight of the array should be closely aligned with r_2. The vector $r_3 \in \mathbb{R}$ connects the center of the reflector to the mobile node. The vector r_g is a *goal* boresight direction of the array. The Euclidean norm of this vector ($|r_g|_2$) is $d^* \in \mathbb{R}$, which is the UGV-reflector spacing for maximum array gain. The reflector boundary and UGV have coordinate frames defined by the unit vectors $x_1, y_1 \in \mathbb{R}^2$ and $x_2, y_2 \in \mathbb{R}^2$, respectively. The reflector's imaginary boundary is zero distance from the origin of the reflector and is defined such that y_1 is aligned with r_2. The UGV's coordinate frame has x_2 aligned with the forward direction of the UGV. The kinematics of this UGV are described in the following equations.

$$\begin{aligned} \dot{r_2} &= x_2 u_\ell \\ \dot{x_2} &= y_2 u_\theta \\ \dot{y_2} &= \text{-}x_2 u_\theta \end{aligned} \tag{4.1}$$

In this equation, $u_\ell \in \mathbb{R}$ is the linear velocity control input of the UGV, and $u_\theta \in \mathbb{R}$ is the rotation velocity control input. The rotational control input has sign and magnitude components. The magnitude component, described more generally in [121], defines how the UGV rotates to approach and follow an orbit path around the reflector. While this magnitude is a function, we omit its arguments in the sequel.

$$u_2 = \underbrace{\mu(x_1 \cdot y_2)}_{\text{align to tangent}} + \underbrace{\left(\frac{x_1 \cdot x_2}{1 - |\kappa_1||r_2|_2}\right)\kappa_1}_{\text{follow boundary curve}} - \underbrace{f(r_2, r_g)\left(\frac{r_2}{|r_2|_2} \cdot y_2\right)}_{\text{maintain distance}} \tag{4.2}$$

The first term aligns the UGV to a vector tangent to the curve of the reflector boundary. The parameter $\mu \in \mathbb{R}$ tunes how tightly the UGV will turn to achieve this alignment; the sign of μ determines whether the UGV circles the boundary in a clockwise or counterclockwise direction, but it is positive in this implementation. The middle term enables the UGV to respond to the nonzero curvature of the boundary. The parameter $\kappa_1 \in \mathbb{R}$ is constant in this implementation and

relates to the ranging capability of the sensor detecting the boundary. The last term maintains the UGV's distance to the boundary. The function $f(r_2, r_g) \in \mathbb{R}$ uses r_g to set the UGV-reflector distance.

$$f(r_2, r_g) = \alpha \left[1.0 - \left(\frac{r_0(r_g)}{|r_2|_2} \right)^2 \right] \tag{4.3}$$

The parameter $\alpha \in \mathbb{R}$ is a positive constant and $r_0(r_g) \in \mathbb{R}$ determines the desired separation between the UGV and the reflector's boundary. It is not linearly related to the separation distance so we use a quadratic equation to relate r_0 to the desired UGV-reflector spacing.

$$r_0(r_g) = \frac{\sqrt{(4a(|r_g|_2 - c) + b^2) - b}}{2a} \tag{4.4}$$

The value $|r_g|_2$ specifies the desired distance of the UGV from the reflector. Using linear regression, we determine that $a = 0.001$, $b = 0.6$, and $c = 0.3$ are appropriate for maintaining the UGV at 1-3 m from the reflector.

With the magnitude of the rotation defined such that the UGV orbits the reflector, we can define the direction (clockwise or counterclockwise) that it orbits to r_g as follows.

$$\beta(r_2, r_g) = \gamma \left| \begin{bmatrix} \frac{r_2^T}{|r_2|_2} \\ \frac{r_g^T}{|r_g|_2} \end{bmatrix} \right| \tag{4.5}$$

The value $\gamma \in \{-1, 1\}$ defines if the UGV is locked such that forward motion is clockwise or counterclockwise. The next term is the z component of the cross product of r_2 and r_g which returns either -1 or 1 depending on whether r_2 or r_g is to the right. In the case where the vectors are antiparallel, we specify that the UGV drives forward to orbit towards r_g. If the vectors are already aligned then the UGV is at the goal. Using this term and u_2 we can define the following rotation control input.

$$u_\theta = \beta(r_2, r_g) u_2 \tag{4.6}$$

We set the linear velocity u_ℓ using the following equation.

$$u_\ell = \begin{cases} 0, & (\phi(r_2,r_g) < \phi_{tol}) \cap (|d^* - |r_2|_2| < d_{tol}) \\ v_{min}\beta(r_2,r_g), & \phi(r_2,r_g) < \pi/8 \\ v_{max}\beta(r_2,r_g), & \text{otherwise} \end{cases} \tag{4.7}$$

This allows the UGV to move quickly at $v_{max} \in \mathbb{R}$ speed when the boresight is not pointed in the desired direction. When the UGV is close to r_g, it slows to $v_{min} \in \mathbb{R}$ to prevent high accelerations when the UGV stops near r_g. We calculate the relative angle between r_2 and r_g as $\phi(r_a, r_b) = \arccos\left((r_a \cdot r_b)/(|r_a||r_b|)\right)$ where $r_a = r_2$ and $r_b = r_g$. This angle is compared with the parameter ϕ_{tol} to check if the boresight is sufficiently aligned while preventing forward/backward oscillation around r_g caused by sensor noise in measuring r_2. Since the UGV smoothly approaches d^*, it is possible that the UGV may arrive at an angle that closely aligns r_2 with r_g, but not spacing the UGV and reflector within $d_{tol} \in \mathbb{R}$. Positioning the UGV within d_{tol} of the desired spacing is necessary for achieving the array gain. To address this issue, we intermittently recalculate $\beta(r_2, r_g)$ so that the UGV can reverse its direction toward the goal to avoid completing a full orbit of the reflector before reaching r_g. The following algorithm describes how the array rotates the boresight to align with a vector r that originates at the reflector.

Algorithm 2 RotateToGoal(r)

1: **if** $\phi(r_2, r) > 1.6\phi_{tol}$ **then**
2: $\quad r_g \leftarrow d^* \frac{r}{|r|_2}$
3: **end if**
4: **while** $|u_\ell| > 0$ **do**
5: $\quad$ wait(0.1 s)
6: **end while**

In Alg. 2, we first check that the angle between the vector r and the boresight, estimated as r_2, is large enough that rotating the boresight would increase RSS. We specify $1.6\phi_{tol}$ is an appropriate angular tolerance given the beamwidth and measurement sensitivity of our system. If this condition is met then r_g is set. The while loop ensures that the UGV cannot assign a new r_g until the UGV aligns the array's boresight with the current r vector.

4.1.2 Actuating the Array to Maximize RSS

We consider a *mid-range* and *long-range* spacing scenario between the array and the mobile node in a complex environment where the ground does not impinge on the r_3. In both cases, the robotic parasitic array can be rotated so that the maximum RSS is measured by the UGV from a mobile node transmitting a signal. In mid-ranges, the boresight will need to actively track the mobile node. However, at long ranges, a mobile node with a fixed speed will vary the angle between r_3 and r_2 more slowly when $|r_3|_2 >> |r_2|_2$. Simultaneously, as $|r_3|_2$ increases, RSS decreases to the point where communication between the array and the mobile node is not possible but the signal is still measurable. In this case, the robotic parasitic array will rotate to increase RSS.

For mid-range tests, we hypothesize that we can maintain RSS at its maximum by directing the boresight in the direction of the mobile node. This approach requires telemetry from the mobile node to resolve r_3. In cases where the mobile node and UGV can communicate, this alignment can be achieved by setting **RotateToGoal**(r_3) for all telemetry available from the mobile node. Our hypothesis is that the robotic parasitic array can rotate quickly enough while maintaining the formation of the array's antennas as the mobile node traverses the environment.

For the long-range test when communication is not possible (i.e., the signal RSS is close to the background noise level), the mobile node remains in one position while the robotic parasitic array rotates to increase RSS. We use gradient ascent as described in Alg. 3 to control the rotation of the robotic parasitic array. In this algorithm implementing gradient ascent, we use a 2-D

Algorithm 3 Gradient Ascent Control

1: **RotateToGoal**($R(\text{-}0.1)r_2$)
2: Begin Collecting RSS
3: **RotateToGoal**($R(0.2)r_2$){Collect RSS samples}
4: Stop Collecting RSS
5: **RotateToGoal**($R(\eta\nabla_\theta \text{RSS}(\theta))r_2$)

rotation matrix to calculate r_g.

$$R(\phi) = \begin{bmatrix} cos(\phi) & -sin(\phi) \\ \sin(\phi) & cos(\phi) \end{bmatrix} \tag{4.8}$$

In the first step of this gradient ascent, the UGV takes RSS samples within $\pm 0.1\,\mathrm{rad}$ which is sufficient to estimate the gradient despite sensor noise. Then it estimates the RSS gradient, $\nabla_\theta \mathrm{RSS}(\theta)$, at a given boresight orientation, $\theta \in \mathbb{R}$, using these collected samples. In the next step, we calculate the change in array rotation as $\eta \nabla_\theta \mathrm{RSS}(\theta)$ to ascend the RSS gradient. The parameter $\eta = 0.25$ is the gradient ascent step size. Afterward, we repeat the two steps in Alg. 3 until RSS values converge.

4.2 Experiments

In our experimental instantiation of a 2 antenna robotic parasitic array, there is a 1/4 λ monopole that serves as the reflector and a UGV with an ESA described in [122], which has a $\lambda/37.5$ ($20\,\mathrm{cm}$) height and the UGV platform acts as its ground plane. The mobile node is an off-road vehicle. This experimental setup is shown in Fig. 4.2. The UGV is a Clearpath Husky with a computer that runs ROS Kinetic. This computer is connected to an Ettus USRP N210 software-defined radio (SDR) outfitted with a basicTx daughtercard. The UGV also has a Ubiquity PicoStation for communicating with the mobile node when possible and a Point-Grey Chameleon camera. The camera imagery detects the four AprilTags [115, 116] mounted on the reflector, as visible in Fig. 4.2. Using the AprilTags, the UGV can localize itself in relation to the reflector. For rotating the array, we set the following speed parameters: $v_{max} = 0.5\,\mathrm{m/s}$ and $v_{min} = 0.2\,\mathrm{m/s}$. We lock forward to a clockwise rotation, such that $\gamma = -1$ to ensure that the reflector is always visible from the UGV's camera. We empirically determine and set $\mu = 5.0$, $\alpha = 1.0$, and $\kappa_1 = 1.0$ to achieve the appropriate response from the boundary following controller in Eqn. 4.2. This localization approach allows us to have an angular tolerance of $\phi_{tol} = 0.05\,\mathrm{rad}$ and a

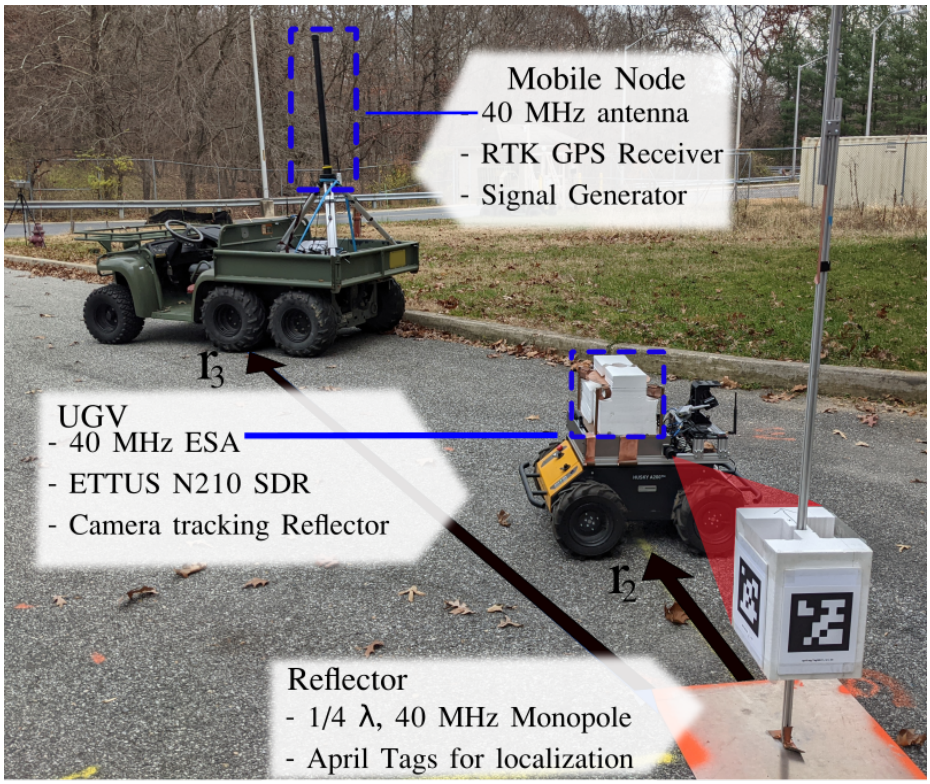

Figure 4.2: The robotic parasitic array is formed by the UGV and reflector. A camera on the UGV allows it to localize the reflector.

spacing tolerance of $d_{tol} = 0.1\,\mathrm{m}$. The mobile node has a computer and Ubiquity PicoStation as well. It is equipped with a $\lambda/6$ antenna that is driven by a signal generator transmitting a sine wave at $40.5\,\mathrm{MHz}$. It also has a Ublox C94-M8P real-time kinematic (RTK) global positioning system (GPS) that is running in rover mode. We deployed an RTK-GPS base station that had performed a self-calibration for 10 minutes. This is sufficient for localizing the mobile node with $\sim 1\,\mathrm{m}$ precision. The relevant coordinate frames for localizing the reflector, UGV, and the mobile node are shown in Fig. 4.3. The reflector's position and orientation are surveyed in the Universal Transverse Mercator (UTM) coordinate system, forming the highest level coordinate frame. The AprilTags are calibrated with respect to the base of the reflector. When these April Tags are observed by the camera on the UGV, it can infer the transform from the base of the reflector to the odometry frame of the UGV. The odometry frame is related to the chassis of the UGV using an Extended Kalman Filter (EKF). This EKF consumes encoder information

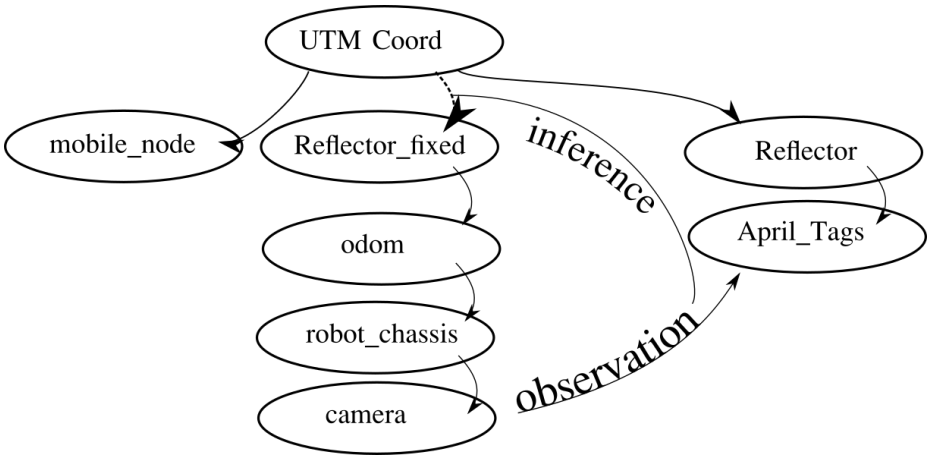

Figure 4.3: This is a system of coordinate frames for localizing the reflector, UGV, and the mobile node.

from the wheels of the ClearPath Husky and rotational information from a Microstrain inertial measurement unit [123]. A fixed transform relates the chassis to the camera. Using the described combination of GPS and AprilTags allows the reflector, UGV, and mobile node to be placed in UTM coordinates when the mobile node and the UGV can communicate through the PicoStation radios. The RSS is measured on the UGV using the SDR. For each signal power sampling, the radio records $M = 100,000$ magnitude and phase (I/Q) samples over $0.05\,\mathrm{s}$. The RSS is calculated as follows:

$$\text{RSS} = 10\log_{10}(\frac{1}{M}\sum_{j=1}^{M}(I_j^2 + Q_j^2)) \tag{4.9}$$

The RSS is the received power of the signal from the mobile node at a given θ angle around the reflector. The signal magnitude $I \in \mathbb{R}^M$ and the phase $Q \in \mathbb{R}^M$ samples are values that are measured by the SDR.

In order for array gain to be maintained, the UGV must maintain the formation of the array as it rotates the boresight at close-range in LOS. In Fig. 4.4 we plot the gain in RSS from adding the reflector to the UGV as the UGV varies the θ and d^*. In this figure, the $\theta = 0\,\mathrm{rad}$ is the direction of the boresight. At its maximum, the array achieves $\sim 2\,\mathrm{dB}$ of gain. Greater array gain is theoretically possible with additional antenna research, which is outside of the scope of

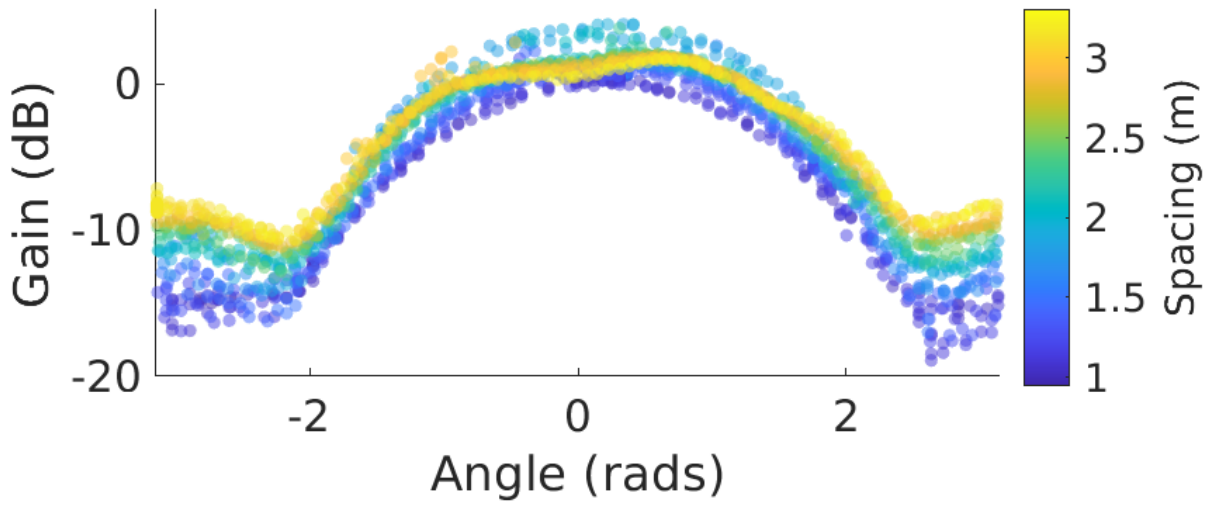

Figure 4.4: Array gain at different boresight angles and reflector-UGV spacings

this dissertation. The mobile node is fixed at a distance of $17\,\mathrm{m}$ away from the robotic parasitic array. Each point in the plot corresponds to an RSS sample collected where $|r_g|_2$ corresponds to the spacing between the reflector and UGV. To collect these points, we specify d^* at a range of $1\,\mathrm{m}$ to $3\,\mathrm{m}$ varied in $0.5\,\mathrm{m}$ increments. The gain of the array rises and falls as the UGV-reflector spacing increases; this test corroborates the findings of [2] as the highest gain is achieved with a spacing of $\sim$1.9 m on asphalt. After setting the desired spacing and parameters in the UGV controller specified in Eqn. 4.6 and 4.7, we collected samples from 3 revolutions of the UGV around the reflector to verify that RSS was maintained as shown in Fig. 4.5.

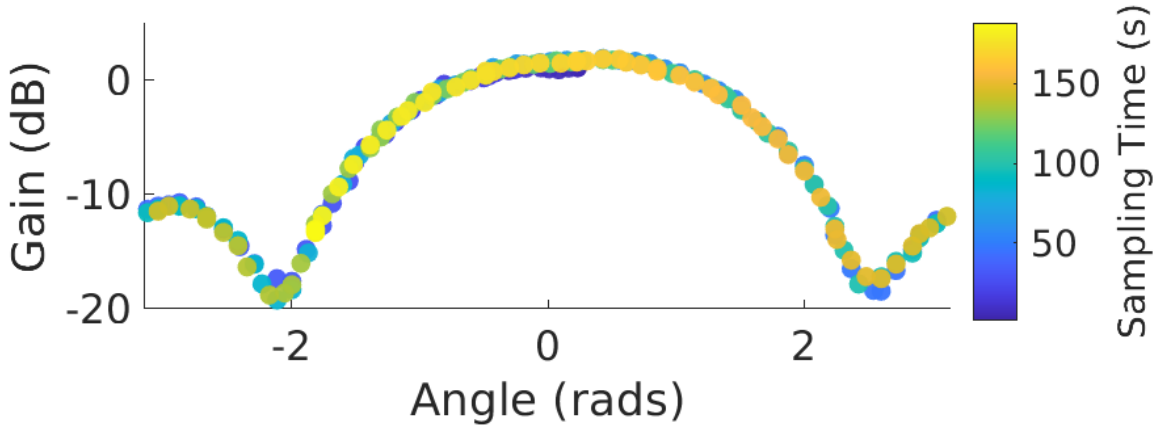

Figure 4.5: RSS v. boresight angle with optimal reflector and UGV spacing.

The variation in RSS is very small ($\pm 0.25\,\mathrm{dB}$) as the UGV orbits the reflector. When comparing samples taken from different revolutions around the reflector, they overlap and are similar to the predicted radiation shown in Fig. 2.2. For reference, at UHF frequencies, it is common for there to be $\pm 1.5\,\mathrm{dB}$ variation without motion of the receiver and transmitter. This test shows that the UGV will repeatably drive to a position and achieve the same array gain since the UGV's error in localizing the reflector is sufficiently small. This validates our hypothesis and approach for rotating the boresight of the array.

Our experiments are conducted in a challenging environment, as shown in Fig. 4.6 where there are wood and cinder-block buildings, trees, metal structures, and some terrain variation. This environment is used for our mid-range and long-range tests. In the mid-range tests, shown in Fig. 4.6a, the red line shows the trajectory that the mobile node follows. The mobile node's trajectory brings it to positions that are between $25\,\mathrm{m}$ and $60\,\mathrm{m}$ away from the UGV. For each test, the mobile node travels at $2\,\mathrm{m/s}$ and performs 3 - 4 loops on this trajectory over which we record 650 - 700 corresponding RSS samples on the UGV. Sampling in this manner allows us to reduce the effects of transient interference and error in localizing the mobile node. In the first mid-range test, the UGV is alone, near the origin, without the reflector present. The RSS samples collected serve as a baseline for low-VHF omnidirectional wave propagation in this complex environment. In the next mid-range test, the UGV drives to an optimal distance from the reflector placed at the origin before the test begins to create the robotic parasitic array. However, the UGV does not move which leaves the boresight static when the mobile node performs its 3-4 loops along the predefined trajectory. In the final test for the mid-range scenario, the UGV rotates the boresight to track the mobile node. In the long-range test shown in Fig. 4.6b, the mobile node is positioned $150\,\mathrm{m}$ away from the robotic parasitic array. Over this range, a dense building and trees create a challenging NLOS environment.

We also performed some preliminary investigation into the effects of impinging ground on the link between the parasitic array and the mobile node. In Fig. 4.7 we look at three different regimes of ground impinging on this signal. The blue plot shows the data recorded from earlier

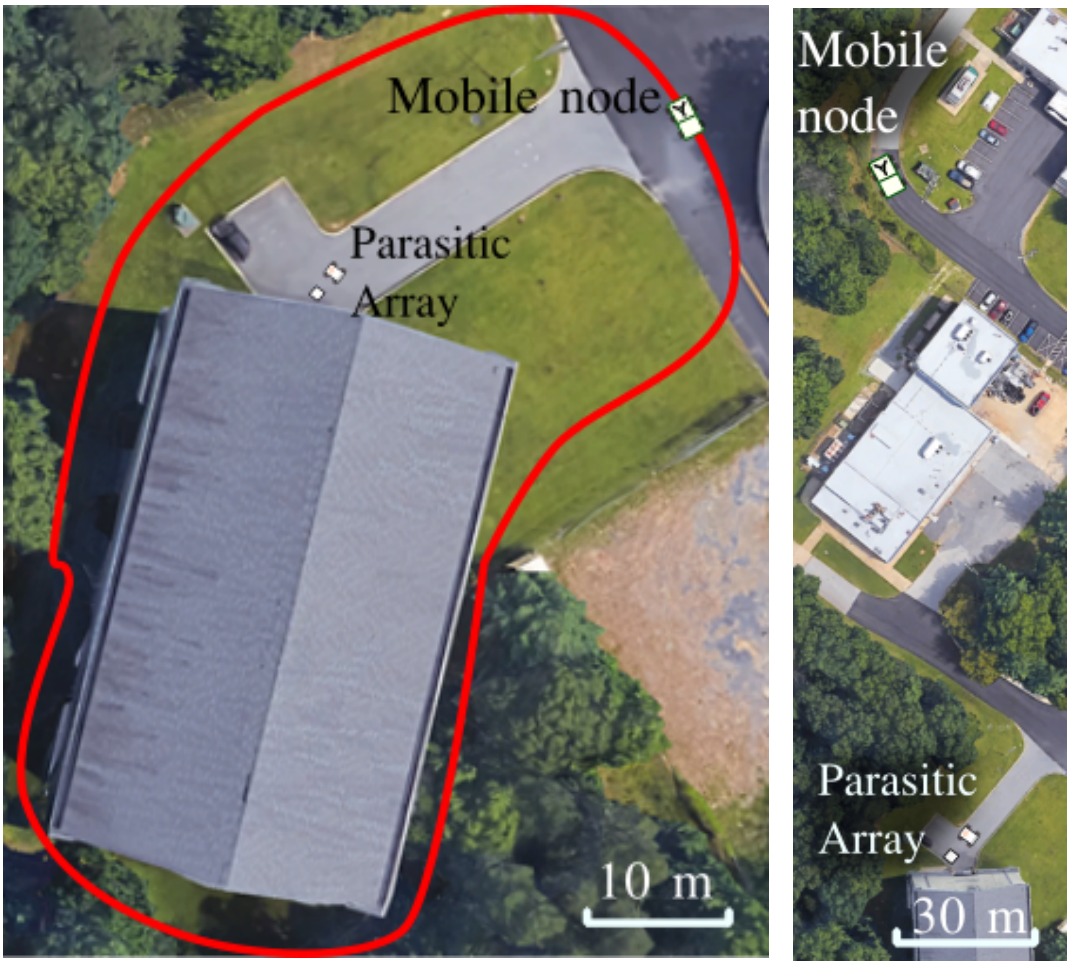

(a) Mid-range: The red line shows the trajectory of the mobile node.

(b) Long Range

Figure 4.6: Satellite view of a complex environment where we test the robotic parasitic array.

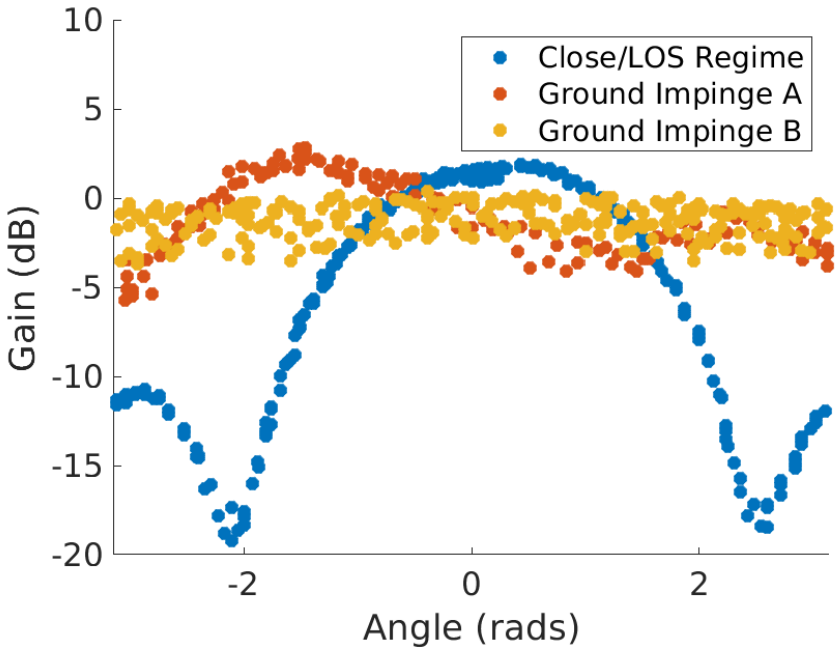

Figure 4.7: Distortion of array pattern when ground impinges on the signal.

tests where the mobile node is $17\,\mathrm{m}$ away. In this situation, the main beam is well defined and aligned with the front of the array. In "Ground Impinge A" the ground is impinging on the line between the array and the mobile node. While there is gain in one direction, this gain is not maximized in front of the array. This indicates that the signal is reflected in the far-field or distorted by mutual coupling in the near-field. Simultaneously, the power does not drop when the boresight is rotated well away from pointing towards the mobile node. This is also surprising. In the test case "Ground Impinge B" there is almost no difference between deploying a parasitic array and an omnidirectional array; the gain is zero regardless of the pointing direction of the boresight. These tests indicate there is significant characterization required for understanding cases where the ground impinges on the signal.

4.3 Results and Discussion

In the mid-range tests, we can calculate the array gain when the boresight is fixed and when it rotates to track the mobile node. This gain is calculated for points that are no less than $8\,\mathrm{m}$ apart

along the trajectory designated in Fig. 4.6. For each of these points, shown as a colored region in Fig. 4.8 and Fig. 4.9, we calculate the difference between the average RSS collected by the robotic parasitic array and the UGV without the reflector. Each colored region is the difference of 20-30 RSS samples. This number of samples collected at different times leads us to be confident in our array gain estimates. The colored circles, denoting array gain for a fixed boresight, show

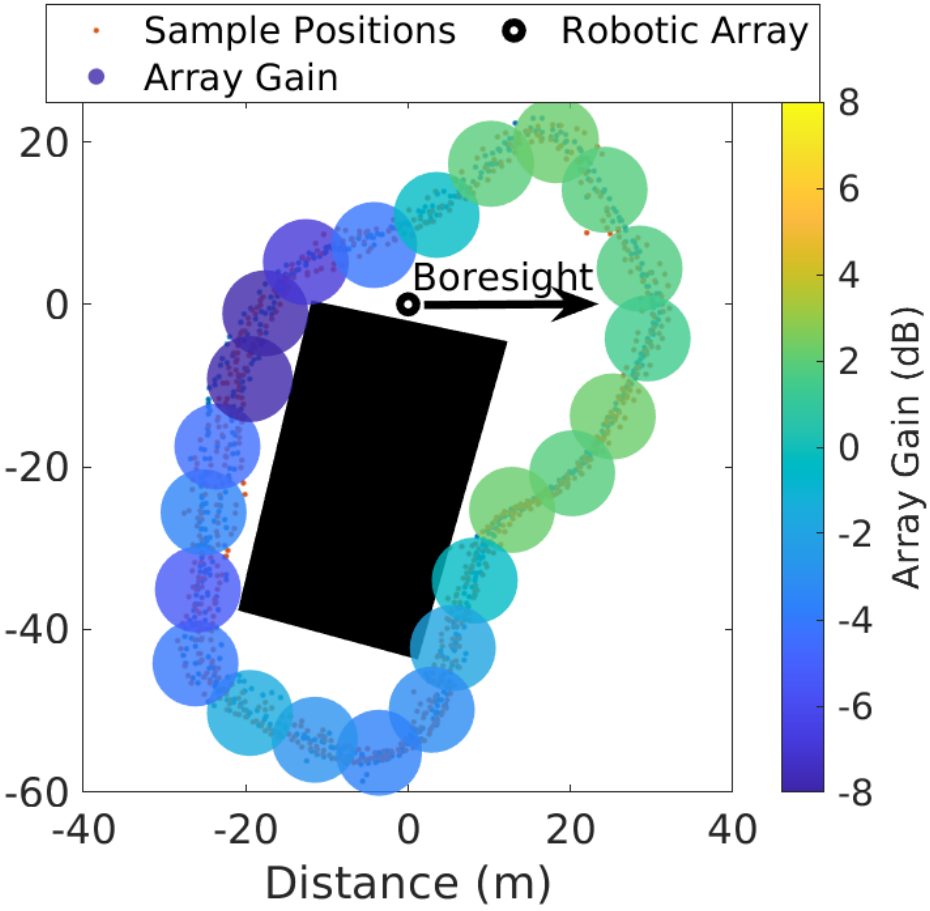

Figure 4.8: Array gain with fixed boresight in LOS and NLOS conditions

that in the direction of the boresight, the array gain is $\sim 2\,\mathrm{dB}$. This gain is present in both LOS and NLOS conditions. However, this gain is limited to $\pm\pi/3$ rad around the boresight. When the mobile node drives out of the boresight, the signal drops as low as -8 dB. Gain is only achieved around the boresight, showing that in these environments and at these ranges, the array pattern is maintained from our tests where the array was characterized in LOS at close range in Fig. 4.5.

However, this result also shows that we can make a signal more covert in complex environments by actuating the boresight away from agents that may be attempting to detect it.

Using this same approach for computing array gain, we compare the omnidirectional radiation of the first mid-range test with the approach for aligning the boresight to the mobile node in our final mid-range test. The resulting array gain is shown in Fig. 4.9.

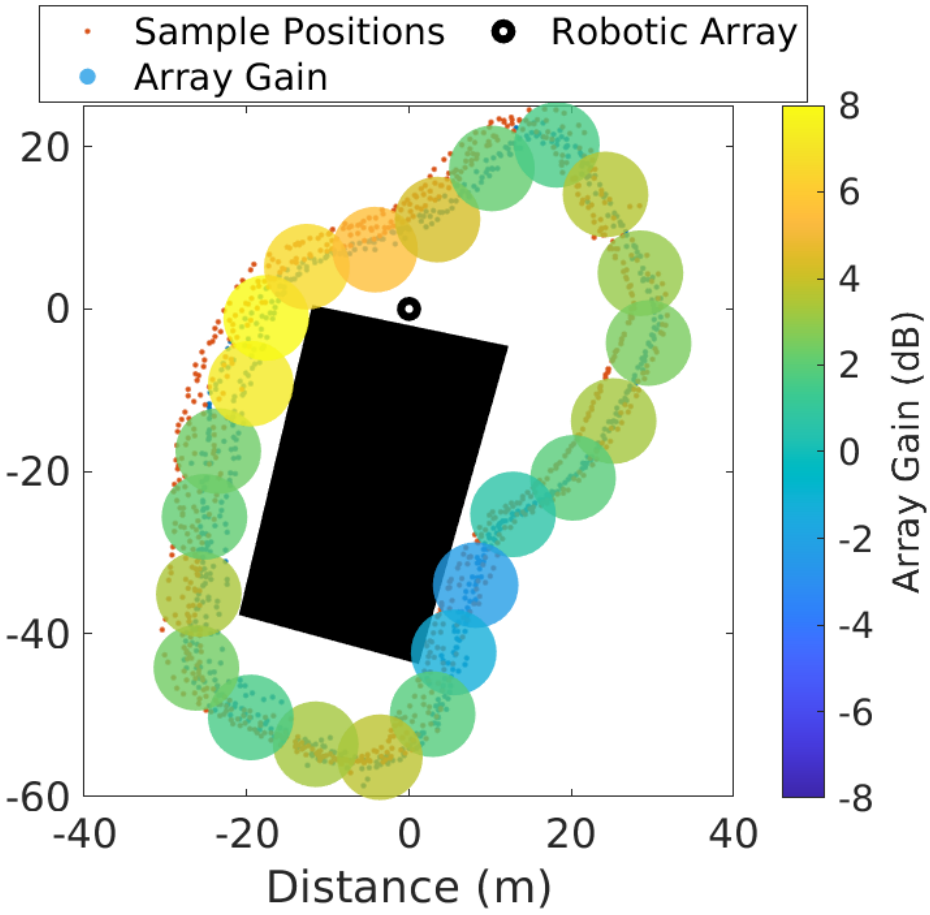

Figure 4.9: Array gain achieved by rotating the boresight using mobile node telemetry at LOS and NLOS positions

This trial shows that the approach to rotating the array is effective for maintaining $2\,\mathrm{dB}$ at almost every point. Near one corner of the building, the gain appears lower. This may have resulted from the antenna on the mobile node transmitting from positions near other metal objects. At another position, we record an $8\,\mathrm{dB}$ gain. This high gain may have also resulted from the presence of a

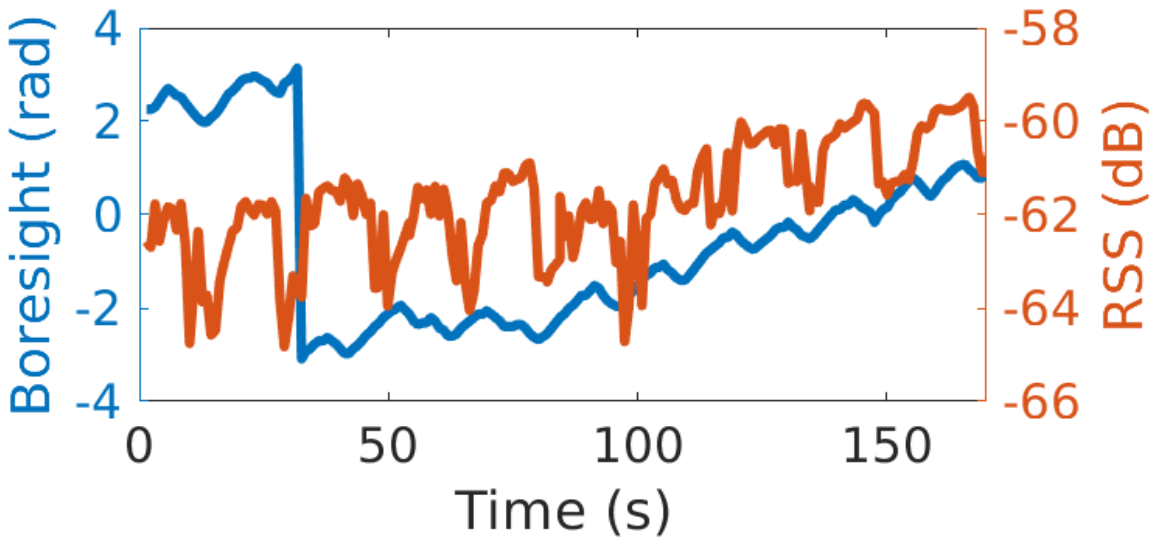

Figure 4.10: The left y-plot shows the change in boresight angle during gradient ascent. The right y-plot shows the steady growth in RSS.

large metal vehicle and an electrical transformer. This gain indicates it may be possible to deploy single antennas or arrays in certain positions within complex environments to leverage mutual coupling. Overall, this approach to rotating the robotic antenna array outperformed the one that did not rotate and showed the ability to maintain array gain in LOS and NLOS conditions.

Finally, we conducted long-range tests where we used gradient ascent to rotate the array to increase RSS. One of these tests is shown in Fig. 4.10 where the array and the mobile node are $150\,\mathrm{m}$ apart in NLOS. In this test, the UGV initializes and measures $-62\,\mathrm{dB}$. As the UGV performs its gradient ascent, it stabilizes at $-60\,\mathrm{dB}$. The noise floor is around $-63\,\mathrm{dB}$ and the signal from the mobile node is barely discernible. The amount of change in RSS that we measure from rotating the array is smaller than what we measured at close-range in Fig. 4.5 since background noise biases our RSS measurements. However, this gradient ascent approach still performs well. At the end of the test, the boresight is pointed at the mobile node.

In this chapter, we demonstrated that in some terrains (i.e., ground media), the ability to increase RSS with a small amount of robotic motion by forming and rotating a robotic parasitic array in a complex, NLOS environment, thereby extending the range of low-VHF antennas demonstrated to perform more reliably in complex environments. This is noteworthy for the

following reason. First, we showed that our implementation of a boundary following controller reliably maintained the RSS gained through forming the robotic parasitic array while changing its orientation. Then we successfully tested an approach for maintaining the gain created by the array by rotating the boresight of the array to track the mobile node in LOS and NLOS conditions. Finally, we successfully tested a gradient ascent-based approach for rotating the array to increase RSS when the mobile node was at an unknown, far position in NLOS.

While robots can drive toward each other to increase RSS, the motion required to increase RSS by rotating the array is smaller than the motion required to drive the UGV closer to the mobile node. In addition, if the position of the mobile node is unknown and the distance between the mobile node and the robotic parasitic array is large, it is difficult to use the RSS gradient to define the correct driving direction towards the mobile node [124]. In complex environments, this capability of increasing the signal power in preferred directions is especially impactful since it is difficult for robots to reliably navigate in these environments [125]. In comparison, the change in RSS caused by rotating the array is large and is not affected by distance. As a result, robotic array formation and control are particularly favorable for improving communication at long ranges in NLOS.

Chapter 5: Optimizing Overall Network Connectivity of Parasitic Arrays

We have investigated optimizing the gain of a two-element parasitic array over the relative positions of robots forming the array in Chapter 3 and rotating the array in Chapter 4. Assuming this approach can be applied to larger arrays with more passive antenna elements, there are critical questions about where robotic parasitic arrays should be formed. Investigating this question is the focus of this chapter. Here, we shift our perspective from controlling robots within an array that create individual communication links to a network of parasitic arrays that move and evolve in size. From this perspective, we abstract the dynamics of parasitic arrays to develop a controller for maximizing the overall connectivity of a network of these antenna arrays. This chapter mirrors our journal paper [1]

To exploit the parasitic coupling for an enhanced beam pattern, we seek to create a controller that guides a multi-robot system over long ranges. Specifically, we utilize low-VHF antennas to form parasitic arrays to communicate over long distances (in the case we study, > 150 m). The objective of our controller is to maintain and improve the connectivity graph of these robotic agents. As shown in Fig. 2.1, we denote the agents communicating at low-VHF as *active antenna agents*. Active antenna agents have low-VHF antennas that are electrically driven/excited (i.e., connected to the radio onboard). There are also *passive antenna agents*, which are robots that have low-VHF passive antennas and therefore require no low-VHF radio. As shown in Fig. 2.2, one or more of these passive antenna agents reflect and spatially focus radiation around the active antenna agents. When properly configured, these agents form a parasitic antenna array. While the agents forming each parasitic array need to control frequency, antenna spacing, and antenna length, this is outside the scope of this research. The electromagnetics of the parasitic

array, including optimization of the antenna placement, are considered in [2]. Here, we focus on the motion control problem of a multi-agent system to enable parasitic array formation so as to establish desired connectivity. Our contributions to solving this problem are the following:

- Introducing a variable state, called parasitic effect, to describe the number of passive antenna agents in a parasitic Yagi-Uda array, a specific type of parasitic array
- Creating a model of the induced beam pattern as a function of the number of agents
- Formulating a Fiedler value maximization approach for groups of parasitic antenna arrays
- Comparing connectivity maintenance with agents that can form parasitic arrays and those that cannot

This work is a first step towards controlling a multi-robot system that can reliably communicate in non-line-of-sight (NLOS) environments using low-VHF, such as safety and rescue contexts (e.g., city building, cluttered outdoor, and urban settings). This is especially important in complex environments, enabling the multi-robot collective to establish and maintain a network topology.

5.1 Approach to Connectivity Maintenance

We assume we have $n \in \mathbb{Z}$ computationally powerful UGVs which act as active antenna agents. In the sequel, we refer to the state of the robotic parasitic arrays and the state of the active antenna agents interchangeably. The states of these robotic agents are described in Table 5.1. If these robotic parasitic arrays can communicate, we assume they can jointly estimate each other's states in the same coordinate system using distributed SLAM [126] or another approach and model their radio propagation. The level of position uncertainty due to noise and the gradual variation in signal strength due to large, signal-attenuating objects and buildings implies that some level of control is required to maintain communication.

Agents can create and control a directional signal if they form a parasitic antenna array. The range and directionality created by forming the array is called array gain with respect to a single omnidirectional antenna on an active antenna agent. For simplicity, we assume each $i \in [0, n]$ agent has states $x_i, y_i \in \mathbb{R}^n$ defining agents' locations. Additionally, $\theta_i \in \mathbb{R}^n$ defines

the direction of maximum array gain for each active antenna array. There is no assumption that the front of the agent or some set of sensors is aligned with the antenna array direction. This assumption partially decouples other tasks the active antenna agent may be engaged with from the connectivity maintenance task. As the positioning of the passive antenna agents controls the array orientation, the gain is controlled by these agents.

Table 5.1: System States and Variables [1] ©2020 IEEE

n	number of active antenna robots (agents) which form robotic parasitic arrays (indexed by i,j)
θ_i	orientation of the array of active antenna robot i
ρ_i	parasitic effect of the array of active antenna robot i
q_i	$[x_i, y_i, \theta_i, \rho_i]$, the state of active antenna robot i
u_i^c	communications maintenance control for active antenna robot i
$P(q_i, q_j)$	Power received at active antenna robot i after transmission from active antenna robot j
$\phi(q_i, q_j)$	Bearing angle of active antenna robot j from active antenna robot i
G_i	Gain of the array of active antenna robot i which is receiving a signal, later defined as $G(\phi(q_i, q_j), q_{i,4})$
G_j	Gain of the array of active antenna robot j which is transmitting a signal, later defined as $G(\phi(q_j, q_i), q_{j,4})$

5.1.1 System Model and Problem Formulation

Passive antenna agents do not require a radio to alter the properties of the array, so these robots can be flyers or some other agile, high-speed robot that has the appropriate electrical properties for forming a parasitic array. In an experiment, the passive antenna agents would use Wi-Fi radios to communicate with the active antenna agents to coordinate array formation. The control and allocation of these passive antenna agents, as well as their ability to rendezvous to form arrays, is outside the scope of this research. We assume that the passive antenna robots will move and position themselves as necessary, and we describe their motion as a state of the robotic parasitic array. We call this state *parasitic effect*, which is characterized by ρ_i, such that $\rho_i \in \mathbb{R}$ is related to the number of passive antenna agents in the array. To be clear, we are abstracting away the dynamics of the passive antenna agents by saying that the orientation and parasitic effect are

states of the robotic array. The array state for each i active antenna agent is $q_i = [x_i, y_i, \theta_i, \rho_i]$ which is indexed by $k \in \{1, 2, 3, 4\}$ so that $q_i \in \mathbb{R}^4$. The degrees of freedom, which are x_i,y_i,θ_i, and ρ_i, are independently actuated, and we assume a single-integrator dynamics model for the agents given by

$$\dot{q}_i = u_i^c. \tag{5.1}$$

In this equation, the connectivity maintenance control is $u_i^c \in \mathbb{R}^4$. This simple model is sufficient for solving the overall system control and passive antenna robot grouping with active antenna robots.

The Friis Transmission Equation (Eqn. 5.2) describes received power at active antenna agent i, $P(q_i, q_j)$, from another j active antenna agent where

$$P(q_i, q_j) = \frac{P_j G_j G_i c^2}{(4\pi R(q_i, q_j) f)^2}. \tag{5.2}$$

We assume that the transmit power P_j of agent j, speed of light c, and the antennas' center frequency f are constant. In our simulations, we choose $P_j = 0.025$ W, $c = 3\text{e}8$ m/s, and $f = 40\text{e}6$ Hz for all agents. The distance between the two active antenna agents is $R(q_i, q_j) = \sqrt{((q_{i,1} - q_{j,1})^2 + (q_{i,2} - q_{j,2})^2)}$. Gains G_j and G_i are unitless multipliers of the transmitting antenna and the receiving antenna, respectively.

The gain for robotic parasitic arrays is a function of q_i and q_j, thus G_i and G_j are not constant. Gain at agent i is a function of angle $\phi(q_i, q_j)$ from the direction of maximum gain of active antenna agent i ($\theta_i \equiv q_{i,3}$) to the relative bearing of agent j ($\tan^{-1}(\frac{q_{j,2}-q_{i,2}}{q_{j,1}-q_{i,1}})$).

$$\phi(q_i, q_j) = \tan^{-1}\left(\frac{q_{j,2} - q_{i,2}}{q_{j,1} - q_{i,1}}\right) - q_{i,3} \tag{5.3}$$

Next, let us approximate the beam pattern of an antenna array for two dimensions. The variable $G_i = G(\phi(q_i, q_j), q_{i,4})$ in parasitic antenna arrays cannot be described by a simple analytical model. Experimental studies [127] show that as more passive antennas are added,

the gain increases, and the beam-width decreases. These results are shown in Table 5.2.

For the purposes of control, we want to approximate the gain G_i as a function of $\phi(q_i, q_j)$ and ρ_i which is continuously differentiable. Normal distributions have been used to approximate gain patterns [128], but a normal distribution model is not differentiable from π to $-\pi$. A Tikhonov distribution, also known as a Von-Misses distribution, or the circular normal distribution, is continuously differentiable, so we adopt this as a beam pattern model.

Another simplifying assumption is that passive antenna agents can configure to form sub-optimal configurations to achieve intermediate gain values. This is how we justify our assumption that $\rho_i \in \mathbb{R}$. The first-order dynamics of ρ_i also help capture the time that it takes for an array to configure and achieve maximum gain. This relation between ρ_i and number of passive antenna agents implies that a parasitic effect of ρ_i requires $\lceil \rho_i \rceil$ (the ceiling of ρ_i) passive antenna agents to form the array. When $\rho_i = 0$, this is a vacuous state of the robotic array i where there are no passive antenna agents; the "array" is an active antenna agent i. In this situation, the orientation is meaningless as the array has no orientation without passive antenna agents; the array orientation is also irrelevant as the active antenna agent radiates omnidirectionally. We choose 6 as the maximum number of passive antenna agents that can participate in an array since there is a point of diminishing returns from adding additional passive antennas to a Yagi-Uda array. Therefore, $\rho_i \in [0, 6]$. The gain of the receiving antenna array in terms of states q_i and q_j is

$$G_i = G(\phi(q_i, q_j), q_{i,4}) = \frac{\exp((q_{i,4}/\alpha)\cos(\phi(q_i, q_j)))}{I_0(q_{i,4}/\alpha)}. \tag{5.4}$$

In Eqn. 5.4 we have already multiplied the Tikhonov distribution by 2π, which cancels out 2π in the denominator. Here, I_0 is a Modified Bessel function of order zero. We find an appropriate value for α to roughly match Table 5.2 is $\alpha = 2.3$. When the parasitic effect is 0, the gain is 1 for all values of ϕ; this is the normalized radiation pattern for an omnidirectional antenna. Note that other connectivity maintenance approaches using the Fiedler value implement a communications model similar to Friis Transmission (Eqn. 5.2) with gain values in reception and transmission

equal to 1.

Table 5.2: Gain of a Yagi-Uda Parasitic Antenna Array [1] ©2020 IEEE

Passive Antennas	Gain (dB)	Gain	Beam Width (°)
0	0	1	–
1	5	1.8	66
2	7.5	2.4	57
3	8.5	2.6	
4	9.5	3.0	48
5	10.5	3.3	40
6	11.5	3.8	

The model in Eqn. 5.4 captures main lobe behavior, but does not capture the beam pattern's nulls or sidelobes. We did not add the additional complexity required to model side-lobes because they create areas of local maxima. Incorporating a multi-lobe beam pattern model is an interesting open problem.

Gain for a parasitic array is symmetric in reception and transmission. Denoting transmission gain as G_j, this is simply G_i with i and j reversed, so $G_j = G(\phi(q_j, q_i), q_{j,4})$. With gain as a function of active antenna agent states for transmission from node j to receive node i, we can update the Friis transmission equation to obtain

$$P(q_i, q_j) = \frac{P_j G(\phi(q_i, q_j), q_{i,4}) G(\phi(q_j, q_i), q_{j,4}) c^2}{(4\pi R(q_i, q_j) f)^2}. \tag{5.5}$$

This final version of Eqn. 5.2 is now in terms of our active antenna agent states q_i. Now that we can approximate the power of a communication connection, we can model the connection quality between agents.

5.1.2 Graph of Agent Connectivity

We relate the received power to communications between the agents and then observe the group connectivity within a graph structure. The values in the adjacency matrix $A(q_i) \in \mathbb{R}^{n \times n}$ are the weights of the edges of the graph corresponding to the agent i's ability to receive data from

agent j. This matrix is a function of $q_i \forall i \in [1, n]$, meaning that the matrix can only be evaluated using state information from all active antenna agents. In the sequel, we continue to use this notation where a matrix $f(q_i)$ is populated using all q_i states. Bearing this in mind, we consider how to use the signal strength to determine the edge weights. An agent's radio must be able to disambiguate the signal from the noise in the environment. This noise sets a threshold for power, P_{low}, below which there is no connection. There is also a power level, P_{high}, above which there is no increase in data received. These values are relative to the specific radio technology. From prior work we find $P_{high} = -45$ dB and $P_{low} = -70$ dB are reasonable values and we adopt these for our simulation [40]. In addition, the large variation in signal strength leads us to favor measuring signal strength in decibels instead of Watts defined as $P_{dB}(q_i, q_j) = 10 \log_{10}(P(q_i, q_j))$. Using Eqn. 5.5 we can create a model of connectivity from agent i to agent j given by

$$A(q_i)_{i,j} = \begin{cases} 0 & i = j \\ 0 & \frac{P_{dB}(q_i,q_j) - P_{low}}{P_{high} - P_{low}} < 0, i \neq j \\ 1 & \frac{P_{dB}(q_i,q_j) - P_{low}}{P_{high} - P_{low}} \geq 1, i \neq j \\ \frac{P_{dB}(q_i,q_j)) - P_{low}}{P_{high} - P_{low}} & \text{o.w.} \end{cases} \tag{5.6}$$

If the power received at agent i is at or above P_{high}, the connectivity is 1. If the power received at agent i is less than P_{low} we say the connectivity along that edge is 0. An agent cannot form an edge with itself, therefore $A(q_i)_{i,j} = 0$ when $i = j$. As per this definition, $A(q_i)_{i,j}$, is piece-wise continuous.

In Fig. 5.1 we show how the connectivity varies as one agent moves around another fixed at $(0, 0)$ using this model. The agents maintain a fixed orientation of $\theta_i = 0$ and a constant parasitic effect. Agent j has $\rho_j = 0$ (i.e., an omnidirectional antenna) and agent i has $\rho_i = 6$ (i.e., it is highly directional with 6 passive antenna agents forming an array). With these values, when the antenna array agents are spaced by 20 m away from each other, there is perfect communication. As the agents move farther apart the communication decreases until communication is lost. In Fig. 5.2, we plot the same data in 3 dimensions. Notice that when agents are close together, the

change in connectivity is greater than when they are farther apart.

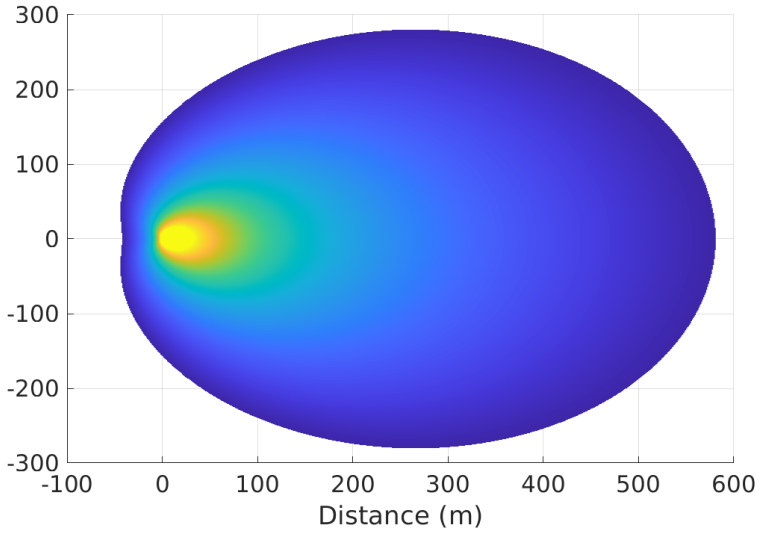

Figure 5.1: Connectivity indicated by the color-scale between agent i, located at (0,0), and agent j in different (x, y) positions, both with fixed values of θ and ρ. [1] ©2020 IEEE

5.1.3 Fiedler Optimization

The Fiedler value, a graph-theoretic metric of connectivity of a multi-agent system, is a function of the adjacency matrix $A(q_i)$. When the Fiedler value is greater than zero, there exists a path along the edges of the graph connecting any pair of agents. The existence of a communication path means that there is connectivity between all agents in the group. The gain in reception is the same in transmission, so the adjacency matrix is symmetric. The values of $P_{dB}(q_i, q_j)$ are all positive, therefore $A(q_i)_{i,j} \geq 0$. The degree of each node as $D(q_i)_{ii} = \sum_{j=1}^{n} A(q_i)_{i,j}$ where $D(q_i) \in \mathbb{R}^{n \times n}$. The Laplacian $L(q_i) \in \mathbb{R}^{n \times n}$ is defined as $L(q_i) = D(q_i) - A(q_i)$. It is positive semidefinite as it is symmetric and all of its eigenvalues are non-negative. The Fiedler value λ_2 is the second smallest eigenvalue of the Laplacian; the smallest eigenvalue is always zero.

The overall control objective is to configure the agents and parasitic elements to maximize the connectivity of the network. This goal, when expressed through the Fiedler value, is given as

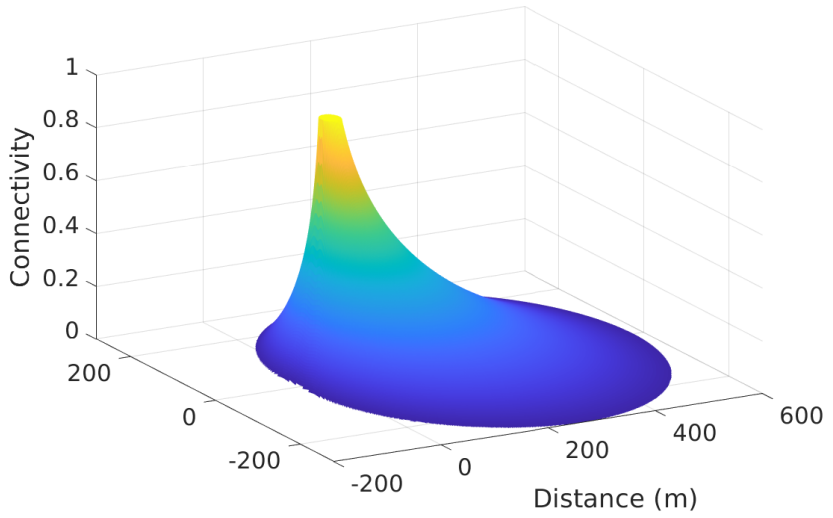

Figure 5.2: Connectivity indicated by colorscale and z-axis plotted between agent i, located at (0,0), and agent j in different (x, y) positions, both with fixed values of θ and ρ.

$$\max_{q_i, \forall i \in [1,n]} \quad \lambda_2(L(q_i)) \tag{5.7}$$

Note that, given the 4 degrees of freedom for each robotic array, we have created a non-convex optimization problem. There are multiple maxima when optimizing connectivity between active antenna agents. Agents can maneuver to decrease their relative distance or increase their gain. This creates an interesting set of trade-offs based on the speed of active antenna agents, the availability of passive antenna agents, and the time required to form and optimize an antenna array.

In [57, 59, 95] the authors formulate a subgradient method for increasing the Fiedler value. We follow the definition of Fiedler as described in Eqn. 2.15.

$$\begin{aligned} \lambda_2(L(q_i)) &= \min_{p \neq 0, p \perp \mathbf{1}} \quad \frac{p^T L(q_i) p}{p^T p} \\ &= \min_{p \neq 0, p \perp \mathbf{1}} \quad \frac{\sum_i^n \sum_j^n A(q_i)_{i,j} (p_i - p_j)^2}{p^T p}, \end{aligned} \tag{5.8}$$

where $\mathbf{1} \in 1^n$ is a vector of size n and p is any unit vector. In this equation, we replace p with v_2, the normalized ($||v_2|| = 1$) left eigenvector corresponding to the Fiedler value. In the sequel, we

sometimes omit stating that λ_2 is a function of q_i explicitly for the sake of brevity.

The differential of λ_2, is

$$\begin{aligned}\frac{\partial \lambda_2(L(q_i))}{\partial q_{i,k}} &= \frac{\partial v_2^T L(q_i) v_2}{\partial q_{i,k}} \\ &= \frac{\partial v_2^T}{\partial q_{i,k}} L(q_i) v_2 + v_2^T \frac{\partial L(q_i)}{\partial q_{i,k}} v_2 + v_2^T L(q_i) \frac{\partial v_2}{\partial q_{i,k}}.\end{aligned} \tag{5.9}$$

Since $L(q_i)^T = L(q_i)$, it follows that

$$\begin{aligned}v_2^T L(q_i) \frac{\partial v_2}{\partial q_{i,k}} &= \frac{\partial v_2^T}{\partial q_{i,k}} L(q_i) v_2 = \lambda_2 \frac{\partial v_2^T}{\partial q_{i,k}} v_2 \\ &= \frac{1}{2} \frac{\partial v_2^T v_2}{\partial q_{i,k}} = \frac{1}{2} \frac{\partial ||v_2||^2}{\partial q_{i,k}} = 0.\end{aligned} \tag{5.10}$$

Following Eqn.5.10 certain terms in Eqn. 5.9 are zero; we can determine a simpler relationship [95].

$$u_{i,k}^c = \dot{q}_{i,k} = \frac{\partial \lambda_2}{\partial q_{i,k}} = v_2^T \frac{\partial L(q_i)}{\partial q_{i,k}} v_2 \tag{5.11}$$

From Eqn. 5.11 it follows that the control for each agent is

$$u_{i,k}^c = v_2^T \frac{\partial L(q_i)}{\partial q_{i,k}} v_2 = \left(\sum_j^n \frac{\partial A(q_i)_{i,j}}{\partial q_{i,k}} (v_{2,i} - v_{2,j})^2 \right). \tag{5.12}$$

Here, i and j are indexing the eigenvector v_2. Using this controller, agents are able to improve connectivity of the system. As in, [59,95] we are implementing a subgradient approach to control agents to maximize the Fiedler value. Agents implementing this controller will always improve the global connectivity of the group. However, since this is a subgradient approach, the controller does not guide the robots on the most efficient trajectory towards better communication.

The partial derivative of the adjacency matrix is

$$\frac{\partial A(q_i)_{i,j}}{\partial q_{i,k}} = \frac{10}{\ln(10) P(q_i, q_j)(P_{high} - P_{low})} \times \frac{\partial P(q_i, q_j)}{\partial q_{i,k}} \tag{5.13}$$

where $\ln$ is the natural logarithm. The derivative $\frac{\partial A(q_i)_{i,j}}{\partial q_{i,k}}$ exists everywhere that a link is sub-optimal. It follows that $\frac{\partial A(q_i)_{i,j}}{\partial q_{i,k}} = 0$ when $A(q_i)_{i,j} = 1$ as the link between i and j cannot be improved.

5.2 Derivation of Controller

The partial derivative of the power with respect to the each of the 4 state variables for agent i is as follows, as defined by Eqn. 5.13: The gain functions are written as $G_i = G(\phi(q_i, q_j), q_{i,4})$ and $G_j = G(\phi(q_j, q_i), q_{j,4})$ to make the following equations easy to read.

$$\frac{\partial P(q_i, q_j)}{\partial q_{i,k}} = \frac{P_j c^2}{(4\pi f)^2} \left(\frac{R(q_i, q_j)^2 \times \frac{\partial}{\partial q_{i,k}} (G_i G_j))}{(R(q_i, q_j)^2)^2} - \frac{(G_i G_j) \times \frac{\partial R(q_i, q_j)^2}{\partial q_{i,k}}}{(R(q_i, q_j)^2)^2} \right), k = \{1, 2, 3, 4\} \tag{5.14}$$

This function is defined for all 4 state variables of active antenna agent i (i.e., $k = \{1, 2, 3, 4\}$).

Let us focus on the x and y states where $k = 1$ is the x component and $k = 2$ is the y component. Here, $R(q_i, q_j)$ is a function of states x_i and y_i.

$$\frac{\partial (R(q_i, q_j)^2)}{\partial q_{i,k}} = 2(q_{i,k} - q_{j,k}), k = \{1, 2\} \tag{5.15}$$

Eqn. 5.14 for $k = 1, 2$ is simplified in Eqn. 5.16

$$\frac{\partial P(q_i, q_j)}{\partial q_{i,k}} = \frac{P_j c^2}{(4\pi R(q_i, q_j) f)^2} \times \left(\frac{\partial}{\partial q_{i,k}} (G_i G_j) - \frac{2(q_{i,k} - q_{j,k})(G_i G_j)}{R(q_i, q_j)^2} \right), k = \{1, 2\} \tag{5.16}$$

As G_i and G_j are functions of all the state variables, we must take the partial derivative of the product of these functions.

$$\frac{\partial}{\partial q_{i,k}} (G_i G_j) = \frac{\partial G_i}{\partial q_{i,k}} G_j + G_i \frac{\partial G_j}{\partial q_{i,k}}, k = \{1, 2, 3, 4\} \tag{5.17}$$

$$\frac{\partial G_i}{\partial q_{i,k}} = \frac{\partial G(\phi(q_i, q_j), q_{i,4})}{\partial \phi(q_i, q_j)} \frac{\partial \phi(q_i, q_j)}{\partial q_{i,k}}, k = \{1, 2, 3, 4\} \tag{5.18}$$

Where $\phi(q_i, q_j)$ is a function of the positions of agents i and j and the orientation of agent j. When the variable $k = 3$, this corresponds to the orientation and $k = 4$ corresponds to the parasitic effect. The parasitic effect of either array has no effect on $\phi(q_i, q_j)$, so it follows that

$$\frac{\partial G(q_i, q_j)}{\partial \phi(q_i, q_j)} = -(q_{i,4}/\alpha) \sin(\phi(q_i, q_j)) \times \frac{\exp((q_{i,4}/\alpha) \cos(\phi(q_i, q_j))}{I_0(q_{i,4}/\alpha)}, k = \{1, 2, 3\} \tag{5.19}$$

and

$$\frac{\partial \phi(q_i, q_j)}{\partial q_{i,k}} = \frac{q_{j,k} - q_{i,k}}{R(q_i, q_j)^2}, k = \{1, 2\}. \tag{5.20}$$

After substituting Eqn. 5.19 and Eqn. 5.20 into Eqn. 5.18 we have the partial derivative of G_i. Note that these equations can be used to find G_j by transposing i and j as shown in Eqn. 5.21.

$$\frac{\partial G_j}{\partial q_{i,k}} = \frac{\partial G(\phi(q_j, q_i), q_{j,4})}{\partial \phi(q_j, q_i)} \frac{\partial \phi(q_j, q_i)}{\partial q_{i,k}} \tag{5.21}$$

We now have all of the necessary components to determine the values of Eqn. 5.16 for $k = 1, 2$. Now, let us look at the partial derivatives with respect to orientation and parasitic effect. In Eqn. 5.16, only $G_i = G(\phi(q_i, q_j), q_{i,4})$ is a function of $q_{i,3}$ or $q_{i,4}$. As a result, several terms drop out as the partial derivatives of $R(q_i, q_j)$ and G_j with respect to $q_{i,3}$ and $q_{i,4}$ are both zero.

$$\frac{\partial P(q_i, q_j)}{\partial q_{i,k}} = \frac{P_j c^2}{(4\pi R(q_i, q_j) f)^2} \frac{\partial G_i}{\partial q_{i,k}} G_j, k = \{3, 4\} \tag{5.22}$$

Eqn. 5.19 and 5.20 can be substituted into this equation. Knowing that $\partial \phi(q_i, q_j)/\partial q_{i,3} = -1$, we can solve Eqn. 5.22 for $k = 3$. Finally, we need the partial derivative of G_i with respect to the parasitic effect $q_{i,4}$ to solve Eqn. 5.22 for $k = 4$.

$$\frac{\partial G_i}{\partial q_{i,4}} = \frac{1}{\alpha}\exp(q_{i,4}/(\alpha\cos(\phi(q_i,q_j)) \times \left(\frac{I_0(q_{i,4}/\alpha)\cos(\phi(q_i,q_j)) - I_1(q_{i,4}/\alpha)}{I_0(q_{i,4}/\alpha)^2}\right) \tag{5.23}$$

This completes the derivation of values in Eqn. 5.13.

5.2.1 Maintaining Connectivity While Pursuing Other Objectives

We make a small change to our system model to incorporate other control inputs. These inputs may be used to guide the translational control of active antenna agents to other control objectives. Thus we update the system model to include this additional controller given by

$$\dot{q}_i = u_i^c + u_i^{mc} \tag{5.24}$$

where $u_i^{mc} \in \mathbb{R}^4$. The control u_i^{mc} must have additional constraints so that our control formulation can maintain communication. First, $u_{i,3}^{mc} = u_{i,4}^{mc} = 0$ for all i. We must also maintain that the translational control component of u_i^{mc} (i.e., $u_{i,1}^{mc}$ and $u_{i,2}^{mc}$) must be bounded as described in [60]. As in [60], we modify our controller defined in Eqn. 5.12 with the addition of $\text{csch}^2(\lambda_2 - \epsilon)$, where

$$\begin{aligned} u_{i,k} &= \text{csch}^2(\lambda_2 - \epsilon) v_2^T \frac{\partial L}{\partial q_{i,k}} v_2 \\ &= \text{csch}^2(\lambda_2 - \epsilon) \left(\sum_j^n -\frac{\partial A(q_i)_{i,j}}{\partial q_{i,k}} (v_{2,i} - v_{2,j})^2 \right). \end{aligned} \tag{5.25}$$

In this equation, $\epsilon \in \mathbb{R}$ is a lower bound for the Fiedler value. Since $\text{csch}^2(\lambda_2 - \epsilon)$ approaches infinity as λ_2 approaches ϵ, the magnitude of control for connectivity becomes large when $\lambda_2 - \epsilon \to 0$, guaranteeing that the system maintains at least this value of global connectivity. Note, $\epsilon < \lambda_2$ at the beginning of every trial. Since the control for other objectives (u_i^{mc}) is bounded, the control for maintaining connectivity u_i^c will always be larger than u_i^{mc} as the Fiedler value approaches ϵ.

5.3 Simulations

We compare our controller from Eqn. 5.25 with the standard approach of moving to increase Fiedler value in the absence of other controllers. Then, we show the capability to form parasitic arrays to enable operation at an extended range when u_i^{mc} is pulling two arrays apart. For our simulations to execute we must make some additional considerations. First, we alter Eqn. 5.24 to be $\dot{q}_i = \text{diag(h)}u_i^c + u_i^{mc}$. This scaling factor $h \in \mathbb{R}^4$, $h_k > 0$, does not affect our previous discussions about how the controller maximizes the Fiedler value or the ability of the controller to overcome the bounded control input u_i^{mc}. It compensates for the discrepancy in magnitude between the state positions x_i and y_i, the orientation θ_i, and parasitic effect ρ_i. Another way to view h is as a parameter capturing the arrays' ability to move, re-orient, or form an array. We set the parameter $h = [200, 200, 1, 1]$ for a scenario where active ground antenna robots move slowly relative to flying passive antenna robots.

Another practical question is how to overcome saddle points in our optimization. When $\rho_i \equiv q_{i,4} = 0$, saddle points exist for our sub-gradient method controlling orientation. From Eqn. 5.19 we can see that $\rho_i = 0$ results in $\frac{\partial A(q_i)_{i,j}}{\partial \theta_i} = 0$. This is a problem when the array is facing away from the optimal direction where $\frac{\partial A(q_i)_{i,j}}{\partial q_{i,4}} < 0$. We assume the passive antenna robot UAVs can fly directly over the active ground antenna robot in response to this negative value to change orientation by π radians when $\frac{\partial A(q_i)_{i,j}}{\partial q_{i,4}} < 0$ and $\rho_i = 0$. As a result, there are discontinuities in orientation, but these discontinuities occur only when $\rho_i = 0$ for a given i. Other saddle points may be present, but in simulation, the controller escaped them.

5.3.1 Verifying Communications Maintenance

We compare active antenna agents, which can acquire up to 6 passive antenna agents, with the case when active antenna agents do not have passive antenna agents. In the single active antenna agent case, the beam pattern is uniformly omnidirectional; therefore it is implementing a disk connectivity model approach. In both cases, we initialize the simulation with $n = 4$ active

agents, $q_1 = [-100, 0, 0, 0]$, $q_2 = [100, 0, 0, 0]$, $q_3 = [-50, 25, 0, 0]$, $q_4 = [50, -25, 0, 0]$. We set $u_i^{mc} = [0, 0, 0, 0]$ to test the Fiedler value maximization without other controllers present. Initially, all of the agents share an edge (i.e., $A(q_i)_{i,j} > 0, i \neq j$). We set time step $d_t = 0.4$ s and $\epsilon = 0$. For active antenna agents that cannot form parasitic antenna arrays, we set $\rho_i = 0$ regardless of the control input; mathematically, this is the same as the disk model approach described in [60]. The parasitic effect of all agents in both cases is initially zero. In Fig. 5.3 we show the trajectories of both approaches (with and without array forming). Interestingly, in both cases, the agents follow the same paths to maximize the Fiedler value but the agents that cannot form arrays are controlled to move closer together than the agents that can form arrays. Similarly, in Fig. 5.4 our approach achieves a higher Fiedler value in the same amount of time than the agents which cannot form arrays.

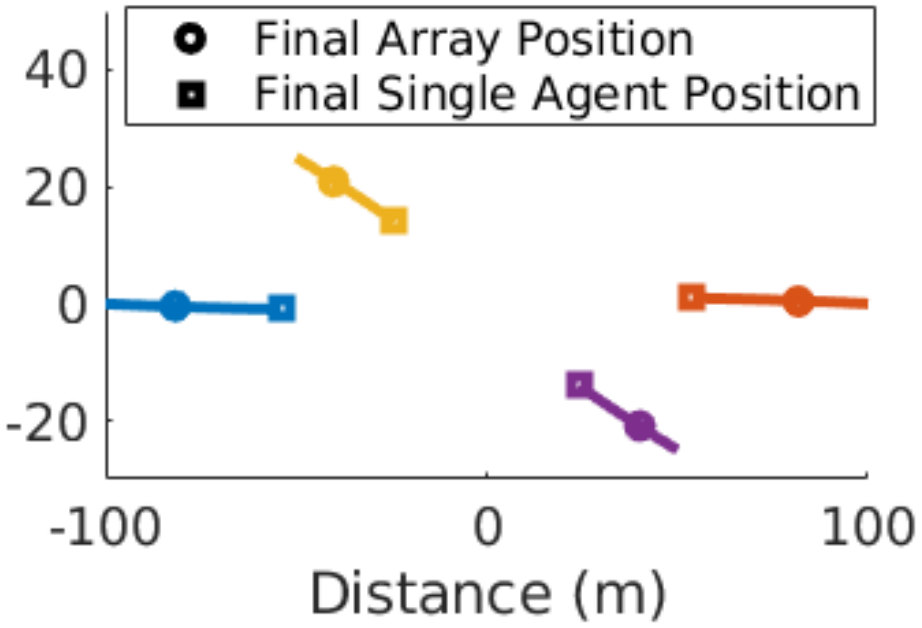

Figure 5.3: Trajectories of active antenna agents. Square markers denote the final positions of the single, non-array-forming agents which employ a disk model. Circle markers denote the final positions of the array forming active antenna agents. [1] ©2020 IEEE

This difference in final position and Fiedler value demonstrates that if the agents can form arrays, they will always outperform existing Fiedler maximization approaches that assume a disk model. The array forming capability allows these array forming agents to have a higher Fiedler

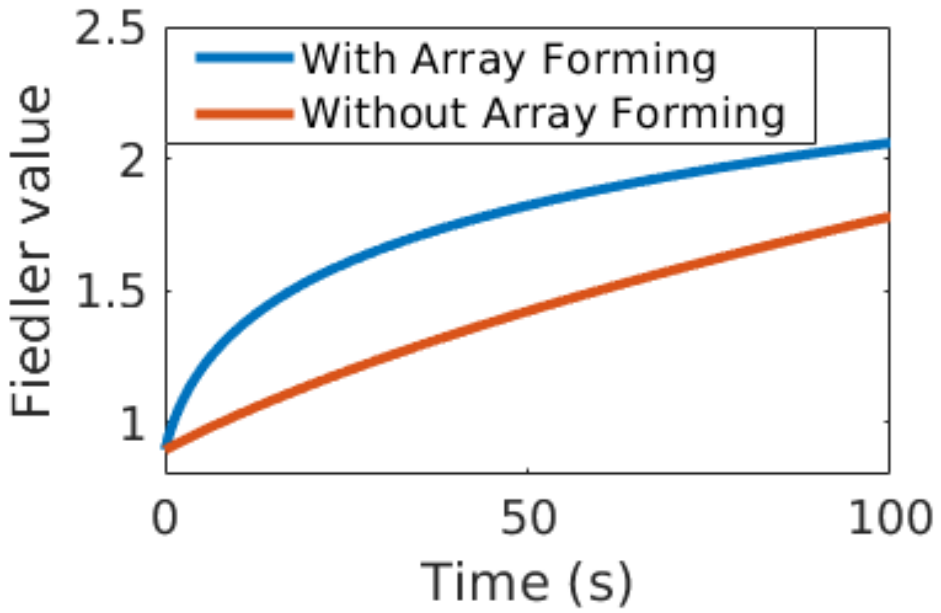

Figure 5.4: Fiedler value over time for both trials of agents shown in Fig. 5.3. [1] ©2020 IEEE

value than the more closely spaced agents which cannot form arrays. If an active antenna agent can easily form an antenna array, communications links between two active antenna agents can be improved far more quickly than if the agents were to drive towards each other.

5.4 Results and Discussion

Another interesting feature of our array forming approach is where active antenna agents form arrays of different sizes. In Fig. 5.5 we plot the parasitic effect of the agents which are able to form antenna arrays from the comparison trial shown in Fig 5.3. Agents 1 (blue) and 2 (red) form larger arrays than agents 3 (yellow) and 4 (purple). As the parasitic effect increases, the beam pattern is more directional. When arrays become more directional, overall connectivity might be reduced by weakening links that are not in the direction of maximum gain. Our subgradient approach is sensitive to this through the summation of link gradients in Eqn. 5.25. As a result, active agents stabilize their arrays at a certain size. Similarly, an antenna array should have a more directional beam pattern when the agents it has links to are confined to a smaller angular range. This angular distribution is more confined when agents are farther from

the centroid of the array forming agents. Consequently, the active antenna agents form larger arrays at larger distances, and hence ,agents 1 and 2 form larger arrays than agents 3 and 4.

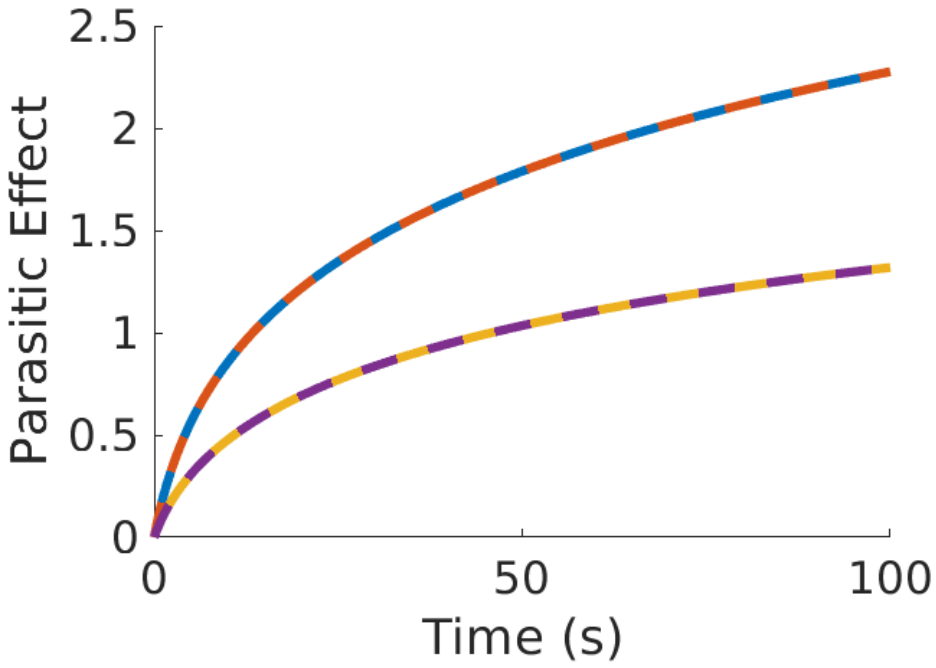

Figure 5.5: Parasitic effect (ρ) of the 4 arrays over time. The plot colors match the agents' colors from the trajectories in Fig.5.3 ending with the circle marker. [1] ©2020 IEEE

5.4.1 Effects of Array Forming on Operational Range

We constructed a simple scenario where there are two active antenna agents with $u_1^{mc} = [-5, 0, 0, 0]$ and $u_2^{mc} = [5, 0, 0, 0]$ in order to determine the effects of the array forming on the operational range. This controller u_i^{mc} causes the active antenna agents to drive away from each other, but our connectivity maintenance controller u_i^c maintains communication between the active antenna agents. These agents begin on the x-axis ($q_1 = [-50, 0, 0, 0], q_2 = [50, 0, 0, 0]$). From this initial configuration, we run 13 tests. We consider up to 12 agents divided between 2 active antenna agents for forming parasitic arrays. If there is an even number of passive antenna agents in the trial, the passive antenna agents are divided equally between active antenna agents 1 and 2. If there is an odd number of passive antenna agents, agent 1 is allowed 1 more than agent

2. All parameters are the same as in earlier simulations. The results of this set of tests can be seen in Fig. 5.6.

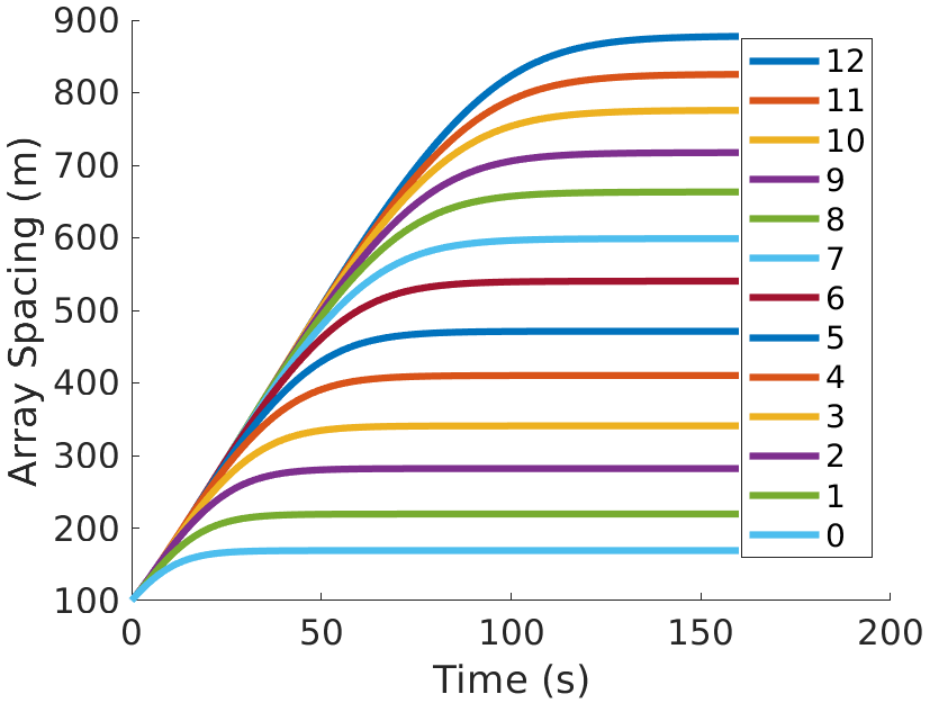

Figure 5.6: Maximum distance between 2 active antenna agents which form parasitic arrays. Each plot corresponds to the number of passive agents available to form arrays. [1] ©2020 IEEE

These results demonstrate that there is a range benefit with the addition of each successive passive antenna agent in this simple scenario with only 2 active antenna agents. At the end of the test, all of the arrays had reached an equilibrium between u_i^c and u_i^{mc} controllers. This equilibrium is between u_i^c pushing the active antenna agents closer together to maintain good communication and u_i^{mc} pulling the active antenna agents apart.

5.4.2 Multiple Trials

We also conducted 100 trials with these four active antenna agents from random initial positions. In Fig. 5.7, we have overlaid all of the trajectories from these four agents from all 100 trials. The random start locations are taken from a uniform distribution. The four colors correspond to each of the four active antenna agents. In all of these trials, the trajectories of each

of the four active antenna agents converge towards each other.

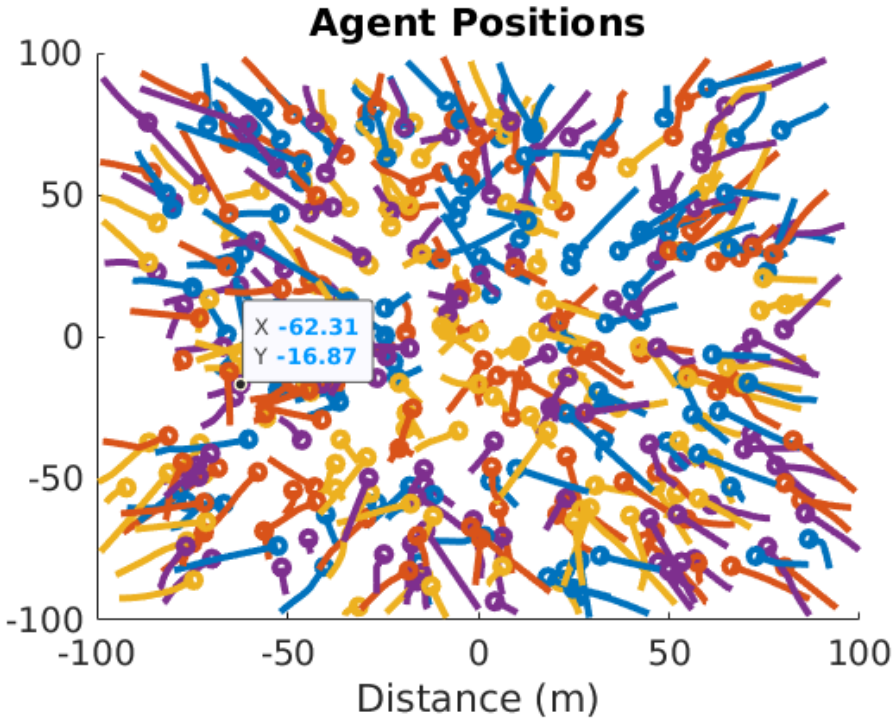

Figure 5.7: Trajectories and final positions of each of the four active antenna agents is initialized at random locations

Fig. 5.8, has the plots of the Fiedler values from each of these 100 trials. In each trial, our controller increases Fiedler value. This result validates our simulation implementation. It also demonstrates that in many initial configurations, the controller will increase Fiedler value by moving agents closer together, increasing the parasitic effect, and rotating to increase gain. In Chapter 6, we go further to prove our controller's ability to maintain or increase the Fiedler value, our metric for overall network connectivity by showing that the Fiedler value is lower bounded.

In this chapter, we have proposed a more general model of power transmitted and received to and from networked agents. This model relates the size of parasitic arrays to their directionality and seamlessly integrates into an approach for maximizing the Fiedler value, a metric of overall network connectivity.

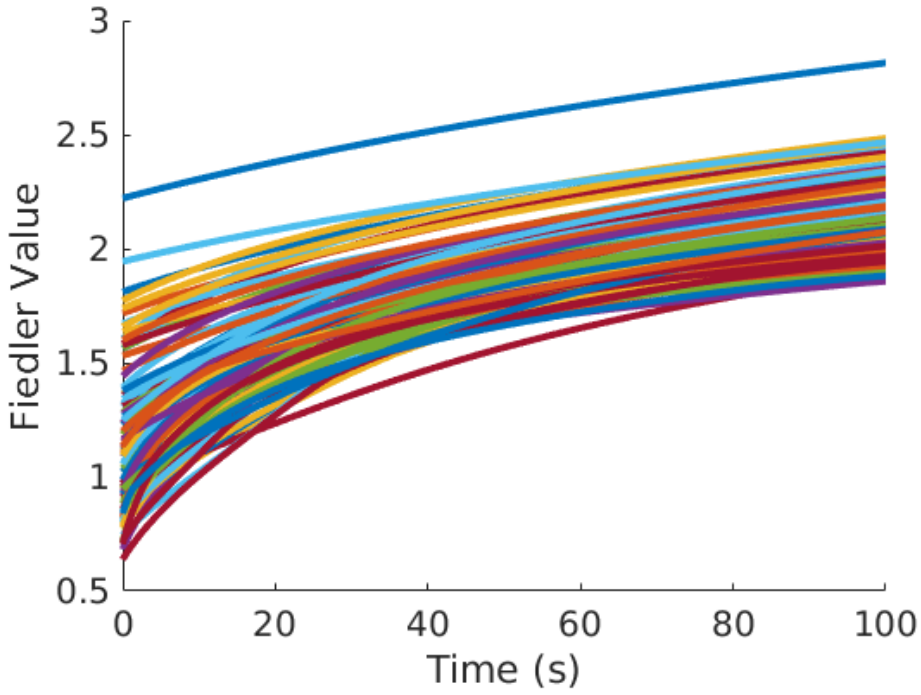

Figure 5.8: Fiedler value of each of the four active antenna agents initialized at random locations.

Chapter 6: Reallocation of Array Forming Robots with Constraints

In Chapter 5, we showed how each additional available passive antenna agent increases the distance between two arrays in Fig. 5.6. The passive antenna agents are a discrete resource for extending the communication range of arrays and are shared by all connected arrays. Until this point in the dissertation, we only considered arrays that gained passive antenna agents. However, if a passive antenna agent that is increasing the range/directionality of one array is reallocated to another array, overall array connectivity can decrease instantaneously; the advantage of reallocating the passive antenna agent is only achieved after it is positioned within the desired array which, requires additional time. This drop in connectivity during reallocation could catastrophically disband the multiagent system of arrays. An integrated approach is required for passive antenna agent allocation and control of array positioning and size to maintain connectivity between arrays. Developing and proving this integrated approach is the focus of this chapter, and the content will be submitted as a journal paper. Fig. 6.1 shows a scenario where such an approach is necessary. In this figure, two different roles for robotic arrays are depicted. *Motion-controlled arrays*, shown with a blue arrow outline, have control inputs that guide them farther apart, as the arrow directions indicate. This control input guides the array in a desired direction for achieving an arbitrary objective. *Relay arrays*, shown with a red circle outline, act as communication relays for the motion-controlled arrays. Without constraints on the available passive antenna agents, simulations from [1] (Chapter 5) show that the motion-controlled arrays increase the number of passive antenna agents in the array as they move farther apart to maintain communication. Therefore, as array roles and motion control input change, an approach is required for allocating passive antenna agents so that the group of arrays can span larger distances while guaranteeing a level of

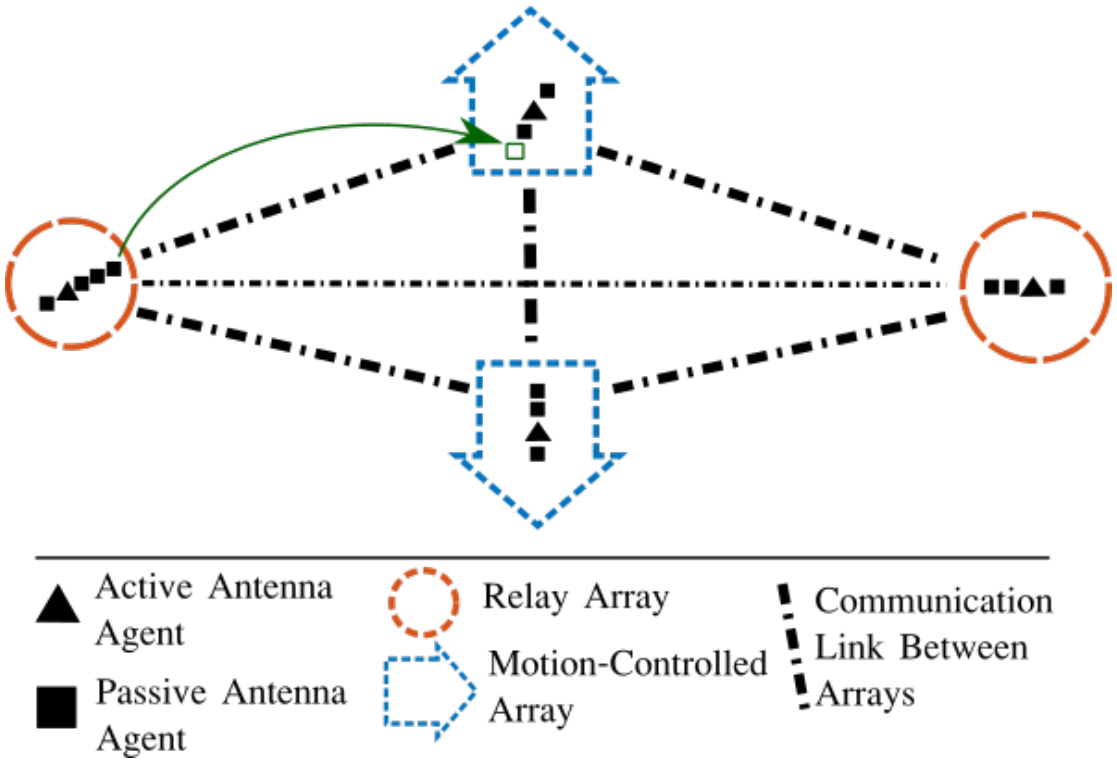

Figure 6.1: A motion-controlled array needs to acquire a passive antenna agent from a relay array to move in a desired direction while maintaining connectivity. However, the proposed reallocation shown by the green arrow can instantaneously reduce the overall connectivity of the arrays.

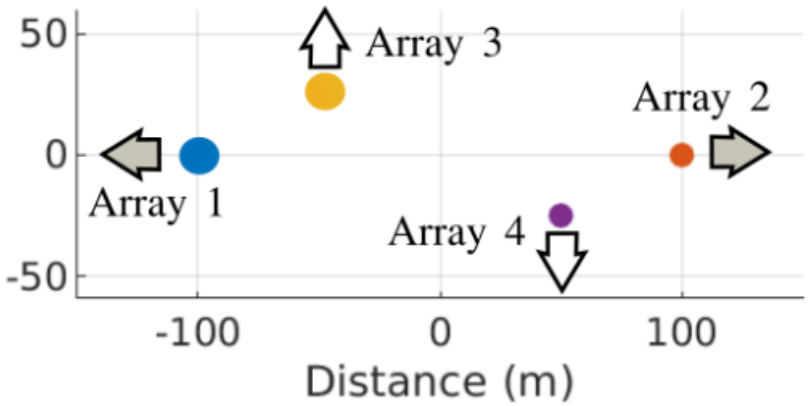

(a) The initial position of robotic antenna arrays with white or grey shaded arrows indicating the direction of their velocity control inputs which are applied at alternating times. The shading for each arrow indicates when these control inputs are applied in Fig. 6.2b.

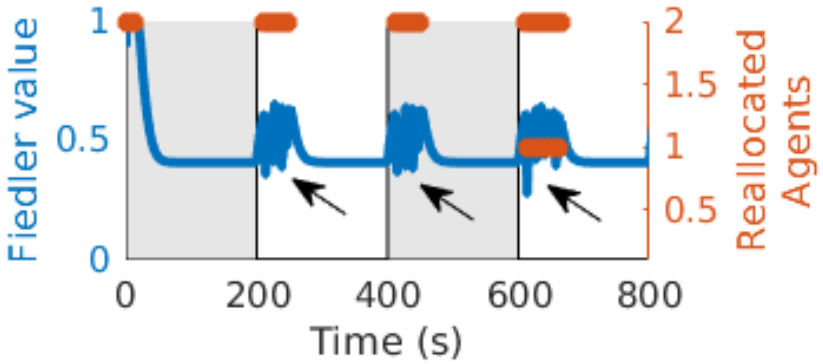

(b) Fiedler value and number of reallocations v. time: Black arrows point to instances where the Fiedler value falls below an acceptable threshold.

Figure 6.2: Trial with a simple approach to reallocating agents

overall network connectivity between arrays.

To illustrate this, we instantiate a simulated scenario where we apply an additional motion control to push specific robotic arrays away from each other as shown in Fig. 6.2. This motion control alternates maximizing the spacing of arrays 1 and 2 along the x-axis for 200 s and then maximizing the spacing of arrays 3 and 4 along the y-axis for 200 s.

Over the duration of this test, the communications maintenance control input increases the Fiedler value, while the additional motion control input forces the agents to alternate maximizing the distance between two robotic arrays. In this simulation, we implement a simple reallocation algorithm that assigns passive antenna agents to arrays so as to increase the Fiedler value at the

greatest rate. This greedy approach to increasing the Fiedler value rapidly oscillates its allocation of passive antenna agents at times indicated by the arrows in Fig. 6.2b. At instances when the reallocation occurs, λ_2 decreases instantaneously, sometimes below a set $\lambda_2 = 0.45$ threshold. Many multi-robot systems need to maintain communication to continue functioning. A sharp drop in communication, as reflected in λ_2, may not allow the multi-robot system to continue functioning in a desired manner. We pursue an approach to reallocating passive antenna agents while ensuring the Fiedler value is lower bounded.

Our contributions to solving this problem in this chapter are as follows. We first demonstrate that in the absence of constraints on passive antenna agents, the connectivity maintenance approach proposed in Chapter 5 maintains a lower bound for overall network connectivity with and without motion control input. Then we specify an algorithm for allocating passive antenna agents under constraints and additionally formulate a control input for deallocating passive antenna agents from a robotic array. Finally, we formulate a controller which complements the allocation algorithm by deallocating passive antenna agents from relay arrays while still guaranteeing array connectivity.

6.1 Related Work

Since individual, discrete agents form the parasitic arrays, it is clear that some portion of this problem is a mixed-integer program (MIP). While algorithms for solving these problems exist, many do not have guaranteed convergence properties. Popular approaches for solving MIPs include branch and bound as well as cutting plane methods that could be used for optimally allocating passive antenna agents given some set of fixed array orientations and positions. However, the results shown in Fig. 6.2b demonstrate that reallocating agents between arrays is more complex than solving a mixed-integer program (MIP) as this might cause a temporary reduction of communication and oscillating reallocation.

In robotics, multi-robot task allocation is achieved by robots using market-based approaches

for bidding on tasks that they estimate they will be able to accomplish [65] and allocate themselves in the presence of communication constraints [42]. This structure is not easy to integrate with the existing robotic array control approach. Game-theoretic approaches are not relevant here as our robotic arrays are working cooperatively to optimize a global metric [129]. Passive agent allocation is not a submodular problem, so we cannot deploy solvers that take advantage of submodularity. Adding passive antennas to a robotic array increases signal power within a sector but decreases power elsewhere. When there are more than two robotic arrays it is easy to construct a scenario where adding passive antenna agents does not yield positive yet diminishing returns [130]. An appropriate approach would solve the MIP while remaining within the feasible set, like an interior point method [131]. However, such an allocation approach is one side of a feasible solution for reallocating passive antenna agents. An approach for safely reducing the gain magnifying effect of a passive antenna agent is necessary so that it can leave an array without dangerously reducing connectivity.

6.2 Approach

As in Chapter 5, the arrays are approximated by the following single integrator dynamics. However, in the following equation, the control inputs are updated.

$$\dot{q}_i = \text{diag}(h)u_i^c + u_i^{mc} + u_i^{pd} \tag{6.1}$$

In this equation, $u_i^c \in \mathbb{R}^4$, the *connectivity* maintenance control, actuates each of the 4 states with the objective of increasing communication. This controller, described in [1], continuously increases the Fiedler value. The parameter $h \in \mathbb{R}^{+4}$ is a gain value that determines how sensitive each state is to the controller, where $\mathbb{R}^+$ is the set of positive real numbers. We choose values for h that make the controller actuate parasitic effect and orientation states more than translation states as the passive antenna agents are more agile and quickly adjust the orientation and parasitic effect of the robotic arrays. The function, $\text{diag}(\cdot)$, places the values of h on the diagonal of a

4×4 matrix. The *motion control* input, $u_i^{mc} \in \mathbb{R}^4$, is bounded and actuates the first two states to push motion-controlled arrays towards positions to achieve an arbitrary goal. The *passive antenna agent deallocation* control input $u_i^{pd} \in \mathbb{R}^4$ is defined in Sec. 6.2.4 and enables the deallocation of passive antenna agents from relay arrays so that they can be reallocated to a motion-controlled array. By definition, motion-controlled robotic arrays have a motion control input (i.e., $\left\|u_{i,1:2}^{mc}\right\| > 0$ and $u_{i,k}^{pd} = 0$) where $i \in N_{mc}$ is the set of motion-controlled arrays. Otherwise, it is a relay array where $u_{i,k}^{mc} = 0$ and $i \in N_r$ is the set of relay arrays. The roles of the motion-controlled and relay arrays are mutually exclusive and $N_{mc} \cup N_r = N$. The control inputs and states for these arrays are shown in Tab. 6.1.

Table 6.1: Robotic Array i States and Control Inputs

x_i, y_i	position of robotic array i
θ_i	orientation of robotic array i
ρ_i	parasitic effect of robotic array i
q_i	$[x_i, y_i, \theta_i, \rho_i]$, state of robotic array i
u_i^c	connectivity maintenance control of robotic array i
u_i^{mc}	motion control input of robotic array i
u_i^{pd}	passive antenna agent deallocation and motion compensating controller of robotic array i

6.2.1 Connectivity Maintenance Control for All Arrays

The Fiedler value, λ_2, is continuously improved among the robotic arrays by descending an energy function.

Definition 1 The following energy function $V(q_i) = V(\lambda_2(L(q_i))), \forall i \in N : \mathbb{R}^4 \mapsto \mathbb{R}$ is

$$V(\lambda_2(L(q_i))) = \begin{cases} \coth(\lambda_2(L(q_i)) - \epsilon)), & \lambda_2(L(q_i)) > \epsilon \\ 0 & \text{o.w.} \end{cases} \tag{6.2}$$

The value $\epsilon \in \mathbb{R}^+$ is a parameter which we will show lower bounds λ_2. As shown in Fig. 6.3, $\lim_{\lambda_2 \to \epsilon} V(q_i) = \infty$. Since $\max(\lambda_2) = n$, then $V(q_i)$ converges to $\coth(n - \epsilon)$. Using this

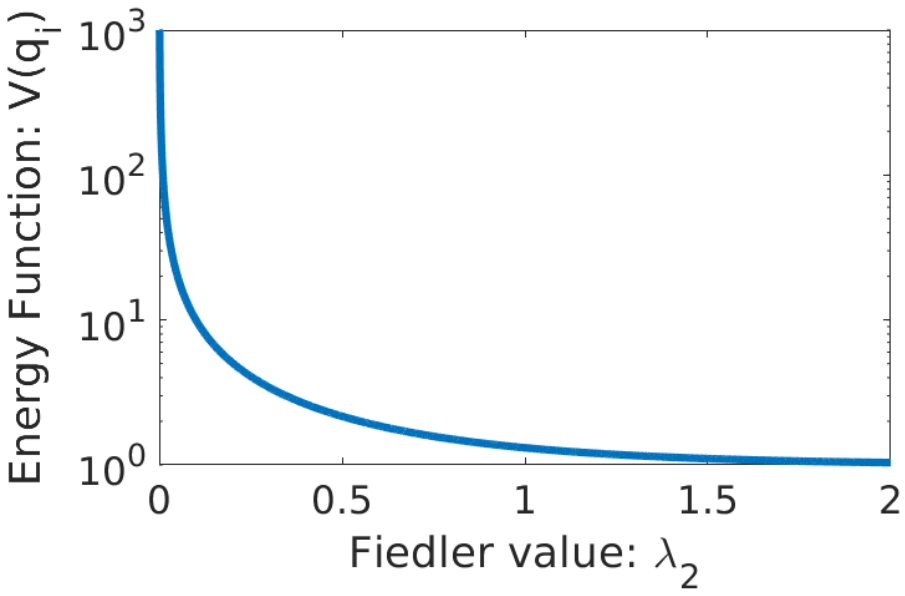

Figure 6.3: The energy function of λ_2 where $\epsilon = 0$

notation, we formulate the connectivity maintenance control input that descends the gradient of $V(q_i)$, as

$$u^c_{i,k} = -\frac{\partial V(q_i)}{\partial q_{i,k}} = -\frac{\partial V(q_i)}{\partial \lambda_2(L(q_i))}\frac{\partial \lambda_2(L(q_i))}{\partial q_{i,k}}. \tag{6.3}$$

Using a subgradient method, the connectivity maintenance control $u^c_i(q_i)$ can be formulated as follows.

$$\begin{aligned} u^c_{i,k} &= \operatorname{csch}^2(\lambda_2 - \epsilon)\frac{\partial \lambda_2}{\partial q_{i,k}} \\ &= \operatorname{csch}^2(\lambda_2 - \epsilon)\left(\sum_j^n \frac{\partial A(q_i)_{i,j}}{\partial q_{i,k}}(v_{2,i} - v_{2,j})^2\right) \end{aligned} \tag{6.4}$$

In this equation, v_2 is the normalized ($||v_2|| = 1$) left eigenvector corresponding to λ_2. The Fielder value, λ_2, is piece-wise continuously differentiable with respect to $q_{i,k}$, so $V(q_i)$ smoothly decreases. Consider the case when $u^{mc}_{i,k} = u^{pd}_{i,k} = 0, \forall i$, and hence from Eqn. 6.1, $\dot{q}_i = \operatorname{diag}(h)u^c_i = \operatorname{diag}(h)\nabla_q V(q_i)$; differentiating $V(q_i)$, we get the following.

$$\dot{V}(q_i) = \nabla^T_q V(q_i)\dot{q}_i = -\left(\nabla^T_q V(q_i)\right)\operatorname{diag}(h)\nabla_q V(q_i) \leq 0 \tag{6.5}$$

Since diag(h) is positive definite we can deduce the following.

$$\sum_{i \in N} \dot{V}(q_i) \leq 0 \tag{6.6}$$

Hence, if $\lambda_2 > \epsilon$ at $t = 0$, then $\lambda_2 > \epsilon, \forall t \geq 0$.

6.2.2 Additional Motion Control Input for Motion-Controlled Arrays

One advantage of this connectivity maintenance strategy is that u_i^c is small when $\lambda_2 - \epsilon >> 0$. This allows us to specify the additional control input u_i^{mc}, which can guide robotic arrays in desired directions but may also reduce λ_2. Since motion-controlled arrays have $u_{i,k}^{pd} = 0$, only u_i^{mc} could reduce λ_2 below ϵ. Potential functions are often used for obstacle avoidance and planning to a goal [132]. In an approach similar to [133], this connectivity maintenance controller will guarantee connectivity is maintained if the motion control input takes the form $u_i^{mc} = -\operatorname{diag}(h)\nabla_q U(q_i)$ where $U(q)$ is a positive-definite potential function.

Proposition 1: Consider the closed-loop system dynamics described in Eqn. 6.1 and Eqn. 6.4. Let $u_i^{mc} = -\operatorname{diag}(h)\nabla_q U(q_i)$ and $u_{i,k}^{pd} = 0$. If $\lambda_2 > \epsilon$ at $t = 0$, then $\lambda_2 > \epsilon, \forall t \geq 0$.

Proof. Let

$$T(q) = \sum_{i \in N} V(q_i) + U(q_i) \tag{6.7}$$

We compute the time derivative of T(q):

$$\begin{aligned}
\dot{T}(q) =& \sum_{i \in N} \left(\nabla_q^T V(q_i) + \nabla_q^T U(q_i) \right) \dot{q}_i \\
=& \sum_{i \in N} \left(\nabla_q^T V(q_i) + \nabla_q^T U(q_i) \right) (- \operatorname{diag}(h) \nabla_q V(q_i) \\
& - \operatorname{diag}(h) \nabla_q U(q_i)) \\
=& - \sum_{i \in N} \left(\nabla_q^T V(q_i) + \nabla_q^T U(q_i) \right) \operatorname{diag}(h) \\
& (\nabla_q V(q_i) + \nabla_q U(q_i)) \\
\leq& 0
\end{aligned} \tag{6.8}$$

With a slight abuse of notation, for this discussion, we will refer to $T(t)$ and $V(t)$, even though $T(\cdot)$ and $V(\cdot)$ are not explicit functions of time. It is evident that $V(t) \leq T(0), \forall t$ and hence is bounded. Consequently, $\lambda_2 > \epsilon, \forall t \geq 0$. □

Now consider a more general motion controller which is not necessarily the gradient of a potential function with a bounded input where $\|u_i^{mc}\|_2 \leq u^{max} \in \mathbb{R}$. As shown in [60], this bounded control input does not push λ_2 below ϵ when there is no deallocation control input (i.e., $u_{i,k}^{pd} = 0$). We include the following proof for the sake of completeness.

Proposition 2: Consider the closed-loop system dynamics described in Eqn. 6.1 and Eqn. 6.4. Let $\|u_i^{mc}\|_2 \leq u^{max}$ and $u_{i,k}^{pd} = 0$. If $\lambda_2 > \epsilon$ at $t = 0$, then $\lambda_2 > \epsilon, \forall t \geq 0$.

Proof. Evaluate the time derivative of energy function $V(q_i)$ after substituting the system model in Eqn. 6.1.

$$
\begin{aligned}
\dot{V}(q_i) &= \nabla_q^T V(q_i)\dot{q}_i, \\
&= \sum_{i\in N}\sum_{k=1}^{4}\left[\frac{\partial V(q_i)}{\partial q_{i,k}}\right]\dot{q}_{i,k} \\
&= \sum_{i\in N}\sum_{k=1}^{4}\frac{\partial V(q_i)}{\partial \lambda_2}\frac{\partial \lambda_2}{\partial q_{i,k}}\left(-\frac{\partial V(q_i)}{\partial \lambda_2}\frac{\partial \lambda_2}{\partial q_{i,k}}h_k + u_{i,k}^{mc}\right) \\
&= \frac{\partial V(q_i)}{\partial \lambda_2}\sum_{i\in N}\sum_{k=1}^{4}\frac{\partial \lambda_2}{\partial q_{i,k}}\left(-\frac{\partial V(q_i)}{\partial \lambda_2}\frac{\partial \lambda_2}{\partial q_{i,k}}h_k + u_{i,k}^{mc}\right)
\end{aligned}
\tag{6.9}
$$

Since u_i^{mc} is bounded with magnitude u^{max}, the time derivative $\dot{V}(q_i)$ can be restated as the following.

$$
\begin{aligned}
\dot{V}(q_i) \leq \underbrace{\frac{\partial V(q_i)}{\partial \lambda_2}}_{\leq 0}\sum_{i\in N}\Bigg[&\underbrace{-\frac{\partial V(q_i)}{\partial \lambda_2}\left\|\mathrm{diag}(h)\frac{\partial \lambda_2}{\partial q_i}\right\|_2^2}_{\geq 0} \\
&\underbrace{-\left\|\mathrm{diag}(h)\frac{\partial \lambda_2}{\partial q_i}\right\|_2 u^{max}}_{\geq 0}\Bigg]
\end{aligned}
\tag{6.10}
$$

As indicated by the brackets under terms in the equation, $\dot{V}(q_i) < 0$ if the difference of the two terms is positive for each $i \in N$; the following inequality maintains this positive difference between the two terms with $-\operatorname{csch}^2(\lambda_2 - \epsilon)$ substituted for $\frac{\partial V(q_i)}{\partial \lambda_2}$.

$$
\begin{aligned}
\sum_{i\in N}&\left(\operatorname{csch}^2(\lambda_2-\epsilon)\left\|\mathrm{diag}(h)\frac{\partial \lambda_2}{\partial q_i}\right\|_2^2\right) \\
&\geq \sum_{i\in N}\left(\left\|\mathrm{diag}(h)\frac{\partial \lambda_2}{\partial q_i}\right\|_2 u^{max}\right)
\end{aligned}
\tag{6.11}
$$

Assuming that $\left\|\frac{\partial \lambda_2}{q_i}\right\|_2 \neq 0$, the inequality in Eqn. 6.11 can be evaluated as follows:

$$
\operatorname{csch}^2(\lambda_2-\epsilon) \geq u^{max}\frac{\sum_{i\in N}\left\|\mathrm{diag}(h)\frac{\partial \lambda_2}{\partial q_i}\right\|_2}{\sum_{i\in N}\left\|\mathrm{diag}(h)\frac{\partial \lambda_2}{\partial q_i}\right\|_2^2}
\tag{6.12}
$$

Note that this condition is always satisfied as $\lim_{\lambda_2 \to \epsilon} \operatorname{csch}^2(\lambda_2 - \epsilon) = \infty$. Solving for λ_2:

$$\lambda_2(q_i) \geq \operatorname{csch}^{-1}\left(\left(u^{max}\frac{\sum_{i\in N}\left\|\operatorname{diag}(h)\frac{\partial\lambda_2}{\partial q_i}\right\|_2^2}{\sum_{i\in N}\left\|\operatorname{diag}(h)\frac{\partial\lambda_2}{\partial q_i}\right\|_2^2}\right)^{\frac{1}{2}}\right) + \epsilon \tag{6.13}$$

The function $\operatorname{csch}^{-1}(\cdot)$ is the inverse function of $\operatorname{csch}(\cdot)$. The condition in Eqn. 6.12 is always maintained, and therefore $\lambda_2 \geq \epsilon$ always exists. If the q_i states are initialized at time $t = 0$ such that the condition in Eqn. 6.12 is maintained, then $\lambda_2 \geq \epsilon, \forall t \geq 0$. In cases where $\left\|\frac{\partial\lambda_2}{q_i}\right\|_2 = 0$, λ_2 is not changing, and therefore λ_2 is trivially lower-bounded by its initial value. Therefore, from Eqn. 6.13 $\lambda_2 \geq \epsilon, \forall t \geq 0$.

□

6.2.3 Allocating Constraints on the Number of Passive Antenna Agents for All Arrays

In order to set up our allocation problem, we prescribe that $\rho_i^{max} \in \mathbb{Z}$ is the most passive antenna agents that can be acquired by motion-controlled or relay robotic array i. It should be noted that the connectivity maintenance controller increases $\rho_i \equiv q_{i,4}$ when $\frac{\partial\lambda_2}{\partial q_{i,4}} > 0$ and hence when $\rho = \rho^{max}$ we set the control input $u_{i,4}^c = 0$ where $\dot{q}_i = h_4 u_{i,4}^c + u_{i,4}^{mc} + u_{i,4}^{pd}$ as stated in Eqn. 6.1. This stops ρ_i from becoming larger than ρ_i^{max}. The value, λ_2 is still lowered bounded in this situation as the motion and orientation of the parasitic arrays can still be actuated to descend the gradient of $V(q_i)$ with respect to q_i.

The following are considerations for setting ρ_i^{max}. For Yagi-Uda arrays, the benefit of each additional passive antenna diminishes [127]. Correspondingly, we should limit ρ_i^{max} to an arbitrary number of passive antenna agents as the cost and benefit of scaling a robotic parasitic antenna array is an open research question. For this paper, we prescribe that $\rho_i^{max} \leq 6$. We also assume there is a finite pool of m passive antenna agents. To address this practical constraint we need an algorithm that can set ρ_i^{max} such that $\sum_{i\in N}\rho_i^{max} \leq m$. When $\sum_{i\in N}\rho_i^{max} < m$, there

are passive antenna agents that are not allocated to an array and are free to join any array. We formulate Alg. 4 to allocate these free passive antenna agents by calculating ρ_i^{max} for all i robotic arrays.

Algorithm 4 Constrained Passive Allocation Algorithm

1: $\rho_i^{max} \leftarrow \lceil \rho_i \rceil$
2: $m_{free} \leftarrow m - \sum_i^n \rho_i^{max}$
3: $N_{sorted} \leftarrow SORT([\partial\lambda_2/\partial q_{i,4}, N], "descending")$
4: **for each** $i \in N_{sorted}$ **do**
5: **if** $\{m_{free} > 0\} \cap \{\rho_i^{max} < 6\}$ **then**
6: $\rho_i^{max} \leftarrow \rho_i^{max} + 1$
7: $m_{free} \leftarrow m_{free} - 1$
8: **end if**
9: **end for**

Alg. 4 allocates free passive antenna agents to active antenna agents with greater $\frac{\partial\lambda_2}{\partial q_{i,4}}$ values. We hypothesize this allocation will lead to a greater increase in λ_2 since this term in Eqn. 6.4 causes ρ_i to increase in order to maintain connectivity. In this algorithm, line 2 calculates $m_{free} \in \mathbb{Z}$, the number of free passive antenna agents that are not part of an array. The list, N_{sorted}, is arranged starting with the robotic array with the greatest value for $\frac{\partial\lambda_2}{\partial q_{i,4}}$. The robotic array at the top of the list is assigned an additional passive antenna agent by increasing ρ_i^{max} if $m_{free} > 0$ and the current $\rho_i^{max} < 6$. The algorithm iterates through this list, assigning additional passive antenna agents if they are available. This algorithm runs periodically, while the control for the robotic arrays is calculated continuously. If a robotic array is not allocated any passive antenna agents, it will simply be omnidirectional. As long as the robotic arrays start with a feasible allocation, any algorithm, including Alg 4, for allocating free passive antenna agents will return a feasible result, and u_i^c will maintain $\lambda_2 > \epsilon$. Note that if an active antenna agent has the ability to gain a passive antenna agent, the algorithm does not imply that active antenna agents will suddenly have a parasitic effect corresponding to ρ_i^{max}. The parasitic effect still follows our single integrator dynamics model when $\rho_i < \rho_i^{max}$. In the case where the parasitic effect for an agent i decreases so that $\rho_i^{max} - \lceil \rho_i \rceil \geq 1$, at least one of the passive antenna agents in array i is available for reallocation. However, the connectivity maintenance controller does

not reduce the parasitic effect unless it increases λ_2. Consequently, passive antenna agents will not necessarily be well allocated after some amount of time. In simulations, we have found that Alg. 4 allocations are strongly determined by the initial states of the active antenna agents and therefore need a deallocation control input to free passive antenna agents.

6.2.4 Passive Antenna Agent Deallocation for Relay Arrays

When a motion-controlled robotic array $j \in N_{mc}$ requires a passive antenna agent and $m_{free} = 0$, we change the control input of the relay arrays so that their passive antenna agents can be deallocated and then reallocated by Alg 4. We set $u^c_{i,4} = 0$ for relay array i so that it cannot increase the parasitic effect of the relay arrays as stated in Sec. 6.2.3. In addition, we apply a control input, $u^{pd}_{i,4}$ that reduces the parasitic effect in relay arrays. In this situation, we set $u^{pd}_{i,4}$ as proportional to the sum of $u^c_{j,4}$ for motion-controlled arrays.

$$\begin{aligned} &u^c_{i,4} = 0, i \in N_r \\ &u^{pd}_{i,1:3} = 0, u^{pd}_{i,4} = -\gamma_i \sum_{j \in N_{mc}} u^c_{j,4}, i \in N_r \end{aligned} \tag{6.14}$$

This approach causes relay arrays to decrease parasitic effect at a rate proportional to that which motion-controlled arrays would increase parasitic effect if passive antenna agents were available. The parameter γ_i is a weighting parameter that determines the rate at which the relay arrays will decrease their parasitic effect. While this approach does not guarantee $\lambda_2 > \epsilon$, we show that this deallocation control works well to deallocate passive antenna agents in Sec 6.3.

6.2.5 Motion Compensation Control for Relay Arrays

Here we consider how relay arrays, which by definition have $u^{mc}_{i,k} = 0$, can reduce parasitic effect without reducing λ_2. As indicated in Eqn. 6.9, a single array can increase $V(q_i)$ by controlling one degree of freedom and decrease $V(q_i)$ by control of a different degree of freedom. Consequently, we control individual relay arrays to move in directions that increase λ_2 to compensate

for reducing ρ_i when the connectivity maintenance controller would otherwise increase ρ_i.

$$u_{i,1:2}^{pd} = \frac{g_{mc}}{a_i}\frac{\partial \lambda_2}{\partial q_{i,1:2}}, u_{i,3}^{pd} = 0, i \in N_r. \tag{6.15}$$

This control input is a vector in the direction of increased λ_2 scaled by gain $g_{mc} \in \mathbb{R}^+$. The value $a_i = \sqrt{\left(\frac{\partial \lambda_2}{\partial q_{i,1}}\right)^2 + \left(\frac{\partial \lambda_2}{\partial q_{i,2}}\right)^2}$ is the magnitude of the x and y direction inputs for increasing λ_2 for each i relay array. Here, a_i and g_{mc} are used in our reformulation of the parasitic effect reduction control input.

$$u_{i,4}^{pd} = -\frac{g_{mc}a_i}{\frac{\partial \lambda_2}{\partial q_{i,4}}}, i \in N_r \tag{6.16}$$

We use $\frac{\partial \lambda_2}{\partial q_{i,4}}$ to weigh how much the parasitic effect can decrease due to the compensated motion from $u_{i,1:2}^{pd}$. From Eqn. 6.4, $\frac{\partial \lambda_2}{\partial q_{i,4}} > 0$ when the connectivity maintenance controller increases the parasitic effect. The product of g_{mc} and a_i of the motion control components are both positive, therefore $u_{i,4}^{pd} < 0$. Consequently, we can demonstrate ρ_i will always be decreased or remain constant by $u_{i,4}^{pd}$, for relay arrays while maintaining $\lambda_2 > \epsilon$.

Proposition 3: Consider the closed-loop system dynamics described in Eqn. 6.1 and Eqn. 6.4. Let $u_{i,4}^{c} = 0$, $u_{i,k}^{mc} = 0$, $u_{i,1:2}^{pd} = \frac{g_{mc}}{a_i}\frac{\partial \lambda_2}{\partial q_{i,1:2}}$, $u_{i,3}^{pd} = 0$, and $u_{i,4}^{pd} = -\frac{g_{mc}a_i}{\frac{\partial \lambda_2}{\partial q_{i,4}}}$ when $\frac{\partial \lambda_2}{\partial q_{i,4}} > 0$. If $\lambda_2 > \epsilon$ at $t = 0$, then $\lambda_2 > \epsilon, \forall t \geq 0$.

Proof. Evaluate $\dot{V}(q_i)$ after substituting in the control inputs for Eqn. 6.1.

$$\begin{aligned}\dot{V}(q_i) =& \nabla_q^T V(q_i)\dot{q}_i, \\ =& \frac{\partial V(q_i)}{\partial \lambda_2}\sum_{i \in N_r}\left(\sum_{k=1}^{3}\left(-\frac{\partial V(q_i)}{\partial \lambda_2}\left(\frac{\partial \lambda_2}{\partial q_{i,k}}\right)^2 h_k\right)\right. \\ &\left. + \sum_{k=1}^{4}\left(\frac{\partial \lambda_2}{\partial q_{i,k}}u_{i,k}^{pd}\right)\right)\end{aligned} \tag{6.17}$$

If $\sum_{k=1}^{4}\left(\frac{\partial \lambda_2}{\partial q_{i,k}}u_{i,k}^{pd}\right) = 0$ then the components of u_i^{pd} cancel each other out. Substituting Eqn. 6.15 and Eqn. 6.16, this term is evaluated as

$$\sum_{k=1}^{4}\left(\frac{\partial\lambda_2}{\partial q_{i,k}}u_{i,k}^{pd}\right)=\sum_{k=\{1,2\}}\left(\frac{\partial\lambda_2}{\partial q_{i,k}}\right)^2\frac{g_{mc}}{a_i}-\frac{\partial\lambda_2}{\partial q_{i,4}}\frac{g_{mc}a_i}{\frac{\partial\lambda_2}{\partial q_{i,4}}}. \tag{6.18}$$

We can also substitute in a_i^2 for $\sum_{k=\{1,2\}}\left(\frac{\partial\lambda_2}{\partial q_{i,k}}\right)^2$.

$$\sum_{k=1}^{4}\left(\frac{\partial\lambda_2}{\partial q_{i,k}}u_{i,k}^{pd}\right)=a_i^2\frac{g_{mc}}{a_i}-\frac{\partial\lambda_2}{\partial q_{i,4}}\frac{g_{mc}a_i}{\frac{\partial\lambda_2}{\partial q_{i,4}}}=0 \tag{6.19}$$

Since this term is 0, the remaining terms are from the connectivity maintenance controller which we have demonstrated maintains $\lambda_2 > \epsilon, \forall t \geq 0$.

□

In cases where a relay array cannot move to increase λ_2, $a_i = 0$ and therefore $u_{i,k}^{pd} = 0$. Consequently, no deallocation will occur and $\lambda_2 > \epsilon, \forall t \geq 0$.

6.3 Simulations

We created a scenario where this reallocation problem often needs to be solved. As in Fig. 6.1, there are four arrays where two arrays initially assume the motion-controlled role and two initially assume the relay array role. The motion-control input pushes motion-controlled arrays farther apart. Periodically, we swap which arrays are in the motion-controlled and relay roles. This role swapping causes the arrays to acquire passive antenna agents, which later should be reallocated to increase λ_2 and enable the motion-controlled agents to span a greater distance while maintaining connectivity. The initial positions for each of the four arrays are shown in Fig. 6.2a and motion control input is stated for each time interval in Tab. 6.2.

In these simulations, all arrays initialize with $\rho_i = 0$. There is a pool of 12 passive antenna agents that can be used by any active antenna agent to build an array. We choose these initial positions to evaluate our approach's sensitivity to initial states. In this scenario, arrays 1 and 2 initialize with a greater distance than arrays 3 and 4. This configuration causes the connectivity maintenance controller to increase the parasitic effect for arrays 1 and 2 more

Table 6.2: The directions that arrays are guided when they assume the motion-controlled role ($u^{mc}_{i,3:4} = 0$).

	t=[0,200)	t=[200,400)	t=[400,600)	t=[600,800)
$u^{mc}_{1,1:2}$	[-1,0]	[0,0]	[-1,0]	[0,0]
$u^{mc}_{2,1:2}$	[1,0]	[0,0]	[1,0]	[0,0]
$u^{mc}_{3,1:2}$	[0,0]	[0,1]	[0,0]	[0,1]
$u^{mc}_{4,1:2}$	[0,0]	[0,-1]	[0,0]	[0,-1]

quickly. Consequently, arrays 1 and 2 have an initial advantage in receiving passive antenna agents; this yields insight into how sensitive each approach is to initial allocations. The control parameters are $h = [1e4, 1e4, 10, 40]$, $\epsilon = 0$, The controller and states are calculated every 0.2 s while the allocating algorithm runs every second for all scenarios. When implementing the deallocation approach $\gamma_{i \in N_r} = 1/n_{mc}$ where n_{mc} is the number of arrays in N_{mc}. In the motion compensation control approach $g_{mc} = 1.0$.

In Fig. 6.4, we show the limitations of an approach where passive antenna agents are allocated using Alg. 4 but $u^{pd}_{i,k} = 0$ by comparing it with an integrated approach using Alg. 4 and $u^{pd}_{i,k}$ as specified in Sec. 6.2.4. The parasitic effect plotted in Fig. 6.4a demonstrates Alg. 4 alone is not sufficient for allocating passive antenna agents. In the first 80 s, Alg. 4 allocates all m of the passive antenna agents from the pool. After this point, the passive antenna agents are already allocated in a way that favors a large distance between arrays 1 and 2. Even though the parasitic effect fluctuates, no reallocation is possible, since no passive antenna agents are deallocated. If this simulation were to continue further in time, arrays 1 and 2 would maintain their allocation of passive antenna agents even when assuming relay array roles. This demonstrates Alg. 4 implemented without a deallocation control input is very sensitive to initialization, which is not desirable.

In comparison, when implementing the deallocation control as described in Sec 6.2.4 in Fig. 6.4b, the effect of this deallocation approach is clear; the number of passive antenna agents that each array is allocated varies, and arrays are allocated more passive antenna agents when in the motion-controlled role. This reallocation demonstrates that the combination of Alg. 4 with

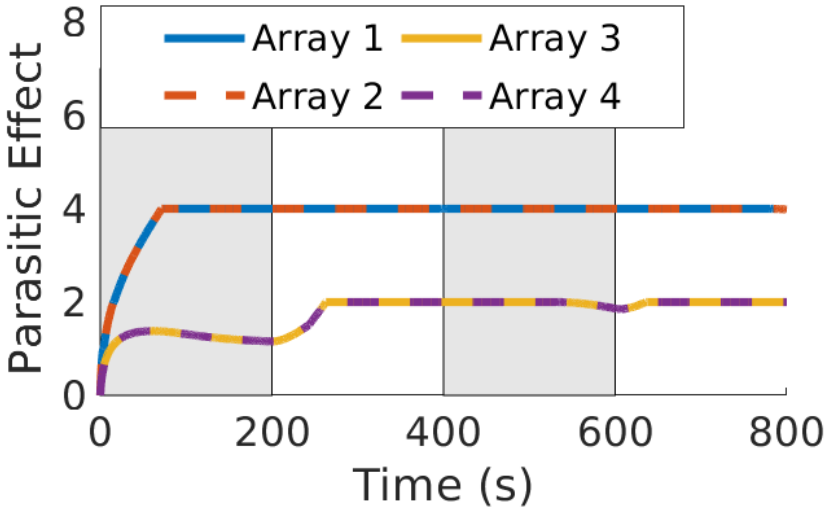

(a) Parasitic effect over time using only Alg. 4

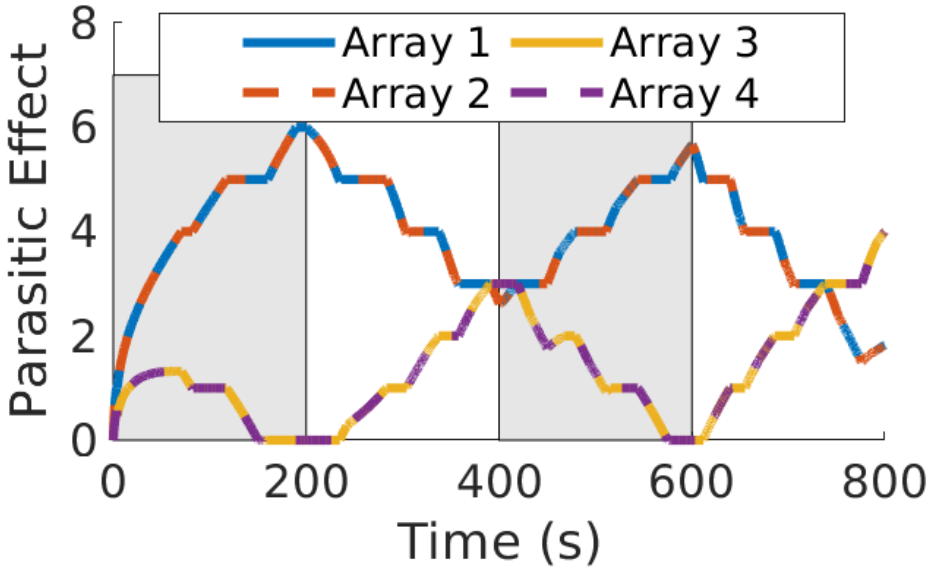

(b) The parasitic effect over time with Alg. 4 implemented with deallocation control (no motion compensation).

Figure 6.4: Comparison of the parasitic effect with and without the deallocation controller described in Sec. 6.2.4

our deallocation controller successfully (re)allocates passive antenna agents and is not sensitive to initial conditions.

6.4 Results and Discussion

Now, we are ready to compare λ_2 of all three approaches. Afterward, we plot something similar to a Pareto Frontier to compare the efficacy of these three approaches for maintaining λ_2 and increasing distance between the motion-controlled arrays. The variation in λ_2 during these simulations arises from three phenomena. In each of the four intervals, there is an increase in λ_2 as u_i^c guides initial array formation and orientation and a decrease in Fiedler when arrays maintain constant size but are still increasing distance. This phenomenon is most clear in the approach using only Alg. 4 (blue). The second source of λ_2 variation is present in the deallocation controller (red) and motion compensating (yellow) control input; there are brief, small-amplitude oscillations in Fiedler as deallocation decreases λ_2 and allocation of the newly free passive antenna agents increase λ_2. The third source of variation is from the motion compensating controller. It drives the motion of the relay arrays towards the centroid of the four arrays with an additional magnitude to the connectivity maintenance controller. As a result, λ_2 is higher, which is the intended result of the motion compensating controller. The motion compensating controller does not remove the brief, small-amplitude oscillations as these oscillations are caused by u_i^{mc} and the corresponding array building. Notice that λ_2 for the first 300s are the same for the Alg. 4 approach and the motion compensation approach as u_i^{pd} is only active when $m_{free} = 0$ and $\frac{\partial \lambda_2}{\partial q_{i,4}} > 0$.

We plot λ_2 vs. motion-controlled array distance to compare the different approaches to (re)allocation in Fig. 6.6. This enables us to evaluate how well our reallocation approaches enable arrays to span greater distances while maintaining connectivity. In our testing scenario, there are four time intervals. We plot Fiedler and motion-controlled array distance of the latter 100 s of each interval to demonstrate the performance after passive antenna agent allocations have been made. As both λ_2 and distances between motion-controlled arrays are increased, the

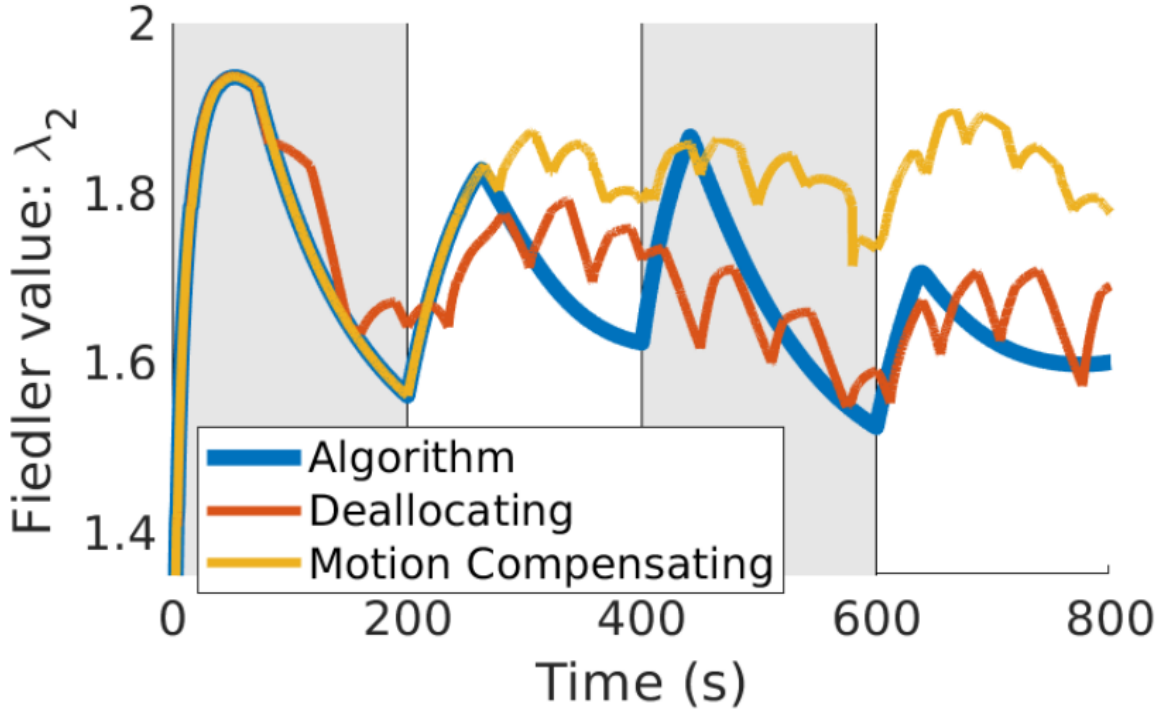

Figure 6.5: Fiedler value over time for 3 different methods of (re)allocating passive antenna agents

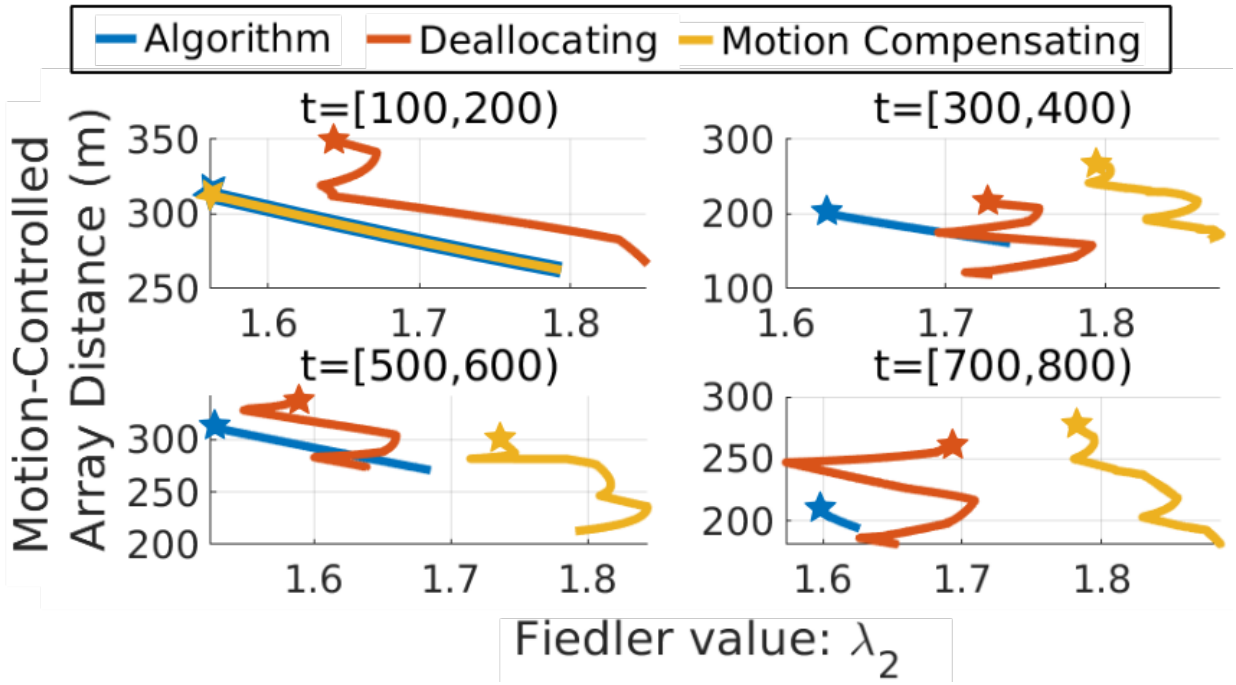

Figure 6.6: Trajectories created by different approaches: Points with the smallest array distances are at the beginning of time interval t as the additional motion control increases the spacing between motion-controlled arrays. The values at the end of each interval are marked with a star.

best approach will have values in the upper right of each plot. When comparing these trajectory-frontiers, the motion compensating control approach performs better with respect to λ_2. The motion compensation approach guides relay arrays to positions that increase λ_2 more quickly (i.e., the centroid of the arrays) and therefore, these closely spaced arrays are at a disadvantage when the arrays swap roles. As a result, the deallocation control sometimes performs better with respect to increasing motion-controlled array distance than the motion compensation control. Overall, the motion-compensation approach to deallocation performs the best when integrated with Alg. 4 for enabling motion controlled arrays to span large distances while maintaining connectivity.

Chapter 7: Contributions and Conclusions

In this dissertation, we describe our investigation into the control of robotic parasitic antenna arrays, a novel method for increasing the range of compact low-VHF antennas. This control work is especially impactful when considering the deployment of agents in complex indoor and outdoor environments in contexts where reliable wireless communication infrastructure does not exist. At the beginning of this research endeavor, we had just discovered the possibility of creating a robotic parasitic antenna array and demonstrated some fundamental properties as to how these arrays may be constructed. Using this foundational work, we developed and tested methods for improving the range of a reliable signal. From two perspectives in this dissertation, we made contributions that enable the control of robotic agents forming parasitic arrays.

7.1 Contributions

From a narrow perspective, we experimentally investigated control to calibrate a single parasitic array to increase the directional gain. We established bounds for antenna element spacing and parasitic element length using simulation and parasitic array design techniques. Using these bounds, we developed an approach for calibrating robot-reflector spacing and reflector length, which we verified experimentally. Finally, we compared the optimal configurations in the presence of different ground media.

From a slightly wider perspective, we investigated and demonstrated the ability to increase the gain of a parasitic array and preserve this gain in NLOS. This investigation was predicated on a hypothesis about how to maintain the calibrated gain by maintaining antenna and robot formations within the array. Using this hypothesis, we proposed a method for rotating a formation

of two antennas through the controlled motion of a UGV carrying one of the antennas. During this rotation of the array, we showed that the array gain is reliably maintained. Then, we described two scenarios where the robotic parasitic array must rotate to maintain or increase RSS when receiving a signal from a transmitting mobile node. In the first scenario, this mobile node must move through a complex environment and communicate with the parasitic array. In response to this motion, the robotic parasitic array must rotate to track the mobile node and maintain enhanced RSS. In the second scenario, the array and mobile node are far apart, but the array can detect the RSS of the mobile node. In response, the robotic parasitic array must rotate to increase RSS. For these two scenarios, we proposed and experimentally tested approaches for controlling the robotic array to increase RSS. The results showed that the robotic parasitic array maintains a higher RSS than a signal transmitted through a single compact low-VHF antenna, which already has an improved range over UHF systems in line-of-sight (LOS) and non-line-of-sight (NLOS) conditions.

From an even wider perspective, we used our insight from this experimental research to develop a model and control approaches for guiding the creation, motion, and evolution of these arrays. This control approach enabled these arrays and their constitutive robotic agents to maintain a metric of overall network connectivity. We introduced a variable state, called parasitic effect, to describe the number of passive antenna agents in a robotic parasitic array. This state indicates how many robots are in the array and how close they are to optimal placement. Then, we developed a model of the induced beam pattern as a function of the parasitic effect. Afterward, we formulated a Fiedler value maximization approach for groups of parasitic antenna arrays. Using this control approach, we compared connectivity maintenance among agents that can form parasitic arrays and those that cannot. This comparison demonstrated that our controller could properly actuate the size of the robotic parasitic arrays.

Finally, we investigated how passive antenna agents forming the array could be safely reallocated to other arrays. We first demonstrated that in the absence of constraints on passive antenna agents, the connectivity maintenance controller maintains a lower bound for overall

network connectivity with and without motion control input. Afterward, we specified an algorithm for allocating passive antenna agents under constraints and additionally formulated a control input for deallocating passive antenna agents from a robotic array. Finally, we formulated a controller that complements the allocation algorithm by deallocating passive antenna agents from relay arrays while still guaranteeing array connectivity.

7.2 Array Gain Control

In Chapter 3, we advanced research that enables robots to increase the directionality of a signal that will penetrate large structures and enable reliable wireless communication in several ways. We described and tested a noise resilient method for robots to optimize their spacing and reflector length. We verified this approach in several different outdoor environments and compared their optimal configurations. Without any additional antenna design, we achieved a gain of 2.2 dB. We focused on the case of using a single excited array element (i.e., the reflector). However, combinations of multiple exciters and passive elements can be employed [88] [89] for greater gain. This is an interesting extension for further study in our context.

In Chapter 4, we demonstrated the ability to increase RSS with a small amount of robotic motion by forming and rotating a robotic parasitic array in a complex, NLOS environment, thereby extending the range of low-VHF antennas demonstrated to perform more reliably in complex environments. First, we showed that our implementation of a boundary following controller reliably maintained the RSS gained through forming the robotic parasitic array while changing its orientation. Then we successfully tested an approach for maintaining gain created by the array by rotating the boresight of the array to track the mobile node in LOS and NLOS conditions. Finally, we successfully tested a gradient ascent-based approach for rotating the array to increase RSS when the mobile node was at an unknown, far position in NLOS.

7.2.1 Future Control Research in Array Creation

There are many ways this research on parasitic array gain optimization from Chapter 3 and Chapter 4 could be extended. Additional characterization is required to understand how non-homogeneous ground media and ground typologies affect the array; in these situations, it is unclear if it is appropriate to have an excited/driven element aligned with the reflector and receiver. It is also important to understand how array configuration affects the gain around the array. Further antenna design and research are probably necessary to make adjustable compact parasitic elements that couple to achieve closer to the theoretical 5 dB gain. Autonomous construction and optimization of robotic parasitic arrays with more than two elements should also be researched. There are interesting trade-offs in gain or directionality and time to configure a robotic parasitic array with more antenna elements.

Subsequent control work could investigate other ways for the mobile node and parasitic array to collaborate and use feedback. Tasking additional robots to form the array would increase the array gain along with the complexity of actuating and optimizing the array. Further research is also required to identify when a telemetry-informed or gradient ascent approach is appropriate and which environmental conditions or ranges cause the directionality of a robotic parasitic array to diminish. Finally, the variation in gain that we see in our experiments as a function of position implies that the passive coupling with the environment is an exciting way of increasing gain for extending the communication range with robotic parasitic arrays.

Another avenue of research is learning models to accelerate the optimization of gain created by forming robotic parasitic arrays. Preliminary research indicates that the complexity of mutual coupling increases as additional passive antennas are added. If these robotic agents could learn a model for spacing themselves in the presence of different ground media, deploying and controlling robotic parasitic arrays could be faster. Similar approaches could be applied to create parasitic arrays that do not mirror the Yagi-Uda designs.

7.3 Network Connectivity Maintenance

In Chapter 5, we described a new model for extending the range of reliable, long-range, low-VHF communication signals. This was accomplished by developing a controller for a robotic array that optimized and appropriately defined a graph-theoretic metric. Our simulations demonstrated that array forming is more useful for improving communication when passive agent motion is less costly than active agent motion, and when traversing the environment is difficult. As a result, this capability should be especially useful in indoor and urban environments where walls induce movement constraints. An additional advantage of using this approach in these complex environments is that the low-VHF signal created by forming the array is more reliable at a longer range than when compared with microwave radio frequency technology (e.g., Wi-Fi and cellular). Parasitic array formation also becomes more valuable as the cost of radios powering the active antennas increases.

In Chapter 6, we demonstrated a controller for maintaining communication through the formation of robotic parasitic antenna arrays that will maintain $\lambda_2 > \epsilon$. Next, we described an algorithm for allocating free passive antenna agents and then an approach for deallocating passive antenna agents from arrays so that they could be allocated. Finally, we computed an appropriate control that uses robotic array motion to compensate for passive antenna agent deallocation in order to maintain $\lambda_2 > \epsilon$. This proves that our approach for controlling robotic parasitic arrays will enable these groups of robotic agents to maintain communication as they move, change size, and alter orientation.

7.3.1 Future Connectivity Research with Robotic Arrays

There are a number of things we could explore further with robotic parasitic arrays that maintain connectivity. First, we could make parasitic array formation more realistic by accounting for the motion constraints imposed by indoor and urban environments. This would mean passive antenna agents take time to transfer into and out of parasitic arrays, and constrain robotic array

orientation and formation. Adding, these complexities would allow us to investigate trade-offs in mission time and motion capabilities. The ability of passive antenna agents to become active therefore, nodes in the graph is another interesting research avenue. In addition, the approach for reallocating passive antenna agents could be decentralized. Research into the formation of shorter-distance links created by passive agents is another area of interest. This could motivate interesting research in multi-level graphs.

7.4 New Research Threads

There are several ways to expand upon the research conducted in this dissertation. Some of these approaches involve removing simplifying assumptions used to abstract the model of the robotic parasitic array for connectivity maintenance control, while others aim to better understand different aspects of parasitic array formation. In our connectivity maintenance research, we do not model the communication between passive antenna agents. However, modeling the communication of the m small, agile agents and n active antenna agents would create a richer network connectivity problem. These agile agents could either be passive agents within the robotic parasitic array or could relay Wi-Fi signals between robotic arrays. There is an optimization problem one would need to solve to maximize communication with respect to how these m agents are allocated. To solve this problem, one would need to model the communication capability of these agents at Wi-Fi with a multi-layer graph. One layer would be low-VHF communication, and another would be Wi-Fi communication. One would need to create a new metric for overall connectivity which does not favor adding nodes. Since $\max(\lambda_2) = n$, where n is the number of nodes in the graph, one would need to remove the bias towards adding nodes to increase Fiedler value. One would also need to create a controller that can (re)allocate passive agents to arrays or to positions where they can act as relays. This research is interesting for several reasons. It would compare array forming with relaying (e.g., how does Wi-Fi range affect the utility of forming an array vs forming a mesh network). Rich, graph-based representations are very popular right now because of machine learning approaches, and our research could draw from or impact that as well. This

complements the research we have done in routing data over different channels. However, it is not clear what the best model or control approach might be. Another drawback might be that the allocation might be difficult to formulate in a way that enables interesting claims to be made. It could be best represented as a mixed-integer programming problem.

One clear direction for future work is a more realistic implementation and simulation of our parasitic array forming controller and platforms. One of the advantages of operating at low-VHF is the reliable, through-wall penetration of the communication signal. However, our controller is implemented assuming that robotic arrays do not have to navigate around obstacles. In order to further compare array forming with multi-hop network communications maintenance, one could remove assumptions that hinder this comparison. Adding a more realistic environment will help us understand how the agility of the active and passive antenna agents affects the value of forming robotic parasitic antenna arrays.

If multiple active agents form a beamforming array, where all agents broadcast at the same time, their coherent signal is much more powerful and their signal will propagate farther as discussed in Chapter 2. The theoretical gain for this type of antenna array is n^2, where n is the number of active antennas forming an array. For simplicity, we could still assume that there is one active antenna agent, around which a robotic antenna array is formed. However, the receive gain for this type of antenna array only scales with n. With this knowledge, we know that we will have to update our model for power. The most important change would be that $P(q_{i,k}, q_{j,k}) \neq P(q_{j,k}, q_{i,k})$. Therefore $A_{i,j} \neq A_{i,j}^T$. As a result, we must consider a directed graph as opposed to an undirected graph. This would require a different control approach to ensure the graph remains strongly connected. Reallocating agents forming this type of array is also a different.. Using the motion of one agent to compensate for losing an agent forming the array will not be possible in some topologies. This research could be impactful as this type of array is more powerful and multi-agent antenna arrays of this type are better researched in the antenna and wireless communication research communities. Optimizing strongly connected graphs is a well researched topic in robotics.

Bibliography

[1] Jeffrey N. Twigg, Nikhil Chopra, and Brian M. Sadler. Communication maintenance of robotic parasitic antenna arrays. *IEEE Robotics and Automation Letters*, 5(4):6475–6482, 2020.

[2] Jeffrey Twigg, Fikadu T. Dagefu, Nikhil Chopra, and Brian M Sadler. Robotic parasitic array optimization in outdoor environments. In *2019 IEEE International Symposium on Safety, Security, and Rescue Robotics (SSRR)*, pages 1–8. IEEE, 2019.

[3] Fikadu T. Dagefu, Jeffrey N. Twigg, Chirag R. Rao, and Brian M. Sadler. Directional communication enabled by mobile parasitic elements. In *2019 International Conference on Military Communications and Information Systems (ICMCIS)*, pages 1–7. IEEE, 2019.

[4] Jason Gregory, Jonathan R. Fink, Ethan Stump, Jeffrey N. Twigg, John Rogers, David Baran, Nicholas Fung, and Stuart Young. Application of multi-robot systems to disaster-relief scenarios with limited communication. In *Field and Service Robotics*, pages 639–653. Springer International Publishing, 2016.

[5] Fikadu. T. Dagefu, Jihun Choi, Morteza Sheikhsofla, Brian M. Sadler, and Kamal Sarabandi. Performance assessment of lower vhf band for short range communication and geolocation applications. *Radio Science*, 50(5), May 2015.

[6] Y. Tadjdeh. Air force must prepare for battle in urban environments. *[Online]. Available: http://www.nationaldefensemagazine.org/articles/2017/9/19/goldfein-air-force-must-prepare-for-battle-in-urban-environments. [Accessed: 24-Sep-2017]*, 2017.

[7] Jeffrey G. Andrews, Stefano Buzzi, Wan Choi, Stephen V. Hanly, Angel Lozano, Anthony C.K. Soong, and Jianzhong Charlie Zhang. What will 5g be? *IEEE Journal on selected areas in communications*, 32(6):1065–1082, 2014.

[8] Xuemin Hong, Jing Wang, Cheng-Xiang Wang, and Jianghong Shi. Cognitive radio in 5g: a perspective on energy-spectral efficiency trade-off. *IEEE Communications Magazine*, 52(7):46–53, 2014.

[9] Theodore S. Rappaport, George R MacCartney, Mathew K. Samimi, and Shu Sun. Wideband millimeter-wave propagation measurements and channel models for future wireless communication system design. *IEEE Transactions on Communications*, 63(9):3029–3056, 2015.

[10] Erik G. Larsson, Ove Edfors, Fredrik Tufvesson, and Thomas L. Marzetta. Massive mimo for next generation wireless systems. *IEEE Communications Magazine*, 52(2):186–195, 2014.

[11] Mahmoud Kamel, Walaa Hamouda, and Amr Youssef. Ultra-dense networks: A survey. *IEEE Communications Surveys Tutorials*, 18(4):2522–2545, 2016.

[12] S. Mohammad Razavizadeh, Minki Ahn, and Inkyu Lee. Three-dimensional beamforming: A new enabling technology for 5g wireless networks. *IEEE Signal Processing Magazine*, 31(6):94–101, 2014.

[13] Grady Williams, Nolan Wagener, Brian Goldfain, Paul Drews, James M Rehg, Byron Boots, and Evangelos A Theodorou. Information theoretic mpc for model-based reinforcement learning. In *International Conference on Robotics and Automation (ICRA)*, 2017.

[14] Alex Kushleyev, Daniel Mellinger, Caitlin Powers, and Vijay Kumar. Towards a swarm of agile micro quadrotors. *Autonomous Robots*, 35(4):287–300, 2013.

[15] Fikadu T. Dagefu, Gunjan Verma, Chirag R. Rao, L. Yu Paul, Jonathan R. Fink, Brian M. Sadler, and Kamal Sarabandi. Short-range low-vhf channel characterization in cluttered environments. *IEEE Transactions on Antennas and Propagation*, 63(6):2719–2727, 2015.

[16] Fikadu T. Dagefu, Jihun Choi, Morteza Sheikhsofla, Brian M. Sadler, and Kamal Sarabandi. Performance assessment of lower VHF band for short-range communication and geolocation applications. *Radio Science*, 50(5):443–452, 2015.

[17] Fikadu T. Dagefu, Jungsuek Oh, Jihun Choi, and K. Sarabandi. Measurements and physics-based analysis of co-located antenna pattern diversity system. *IEEE Transactions on Antennas and Propagation*, 61(11):5724–5734, 2013.

[18] Jungsuek Oh, Jihun Choi, Fikadu T Dagefu, and Kamal Sarabandi. Extremely small two-element monopole antenna for hf band applications. *Antennas and Propagation, IEEE Transactions on*, 61(6):2991–2999, 2013.

[19] Gunjan Verma, Fikadu T. Dagefu, Brian M. Sadler, and Kamal Sarabandi. Localization via the received signal strength gradient at lower VHF. *IEEE AP-S/URSI, to appear*, page 999, 2017.

[20] Fikadu T. Dagefu, Gunajn Verma, Richard Kozick, Brian M. Sadler, and Kamal Sarabandi. Full-wave analysis of time of arrival based localization with polarization diversity. *IEEE AP-S/URSI, to appear*, pages 99–, 2017.

[21] L. J. Chu. Physical limitations of omni-directional antennas. *Journal of Applied Physics*, 19(12):1163–1175, 1948.

[22] J. Choi, F. T. Dagefu, B. M. Sadler, and K. Sarabandi. Electrically small folded dipole antenna for hf and low-vhf bands. *IEEE Antennas and Wireless Propagation Letters*, 15:718–721, 2016.

[23] Gunjan Verma, Fikadu T. Dagefu, Brian M. Sadler, and Predrag Spasojevic. Implications of time/frequency synchronization tradeoff of quasi-synchronous multi-carrier ds-cdma for robust communications at lower VHF. *MILCOM 2016 - 2016 IEEE Military Communications Conference*, pages 694–699, 2016.

[24] Fikadu T. Dagefu, Gunjan Verma, Predrag Spasojevic, and Brian M. Sadler. An experimental study of quasi-synchronous multiuser communications in cluttered scenarios at low VHF. *2017 International Conference on Military Communications and Information Systems (ICMCIS)*, pages 1–7, 2017.

[25] Jihun Choi, Fikadu T. Dagefu, Brian M. Sadler, and Kamal Sarabandi. Low-power low-VHF ad-hoc networking in complex environments. *IEEE Access, submitted*, page 999, 2017.

[26] Fikadu. T. Dagefu, Gunjan Verma, Chirag R. Rao, Paul L. Yu, Jonathan R. Fink, Brian M. Sadler, and Kamal Sarabandi. Short-range low-vhf channel characterization in cluttered environments. *IEEE Transactions on Antennas and Propagation*, 63(6), June 2015.

[27] Fikadu T. Dagefu, Jihun Choi, Brian M. Sadler, and Kamal Sarabandi. A survey of small, low-frequency antennas: Recent designs, practical challenges, and research directions. *IEEE Antennas and Propagation Magazine*, pages 2–14, 2022.

[28] G Thiele. Analysis of yagi-uda-type antennas. *IEEE Transactions on Antennas and Propagation*, 17(1):24–31, 1969.

[29] Eric A Jones and William T Joines. Design of yagi-uda antennas using genetic algorithms. *IEEE Transactions on Antennas and Propagation*, 45(9):1386–1392, 1997.

[30] Constantine A. Balanis. Antenna theory analysis and design 3rd edition. new jersey: John willey & sons. *Inc.[3 Januari 2020]*, 2005.

[31] Jeffrey N. Twigg, Fikadu T. Dagefu, Nikhil Chopra, and Brian M. Sadler. Robotic parasitic array control for increased rss in non-line-of-sight. *IEEE Robotics and Automation Letters*, page NA, 2022.

[32] M. Ani Hsieh, Anthony Cowley, Vijay Kumar, and Camillo J Taylor. Maintaining network connectivity and performance in robot teams. *Journal of Field Robotics*, 25(1-2):111–131, 2008.

[33] Geoffrey Hollinger and Sanjiv Singh. Multi-robot coordination with periodic connectivity. In *2010 IEEE International Conference on Robotics and Automation*, pages 4457–4462. IEEE, 2010.

[34] Micah Corah, Cormac O'Meadhra, Kshitij Goel, and Nathan Michael. Communication-efficient planning and mapping for multi-robot exploration in large environments. *IEEE Robotics and Automation Letters*, 4(2):1715–1721, 2019.

[35] Graeme Best, Michael Forrai, Ramgopal R. Mettu, and Robert Fitch. Planning-aware communication for decentralised multi-robot coordination. In *2018 IEEE International Conference on Robotics and Automation (ICRA)*, pages 1050–1057. IEEE, 2018.

[36] Zhiyong Sun, Marcus Greiff, Anders Robertsson, and Rolf Johansson. Feasible coordination of multiple homogeneous or heterogeneous mobile vehicles with various constraints. In *Proc. of the 2019 International Conference on Robotics and Automation (ICRA'19), Montreal, Canada, IEEE*, 2019.

[37] Derek Mitchell, Micah Corah, Nilanjan Chakraborty, Katia Sycara, and Nathan Michael. Multi-robot long-term persistent coverage with fuel constrained robots. In *2015 IEEE International Conference on Robotics and Automation (ICRA)*, pages 1093–1099. IEEE, 2015.

[38] Isaac Vandermeulen, Roderich Groß, and Andreas Kolling. Turn-minimizing multirobot coverage. In *2019 IEEE International Conference on Robotics and Automation*. IEEE, 2019.

[39] Jonathan R. Fink and Vijay Kumar. Online Methods for Radio Signal Mapping with Mobile Robots. In *2010 {IEEE} International Conference on Robotics and Automation (IRCA)*, Anchorage, AK, May 2010.

[40] Jeffrey N. Twigg, Jonathan R Fink, Paul L. Yu, and Brian M. Sadler. Efficient base station connectivity area discovery. *The International Journal of Robotics Research*, 32(12):1398–1410, 2013.

[41] Jonathan R. Fink, Jeffrey N. Twigg, Paul L. Yu, and Brian M. Sadler. A parsimonious model for wireless connectivity in robotic networks. In *Global Conference on Signal and Information Processing (GlobalSIP), 2013 IEEE*, pages 855–858. IEEE, 2013.

[42] Alessandro Farinelli, Luca Iocchi, and Daniele Nardi. Distributed on-line dynamic task assignment for multi-robot patrolling. *Autonomous Robots*, 41(6):1321–1345, 2017.

[43] Jason M. Gregory, Jeffrey N. Twigg, and Jonathan R. Fink. Enabling autonomous information-gathering and self-recovery behaviors in partially-known, communication-constrained environments. In *Safety, Security, and Rescue Robotics (SSRR), 2016 IEEE International Symposium on*, pages 92–99. IEEE, 2016.

[44] Jeffrey N. Twigg, Jonathan R. Fink, Paul L. Yu, and Brian M. Sadler. RSS gradient-assisted frontier exploration and radio source localization. In *IEEE International Conference on Robotics and Automation*, pages 889–895, Saint Paul, MN, May 2012.

[45] Gunjan Verma, Fikadu T. Dagefu, Brian M. Sadler, and Kamal Sarabandi. Localization via the received signal strength gradient at lower vhf. In *2017 USNC-URSI Radio Science Meeting (Joint with AP-S Symposium)*, pages 7–8, July 2017.

[46] Neeraj Tantubay, Dinesh Ratan Gautam, and Mukesh Kumar Dhariwal. A review of power conservation in wireless mobile adhoc network (manet). *International Journal of Computer Science Issues (IJCSI)*, 8(4):378–383, 2011.

[47] Neha Kumari, Rohit Kumar, and Rohit Bajaj. Energy efficient communication using reconfigurable directional antenna in manet. *Procedia Computer Science*, 125:194–200, 2018.

[48] Gabriel Astudillo and Michel Kadoch. Neighbor discovery and routing schemes for mobile ad-hoc networks with beamwidth adaptive smart antennas. *Telecommunication Systems*, 66(1):17–27, 2017.

[49] Branislav Kusy, David Abbott, Christian Richter, Cong Huynh, Mikhail Afanasyev, Wen Hu, Michael Brünig, Diethelm Ostry, and Raja Jurdak. Radio diversity for reliable communication in sensor networks. *ACM Transactions on Sensor Networks (TOSN)*, 10(2):32, 2014.

[50] Patricio J. Cruz, Brian M. Sadler, and Rafael Fierro. Sensor localization using hybrid rf/optical wireless communications for an aerial data mule. In *American Control Conference (ACC), 2016*, pages 7085–7091. IEEE, 2016.

[51] Ryan J. Marcotte and Edwin Olson. Adaptive forward error correction with adjustable-latency qos for robotic networks. In *Robotics and Automation (ICRA), 2016 IEEE International Conference on*, pages 5283–5288. IEEE, 2016.

[52] Jonathan R. Fink, Alejandro Ribeiro, and Vijay Kumar. Motion planning for robust wireless networking. In *Robotics and Automation (ICRA), 2012 IEEE International Conference on*, pages 2419–2426. IEEE, 2012.

[53] James Stephan, Jonathan Fink, Vijay Kumar, and Alejandro Ribeiro. Hybrid Architecture for Communication-Aware Multi-Robot Systems. In *IEEE International Conference on Robotics and Automation (ICRA)*, pages 5269–5276, 2016.

[54] James Stephan, Jonathan Fink, and Alejandro Ribeiro. System architectures for communication-aware multi-robot navigation. In *ICASSP, IEEE International Conference on Acoustics, Speech and Signal Processing - Proceedings*, volume 2016-May, pages 6395–6399, 2016.

[55] James Stephan, Jonathan R. Fink, Vijay Kumar, and Alejandro Ribeiro. Concurrent Control of Mobility and Communication in Multi-Robot Systems. *IEEE Transactions on Robotics*, 33(5):1–15, 2017.

[56] Mehran Mesbahi and Magnus Egerstedt. *Graph theoretic methods in multiagent networks*, volume 33. Princeton University Press, 2010.

[57] Michael M Zavlanos, Magnus B Egerstedt, and George J Pappas. Graph-theoretic connectivity control of mobile robot networks. *Proceedings of the IEEE*, 99(9):1525–1540, 2011.

[58] Maria Carmela De Gennaro and Ali Jadbabaie. Decentralized control of connectivity for multi-agent systems. In *Proceedings of the 45th IEEE Conference on Decision and Control*, pages 3628–3633. IEEE, 2006.

[59] Ethan Stump, Ali Jadbabaie, and Vijay Kumar. Connectivity management in mobile robot teams. In *2008 IEEE international conference on robotics and automation*, pages 1525–1530. IEEE, 2008.

[60] Lorenzo Sabattini, Cristian Secchi, Nikhil Chopra, and Andrea Gasparri. Distributed control of multirobot systems with global connectivity maintenance. *IEEE Transactions on Robotics*, 29(5):1326–1332, 2013.

[61] David Williams and Oussama Khatib. The virtual linkage: A model for internal forces in multi-grasp manipulation. In *Robotics and Automation, 1993. Proceedings., 1993 IEEE International Conference on*, pages 1025–1030. IEEE, 1993.

[62] Peng Song and Vijay Kumar. A potential field based approach to multi-robot manipulation. In *Robotics and Automation, 2002. Proceedings. ICRA'02. IEEE International Conference on*, volume 2, pages 1217–1222. IEEE, 2002.

[63] J. Spletzer, Aveek K. Das, Rafael Fierro, Camillo J. Taylor, Vijay Kumar, and James P Ostrowski. Cooperative localization and control for multi-robot manipulation. In *Intelligent Robots and Systems, 2001. Proceedings. 2001 IEEE/RSJ International Conference on*, volume 2, pages 631–636. IEEE, 2001.

[64] Jim Mainprice and Dmitry Berenson. Human-robot collaborative manipulation planning using early prediction of human motion. In *Intelligent Robots and Systems (IROS), 2013 IEEE/RSJ International Conference on*, pages 299–306. IEEE, 2013.

[65] Alaa Khamis, Ahmed Hussein, and Ahmed Elmogy. Multi-robot task allocation: A review of the state-of-the-art. In *Cooperative Robots and Sensor Networks 2015*, pages 31–51. Springer, 2015.

[66] Robert Calderbank, Stephen D. Howard, and Bill Moran. Waveform diversity in radar signal processing. *IEEE Signal Processing Magazine*, 26(1):32–41, 2009.

[67] Stephanie Gil, Swarun Kumar, Dina Katabi, and Daniela Rus. Adaptive communication in multi-robot systems using directionality of signal strength. *International journal of robotics research*, 34(7):946–968, 2009.

[68] Andrea Conti, Matteo Guerra, Davide Dardari, Nicolò Decarli, and Moe Z. Win. Network experimentation for cooperative localization. *IEEE Journal on Selected Areas in Communications*, 30(2):467–475, 2012.

[69] Seongah Jeong, Osvaldo Simeone, Alexander Haimovich, and Joonhyuk Kang. Beamforming design for joint localization and data transmission in distributed antenna system. *IEEE Transactions on Vehicular Technology*, 64(1):62–76, 2015.

[70] Shahab Farazi, Kim Chinkidjakarn, and D. Richard Brown. Simultaneous distributed beamforming and nullforming with adaptive positioning. *2016 IEEE Global Conference on Signal and Information Processing (GlobalSIP)*, pages 129–132, 2016.

[71] Jian Hou, Zhiyun Lin, Wenyuan Xu, and Gangfeng Yan. Distributed transmit beamforming with autonomous and self-organizing mobile antennas. In *2010 IEEE Global Telecommunications Conference GLOBECOM 2010*, pages 1–5. IEEE, 2010.

[72] Laura Koch, Raviraj Adve, and Bruce Francis. Optimal beamforming with mobile robots. In *2007 Conference Record of the Forty-First Asilomar Conference on Signals, Systems and Computers*, pages 1652–1656. IEEE, 2007.

[73] Arjun Muralidharan and Yasamin Mostofi. Energy optimal distributed beamforming using unmanned vehicles. *IEEE Transactions on Control of Network Systems*, 2017. to appear.

[74] A. Jafargholi, M. Mousavi, M. Emadi, and M.M. Nayebi. Wide-band vhf nulling by five elements spiral array antenna. In *2006 6th International Conference on ITS Telecommunications*, pages 446–448. IEEE, 2006.

[75] Qi Wu, Yi Cao, Haiming Wang, and Wei Hong. Machine-learning-assisted optimization and its application to antenna designs: Opportunities and challenges. *China Communications*, 17(4):152–164, 2020.

[76] Justin Kong, Fikadu T. Dagefu, and Brian M. Sadler. Performance analysis of distributed beamforming with random phase offsets. In *2020 IEEE Wireless Communications and Networking Conference (WCNC)*, pages 1–6. IEEE, 2020.

[77] Justin Kong, Fikadu T. Dagefu, and Brian M. Sadler. Coverage analysis of distributed beamforming with random phase offsets using ginibre point process. *IEEE Access*, 8:134351–134362, 2020.

[78] Jemin George, Cemal Tugrul Yilmaz, Anjaly Parayil, and Aranya Chakrabortty. A model-free approach to distributed transmit beamforming. In *ICASSP 2020-2020 IEEE International Conference on Acoustics, Speech and Signal Processing (ICASSP)*, pages 5170–5174. IEEE, 2020.

[79] Jemin George, Anjaly Parayil, Cemal Tugrul Yilmaz, Bethany L Allik, He Bai, and Aranya Chakrabortty. Multi-agent coordination for distributed transmit beamforming. In *2020 American Control Conference (ACC)*, pages 144–149. IEEE, 2020.

[80] Justin Kong, Fikadu T. Dagefu, and Brian M. Sadler. Distributed adaptive beamforming and nullforming for covert wireless communications. In *2019 IEEE 90th Vehicular Technology Conference (VTC2019-Fall)*, pages 1–6. IEEE, 2019.

[81] Justin Kong, Fikadu T. Dagefu, and Brian M. Sadler. Simultaneous beamforming and nullforming for covert wireless communications. In *2020 IEEE 91st Vehicular Technology Conference (VTC2020-Spring)*, pages 1–6. IEEE, 2020.

[82] Justin Kong, Fikadu T. Dagefu, and Brian M. Sadler. Distributed beamforming in the presence of adversaries. *IEEE Transactions on Vehicular Technology*, 2020.

[83] Hoi-Shun Lui, Hon Tat Hui, and Mook Seng Leong. A note on the mutual-coupling problems in transmitting and receiving antenna arrays. *IEEE Antennas & Propagation Magazine*, 51(5):171–176, 2009.

[84] Zhiyong Huang, Constantine A Balanis, and Craig R Birtcher. Mutual coupling compensation in ucas: Simulations and experiment. *IEEE Transactions on Antennas and Propagation*, 54(11):3082–3086, 2006.

[85] Bin Liao and Shing-Chow Chan. Adaptive beamforming for uniform linear arrays with unknown mutual coupling. *IEEE Antennas and Wireless Propagation Letters*, 11:464–467, 2012.

[86] John D. Kraus, Ronald J. Marhefka, and Ahmad S. Khan. *Antennas for all applications*. McGraw-Hill, 2002.

[87] Carl Pfeiffer, Fikadu T. Dagefu, Boris Tomasic, Jeffrey N. Twigg, and Bae-Ian Wu. Virtual impedance method for mutual coupling compensation. *IEEE Transactions on Antennas and Propagation*, 69(8):4569–4579, 2021.

[88] S. Zhang, Gregory H. Huff, J. Feng, and Jennifer T. Bernhard. A pattern reconfigurable microstrip parasitic array. *IEEE Transactions on Antennas and Propagation*, 52(10):2773–2776, 2004.

[89] Laurent Petit, Laurent Dussopt, and J-M Laheurte. Mems-switched parasitic-antenna array for radiation pattern diversity. *IEEE Transactions on Antennas and Propagation*, 54(9):2624–2631, 2006.

[90] K. Iigusa, K. Sato, and M. Fujise. A slim electronically steerable parasitic array radiator antenna. In *2006 6th International Conference on ITS Telecommunications*, pages 386–389. IEEE, 2006.

[91] Stylianos C Panagiotou, Themistokis D Dimousios, Stelios A. Mitilineos, and Christos N. Capsalis. Broadband switched parasitic arrays for portable dvb-t receiver applications in the vhf/uhf bands. *IEEE Antennas and Propagation Magazine*, 50(5):110–117, 2008.

[92] Koresh Khateri, Mahdi Pourgholi, Mohsen Montazeri, and Lorenzo Sabattini. A comparison between decentralized local and global methods for connectivity maintenance of multi-robot networks. *IEEE Robotics and Automation Letters*, 4(2):633–640, 2019.

[93] Ethan Stump, Nathan Michael, Vijay Kumar, and Volkan Isler. Visibility-based deployment of robot formations for communication maintenance. In *2011 IEEE international conference on robotics and automation*, pages 4498–4505. IEEE, 2011.

[94] Yiannis Kantaros, Michalis Thanou, and Anthony Tzes. Distributed coverage control for concave areas by a heterogeneous robot–swarm with visibility sensing constraints. *Automatica*, 53:195–207, 2015.

[95] Peng Yang, Randy A. Freeman, Geoffrey J. Gordon, Kevin M. Lynch, Siddhartha S Srinivasa, and Rahul Sukthankar. Decentralized estimation and control of graph connectivity for mobile sensor networks. *Automatica*, 46(2):390–396, 2010.

[96] Jingjin Yu, Steven M. LaValle, and Daniel Liberzon. Rendezvous without coordinates. *IEEE Transactions on Automatic Control*, 57(2):421–434, 2011.

[97] Hasan A. Poonawala and Mark W. Spong. On maintaining visibility in multi-robot-networks with limited field-of-view sensors. In *2017 American Control Conference (ACC)*, pages 4983–4988. IEEE, 2017.

[98] Meng Ji and Magnus Egerstedt. Distributed coordination control of multiagent systems while preserving connectedness. *IEEE Transactions on Robotics*, 23(4):693–703, 2007.

[99] Stephanie Gil, Dan Feldman, and Daniela Rus. Communication coverage for independently moving robots. In *2012 IEEE/RSJ International Conference on Intelligent Robots and Systems*, pages 4865–4872. IEEE, 2012.

[100] Nicola Bezzo, Brian Griffin, Patricio Cruz, John Donahue, Rafael Fierro, and John Wood. A cooperative heterogeneous mobile wireless mechatronic system. *IEEE/ASME Transactions on Mechatronics*, 19(1):20–31, 2012.

[101] Michael M. Zavlanos and George J Pappas. Controlling connectivity of dynamic graphs. In *Proceedings of the 44th IEEE Conference on Decision and Control*, pages 6388–6393. IEEE, 2005.

[102] Jorge Cortes, Sonia Martinez, Timur Karatas, and Francesco Bullo. Coverage control for mobile sensing networks. *IEEE Transactions on robotics and Automation*, 20(2):243–255, 2004.

[103] Maggie X. Cheng, Yi Ling, and Brian M. Sadler. Network connectivity assessment and improvement through relay node deployment. *Theoretical Computer Science*, 660:86–101, 2017.

[104] Yu-Pin Hsu, Eytan Modiano, and Lingjie Duan. Age of information: Design and analysis of optimal scheduling algorithms. In *2017 IEEE International Symposium on Information Theory (ISIT)*, pages 561–565. IEEE, 2017.

[105] Mac Schwager, Daniela Rus, and Jean-Jacques Slotine. Unifying geometric, probabilistic, and potential field approaches to multi-robot deployment. *The International Journal of Robotics Research*, 30(3):371–383, 2011.

[106] Lorenzo Sabattini, Nikhil Chopra, and Cristian Secchi. Decentralized connectivity maintenance for cooperative control of mobile robotic systems. *The International Journal of Robotics Research*, 32(12):1411–1423, 2013.

[107] Anne Marsden. Eigenvalues of the laplacian and their relationship to the connectedness of a graph. *University of Chicago, REU*, 2013.

[108] Jonathan Kelner. Topics in theoretical computer science an algorithmists toolkit: Lecture 3. *[Online]. Available: https://ocw.mit.edu/courses/mathematics/18-409-topics-in-theoretical-computer-science-an-algorithmists-toolkit-fall-2009/lecture-notes/MIT18_409F09_scribe3.pdf [Accessed: 12-Nov-2020]*, 2009.

[109] Wei Ren and Yongcan Cao. *Distributed coordination of multi-agent networks: emergent problems, models, and issues*, volume 1. Springer, 2011.

[110] Lorenzo Sabattini, Nikhil Chopra, and Cristian Secchi. On decentralized connectivity maintenance for mobile robotic systems. In *2011 50th IEEE Conference on Decision and Control and European Control Conference*, pages 988–993. IEEE, 2011.

[111] Juergen Graefenstein, Amos Albert, Peter Biber, and Andreas Schilling. Wireless node localization based on rssi using a rotating antenna on a mobile robot. In *Positioning, Navigation and Communication, 2009. WPNC 2009. 6th Workshop on*, pages 253–259. IEEE, 2009.

[112] Oliver M. Cliff, Robert Fitch, Salah Sukkarieh, Debbie Saunders, and Robert Heinsohn. Online localization of radio-tagged wildlife with an autonomous aerial robot system. In *Robotics: Science and Systems*, 2015.

[113] J.H. Bojsen, Hans Schjær-Jacobsen, E. Nilsson, and J. Bach Andersen. Maximum gain of yagi–uda arrays. *Electronics Letters*, 7(18):531–532, 1971.

[114] Yaser S. Abu-Mostafa, Malik Magdon-Ismail, and Hsuan-Tien Lin. *Learning From Data*. AMLBook, 2012.

[115] Danylo Malyuta. Guidance, Navigation, Control and Mission Logic for Quadrotor Full-cycle Autonomy. Master thesis, Jet Propulsion Laboratory, 4800 Oak Grove Drive, Pasadena, CA 91109, USA, December 2017.

[116] John Wang and Edwin Olson. AprilTag 2: Efficient and robust fiducial detection. In *2016 IEEE/RSJ International Conference on Intelligent Robots and Systems (IROS)*, pages 4193–4198. IEEE, oct 2016.

[117] Asif A. Mulla and Pramod N. Vasambekar. Overview on the development and applications of antenna control systems. *Annual Reviews in Control*, 41:47–57, 2016.

[118] Ahmad Kamal Hassan, Md. Ahsanul Hoque, and Arild Moldsvor. Automated micro-wave (MW) antenna alignment of base transceiver stations: time optimal link alignment. In *Telecommunication Networks and Applications Conference (ATNAC), 2011 Australasian*, pages 1–5. IEEE, 2011.

[119] Md. Ahsanul Hoque and Ahmad Kamal Hassan. Modeling and performance optimization of automated antenna alignment for telecommunication transceivers. *Engineering Science and Technology, an International Journal*, 18(3):351–360, 2015.

[120] Jehn-Ruey Jiang, Chih-Ming Lin, Feng-Yi Lin, and Shing-Tsaan Huang. Alrd: Aoa localization with rssi differences of directional antennas for wireless sensor networks. *International Journal of Distributed Sensor Networks*, 2013, 2013.

[121] Fumin Zhang, Eric W. Justh, and P.S. Krishnaprasad. Boundary following using gyroscopic control. In *2004 43rd IEEE Conference on Decision and Control (CDC)(IEEE Cat. No. 04CH37601)*, volume 5, pages 5204–5209. IEEE, 2004.

[122] Jihun Choi and Fikadu T. Dagefu. A low-profile, top-loaded, multi-element, monopole antenna for compact ugv systems. *IEEE Transactions on Antennas and Propagation*, 2021.

[123] MicroSrain IMU. `http://www.microstrain.com/inertial/3DM-GX3-25`.

[124] Paul L. Yu, Jeffrey N. Twigg, and Brian M. Sadler. Radio signal strength tracking and control for robotic networks. *SPIE Defense, Security, and Sensing*, pages 803116–803116, 2011.

[125] Jeffrey N. Twigg, Jason M. Gregory, and Jonathan R. Fink. Towards online characterization of autonomously navigating robots in unstructured environments. In *Intelligent Robots and Systems (IROS), 2016 IEEE/RSJ International Conference on*, pages 1198–1205. IEEE, 2016.

[126] Siddharth Choudhary, Luca Carlone, Carlos Nieto, John Rogers, Zhen Liu, Henrik I Christensen, and Frank Dellaert. Multi robot object-based slam. In *International Symposium on Experimental Robotics*, pages 729–741. Springer, 2016.

[127] Peter P. Viezbicke. Yagi antenna design. *US Government Printing Office, Washington, DC*, 1976.

[128] Adel Haydar Lazem. Approximation of antenna patterns by means of a combination of gaussian beams, 2012.

[129] Simon Parsons and Michael Wooldridge. Game theory and decision theory in multi-agent systems. *Autonomous Agents and Multi-Agent Systems*, 5(3):243–254, 2002.

[130] Andreas Krause and Daniel Golovin. Submodular function maximization., 2014.

[131] Gerald Gamrath, Timo Berthold, Stefan Heinz, and Michael Winkler. Structure-driven fix-and-propagate heuristics for mixed integer programming. *Mathematical Programming Computation*, 11(4):675–702, 2019.

[132] Daniel E. Koditschek. Robot planning and control via potential functions. *The robotics review*, page 349, 1989.

[133] Lorenzo Sabattini, Cristian Secchi, and Nikhil Chopra. Decentralized connectivity maintenance for networked lagrangian dynamical systems. In *2012 IEEE international conference on robotics and automation*, pages 2433–2438. IEEE, 2012.